Microfluidic technologies for rapid, high-throughput screening and selection of antibodies for disease diagnostics and novel therapeutics

by

Monica Anjuli Kapil

A dissertation submitted in partial satisfaction of the

requirements for the degree of

Joint Doctor of Philosophy
with University of California, San Francisco

in

Bioengineering

in the

Graduate Division

of the

University of California, Berkeley

Committee in charge:

Professor Amy E. Herr, Chair
Professor Dorian Liepmann
Professor Adam Abate
Professor Susan Muller

Spring 2015

Microfluidic technologies for rapid, high-throughput screening and selection of antibodies for disease diagnostics and novel therapeutics

By

Monica Anjuli Kapil

Abstract

Microfluidic technologies for rapid, high-throughput screening and selection of antibodies for disease diagnostics and novel therapeutics

by

Monica Anjuli Kapil

Doctor of Philosophy in Bioengineering

University of California, Berkeley

Professor Amy E. Herr, Chair

With relevance spanning from disease diagnostics such as immunohistochemistry to immunoassays and therapeutics, antibody reagents play a critical role in the life sciences, clinical chemistry, and clinical medicine. Approaches such as immunohistochemistry (IHC), and immunoassays, all work by exploiting the principle that antibodies bind specifically to antigens of interest. IHC uses antibodies to detect antigens on cancerous tissue, and immunoassays use antibodies to identify biomarkers both for a myriad of disease diagnostics for cancer and infections diseases. Currently, antibody-based proteomic approaches such as immunohistochemistry and technologies that serve to diagnose and advance therapeutics are severely limited due to non-specific antibody binding, low specificity, and reproducibility issues. Selecting antibodies based on their antigen binding kinetic properties, such as their association and dissociation rate constants, k_{on} and k_{off}, can provide a quantitative metric that can further optimize and validate immunoreagent selection. These rate constants quantify the ability for an antibody to associate (bind) or dissociate (unbind) to a target analyte and determines inherent binding strength. Therefore a metric such as this has the power to eliminate problems seen by clinicians, researchers, and drug developers alike in regards to false positive, false negatives, and problems with reproducibility seen in antibody-based approaches and inform assay design. Consequently, scalable and efficient analytical tools for informed selection of reliable antibody reagents would have wide impact. In this work, I have developed a highly scalable, rapid, microfluidic screening assay, that is able to assess important but difficult to characterize interaction kinetics for antibodies and protein-protein interactions. This work includes a novel screening assay for quantitative characterization of binding kinetics for the development of new biomarker discovery, disease diagnostics, and novel therapies and advances antibody-based proteomics.

Acknowledgements

I first and foremost would like to thank God for being by my side, and helping me get through everything that life brings me. “Thy will be done in earth, as it is in heaven.” Matthew 6:9-13 and “Thy rod and thy staff they comfort me.” (Psalm 23:4). With God’s will, all things are possible.

I would like to thank my Ph.D. advisor and mentor, Professor Amy Elizabeth Herr. It has been a pleasure and an honor to work with such a wonderful person these past 5 years. Amy is a uniquely kind, compassionate, hard working, extremely intelligent and caring person, incredible mentor and advisor. Amy’s mentoring has provided me with constant and consistent support and motivation that helped me to accomplish my career goals that I have set out for myself. She is always enthusiastic when we are discussing science and often has a sparkle in her eye, which is contagious and motivated me to work even harder and explore questions that I once thought were too difficult to answer. Her passion, enthusiasm, and positivity drove me to continue to solve difficult problems in engineering and science and further push limitations that I often had put on myself. Amy’s ability to inspire, and her commitment to mentoring have made my Ph.D. experience unparalleled. I have learned so much being Amy’s student and I am forever grateful for her and for her always believing in me and pushing for excellence. She is a star.

I would like to also thank Professor Dorian Liepmann for being a fantastic mentor and one of my greatest champions. Thank you Dorian for being there for me since I first stepped onto UC Berkeley campus 6 years ago and sticking with me mentoring me as we worked through my research and career goals.

I would also like to that Professor Steven Conolly for always being there and sharing his many stories of academia, and how to navigate through it all successfully.

My Ph.D. studies would not have been the same without my wonderful labmates from the Herr lab, including all past and present members. Being surrounded by such smart, motivated, interesting, diverse, and inspiring people have made the whole Ph.D. process amazing and made coming into Lab a sheer joy. The people in the Herr lab are phenomenal on all counts! I would like to specifically thank Dr. Kelly (Karns) Gardner for taking me under her wing when I was just starting up in the Herr lab and providing great help and advice. I would like to thank Ms. Sasha Denisin for her support and positivity during the beginning of my Ph.D. Her curiosity, intellect, and kindness are a unique combination and it was a great joy to work with her. I would like to thank Dr. Robert Lin for always being the first to volunteer to help when I needed it and being an excellent labmate and friend. I would like to thank Dr. Todd A. Duncombe for always helping out and coming up with useful and interesting ideas. I would like to thank Ms. Julea Vlassakis for always being a great ear to discuss new findings and providing helpful and meaningful feedback. Lastly, I would like to thank Dr. Augusto M. Tentori for being a great colleague and friend throughout my time in the Herr lab and all of graduate school. I am

especially thankful for his help during my qualifying exam preparation, where he went above and beyond in helping me prepare.

Next, I would like to thank the student organizations that helped me meet the folks that turned into my Berkeley Family - The Latino/a Association of Graduate Students in engineering and sciences (LAGSES) and BEAST (BioEngineering Association of STudents). I would like to thank Dr. Nancy Diaz-Elsayed for her friendship and constant encouragement, always saying "Just keep swimming!" I would like to thank Dr. Laura Rose Croft for her ability to always give good honest advice, and always keeping it real and fun! I would like to thank Dr. Sophie Wong for her endless support, kindness, and compassion. Sophie, you are truly a gem! I would like to thank my dear friend Dawn Spelke for being an amazing friend and a wonderful listener. Dawn, your ability to listen, understand, and always be free to take a quick break with me to get our nails done, you are the best! Thank you! I would like to thank Elisabet Rosas who made my last year in graduate school brighter, her smile is contagious and her energy is just uplifting, I am very happy to have been able to meet and work with such intelligent and kind person. I would like to thank Dr. Joseph Chavarria-Smith, a friend I feel like I have known all my life. Joe, thank you for being there through the fun (crazy fun!) and difficult times. Graduate school would not have been the same without you. I would also like to thank my dear friend Jorge Santiago Ortiz who has been an incredibly supportive and caring friend. Jorge, I know we have more adventures to come!

Lastly, I would like to thank my dear and loving family. I would like to thank by two wonderful brothers, Akshay and Ajay Kapil who have supported and sacrificed so much for me to get to where I am today. Thank you Akshay for reviewing my NSF Graduate Research fellowship and always being ready to help me in a "pinch." Thank you Ajay for sacrificing so much for our family and talking care of our critically ill father all those years, allowing me to continue my dream of going to graduate school to get my Ph.D. I could not have asked for better brothers than the both of you. I love you. I would like to thank my dear, sweet, and kind mother, Ms. Norma Kapil who has given so much to make her children's dreams come true. She is truly a selfless person who would do anything for her family. I love you Mom and thank you for everything. Lastly I would like to thank my father, Mr. Shashi Kant Kapil who taught me so much and raised me as a little girl. Thank you for giving me the confidence to pursue anything I set my heart to and introducing me to math, science, and engineering through your love and fascination for those subjects. Thank you for providing a home built on learning and understanding the importance of an education. Thank you for providing me inspiration to go into the bioengineering field. I hope to one day be able to provide healthcare solutions that will help people, like so many helped us and our family in our struggle to help you survive. Daddy, thank you for everything. You will always live in my heart. I love you. This is dedicated to you.

Dedicated to my loving father and mother,

Mr. Shashi Kant Kapil

And

Mrs. Norma Armida Cervantes-Kapil

Table of Contents

Chapter 1: Motivation

1.0 Microfluidic technologies for rapid, high-throughput screening and selection of antibodies for disease diagnostics and novel therapeutics

Antibody-based proteomic approaches have great promise to provide further advancements in disease diagnostics and novel protein based therapeutics, however these technologies lack in quality, reproducibility, and accuracy and are in great need of thorough optimization[1,2,3]. Approaches such as immunohistochemistry (IHC), protein arrays, and chromatin immunoprecipitation (ChIP) all work by exploiting the principle of antibodies binding specifically to antigens of interest. IHC uses antibodies to detect antigens on tissue, and protein arrays use antibodies to identify biomarkers in serum, both for a myriad of cancer diagnostics [1,4,5] .Similarly, ChIP uses antibodies to purify protein-DNA complexes for drug discovery applications[6].

All of these antibody-based technologies however suffer in problems with accuracy and reproducibility, rooted from poor antibody selection. This results in a multitude of problems including inaccurate diagnosis, with up to 30–60% false negatives[1] and problems with reproducibility[2]. The ability of an antibody to bind to a target protein with high specificity or "binding affinity" to a given target analyte dictates the overall performance of these approaches[7]. An antibody that has a high affinity to a target analyte of interest will result in good attachment of target proteins. This results in a greater signal providing a more confident prediction in diagnosis. Problems with reproducibility in these approaches are derived from variations seen in antibody binding specificity or "binding affinity" to target antigens. Variation in antibody binding affinity has been known to occur between antibodies targeting different epitopes and even between antibodies targeting the same epitope [8]. Variation can also occur between different vendors of antibodies, and even between different batches from the same vendor [2,9]. These variations can result in misdiagnoses and can waste valuable time, samples, and reagents for researchers developing novel antibody based therapeutics and diagnostics. Therefore, technologies that can validate the selection of reliable and consistent antibodies towards uncharacterized proteins of interest are of great need.

Selecting antibodies based on their antigen binding kinetic properties, such as their association and dissociation rate constants, k_{on} and k_{off}, can provide a quantitative metric that can further optimize and validate immunoreagent selection. These rate constants quantify the ability for an antibody to associate (bind) or dissociate (unbind) to a target analyte and determine inherent binding strength. Therefore, a metric such as this has the power to eliminate many of the problems seen in antibody-based proteomic approaches and has the ability to reduce misdiagnosis and reproducibility errors while increasing overall performance.

Overarching Goal of this work: Advance antibody-based proteomics and diagnostics by introducing rapid, multiplexed immunoreagent quality assessment assays for the screening and selection of antibodies for disease diagnostics and novel therapeutics.

Chapter 2: Single-microchannel, multistep assay reports protein size and immunoaffinity

Based on Published article in Analytical chemistry by Chen, X., Kapil, M. A., Hughes, A. J., & Herr, A. E. (2011). Single-microchannel, multistep assay reports protein size and immunoaffinity. Analytical chemistry, 83(17), 6573-6579.

2.0 Abstract

We introduce a fully integrated multi-step protein assay that reports both protein identity and size. To report these two properties, a microfluidic design strategy integrates pore limit electrophoresis (PLE) with a pseudo-heterogeneous immunoassay in a single microchannel (PLE-IA). The PLE-IA assay was applied in a study of follistatin, a 31.5 kDa glycoprotein regulating mammalian cell proliferation and differentiation. In the "single-channel, multi-step" approach, an antibody to follistatin was first pseudo-immobilized in a polyacrylamide PLE gradient gel, near the origin of the separation axis. Subsequently, target and ladder protein species were electrophoretically introduced into the antibody-patterned PLE channel. Species having an affinity for the pseudo-immobilized antibody were detected via heterogeneous immunoassay. Non-interacting and, thus, unbound species electromigrated past the patterned antibodies, along the separation axis and finally separated according to the pore-size limit of each, yielding a log-linear dependence of molecular weight on migration distance. Ten-minute separations yielded an average peak capacity of 18±1.3 (separation resolution (*SR*) =1) in a 10 mm separation distance. Comparison of the separated peaks in two parallel PLE channels in the presence or absence of capture antibody with a protein size ladder revealed good agreement of target molecular weight with reported values. In addition, a more than 50-fold decrease in the detection limit (0.078 nM vs. 5 nM) was achieved using a "concentration front-injection" technique in which sample material was continuously loaded for 40 minutes. Based on this proof-of-principle demonstration with follistatin, PLE-IA should find application in study of cell signaling, including questions related to aging and regeneration.

2.1 Introduction

Given the biochemical diversity of proteins, a major analytical goal is realization of integrated protein analyses that rapidly yield information for multiple physicochemical properties. For instance, immunoblotting assays are coupled with electrophoreses to obtain both size and immuno-identity for proteins.[10] While powerful, these assays require multiple distinct instruments necessitating manual handing as key components of the assay workflow.[11] Consequently, microfluidic integration strategies are promising as means to realize fully integrated, multi-stage protein analysis tools. A major factor in use of microfluidic design strategies is compatibility of the approach with electrokinetic sample/fluid manipulation, rapid electrophoretic separation, low sample volume and the potential for multiplexing.[12]

While microfluidic immunoblotting has recently been introduced[13], a powerful variant of the assay comprises immunoprecipitation (IP) or IP-like processes integrated with subsequent electrophoretic analysis of target protein. Key advances to date have consisted of 'pull-down' of target species onto a solid phase (i.e., beads, silica filter) prior to elution of the target to electrophoresis analysis. A major advantage of IP (or co-immunoprecipitation) concatenated with homogeneous electrophoretic assays is reporting of both immunoaffinity and mobility information for the target, as well as an ability analyzing proteins in their native conformation (e.g., relevant to complexes).[14] As two examples of this approach, Yang et al. [10] developed an assay that detects multiple cancer biomarkers in human sera using microfluidic integration of the IP-release-electrophoresis workflow. An affinity column was formed by immobilization of antibody on the surface of a microfluidic channel, upstream of an electrophoresis channel. Target

was first captured by the immobilized antibody, then captured target was eluted with a low pH buffer and eluate was subsequently analyzed by electrophoresis. In a slightly different integration strategy, Wellner et al[15-17] inserted a small disc of glass fiber filter paper decorated with chemically immobilized antibody into a microfluidic sample reservoir of a t-channel microfluidic network. Sample was introduced into the reservoir and incubated with the immobilized antibodies. Multiple target protein species were later eluted from the glass fiber disc and analyzed by electrophoresis on the chip. In these assays, captured protein is eluted from the solid phase and analyzed by native electrophoresis.

In a complementary approach, on-chip immunosubtraction has been implemented in a wide range of heterogeneous formats (i.e., antibody functionalized magnetic beads[18], filter paper[16] or microcolumns[19]). In immunosubtraction, target proteins are identified via comparison of electropherograms – with and without target extraction. Target is extracted by incubating an aliquot of the sample with the heterogeneous immunoassay phase. Comparison of two electrophoretic assays reports 'subtraction' of target peaks (mobility) for those species that interact with the solid-phase immobilized antibody.[10, 17]. A recent fully homogenous immunosubtraction assay developed by our group benefited from incorporation of non-uniform *in situ* sieving matrices to both i) enhance mobility differences among analytes and improve electrophoresis performance and ii) yield a sharp decreasing pore-size interface to exclude large immune-complexes from subsequent native (non-denaturing, non-reducing) electrophoretic analysis.[20] Thus, the size exclusion filter acted to 'subtract' target analyte from electrophoresis, obviating the need for a heterogeneous stage in the immunosubtraction assay. Immunosubtraction was completed in one integrated chip with a total on-chip analysis time of 2 min.
In the present work, we seek to subtract native protein targets from a subsequent sizing assay. To minimize sample handling, reagent exchange, and inter-assay sample manipulation, we integrate an immunoassay with pore limit electrophoresis (PLE) in a single microchannel. PLE was introduced in the 1960's as a separation technique whereby a mixture of proteins was separated in a decreasing gradient in slab-gel pore-size; in which the gradient extends to pore-sizes much smaller than those used in standard slab-gel electrophoresis[21]. Protein mobility is reduced as species electromigrate along the separation axis, through the decreasing pore-size gel gradient, until electromigration reaches a near stop where the pore-size is smaller than the effective dimension of the analyte (i.e., the pore limit). A logarithmic relationship between migration distance and protein size is reported, which is useful in determining analyte molecular weight.

While conceptually useful, macroscale (slab-gel) PLE has found limited use as an analytical method due to an intensive and difficult to control fabrication process and extensive run times. Importantly, recent adaptation of PLE to microfluidic formats has mitigated both the complexity of gel fabrication and the needed run times – making the assay more accessible.[16] Building on the single-stage microfluidic PLE assay, the format has proven useful as a component in multi-stage assays, including a PLE-based zymography assay. Using a single straight microfluidic channel, enzyme was sized via PLE and the activity of the PLE-immobilized enzyme was quantified from the generation of fluorescent product, after electrophoretic introduction of substrate.[22]

Here, we report on a multi-stage PLE-based immunoassay (PLE-IA) that integrates into a single, straight microchannel a two-stage assay comprised of: (1) a heterogeneous immunoassay (akin to IP or co-IP) and (2) subsequent protein sizing accomplished using PLE . For the first stage, the assay requires no surface immobilization, as the initial heterogeneous stage of the assay is completed by allowing sample to electromigrate through a capture antibody region. The capture antibody has been *a priori* immobilized owing to pore limit exclusion in the PLE gel; thus, eliminating the need for chemical functionalization and surface attachment. For the second stage, surfactant-free sizing (via PLE) greatly simplifies assay integration, eliminating the need to heat treat or mix sample with surfactants on-chip. Both the immunoassay and the protein sizing are characterized. Immunoassay results suggest the strategy is a selective method with a linear dose response behavior that is useful for protein quantitation. In the PLE stage of the assay, log-linear dependence between molecular weight and migration distance allows determination of protein size. Taken together, the assay protocol simplifies chip design and shrinks the overall device footprint, as the design strategy eliminates the need for both a sample injection geometry (cross-t injector) and more than two access wells. Our study forms a promising basis for the multi-stage separation applicable to analysis of sparingly available samples.

2.2 Materials and methods

Reagents: The UV photoinitiator 2,2-azobis[2-methyl-N-(2-hydroxyethyl) propionamide] (VA-086) was purchased from Wako Chemicals (Richmond, VA). 3-(Trimethoxysilyl)-propyl methacrylate (98%), glacial acetic acid (ACS grade), methanol (ACS grade), 2-hydroxyethyl cellulose (HEC), acrylamide, bis-acrylamide were all purchased from Sigma. Premixed 10x Tris/glycine native electrophoresis buffer (25 mM Tris, 192 mM glycine in 1x buffer, pH 8.3) was purchased from Bio-Rad (Hercules, CA). Alexa Fluor 488 labeled trypsin inhibitor (TI) and bovine serum albumin (BSA) were purchased from Invitrogen (Carlsbad, CA). Purified human C reactive protein (CRP), recombinant human S100 beta protein and recombinant human FST protein, mouse monoclonal antibody to S100 and mouse monoclonal antibody to FST were all purchased from Abcam (Cambridge, MA). Proteins and antibodies were fluorescently labeled in-house using Alexa Fluor 488 and 568 protein labeling kits from Invitrogen per the supplier's instruction and purified by P-6 Bio-Gel columns (Bio-Rad, Hercules, CA). A "*" symbol after the name of an analyte (i.e., "BSA*") is used throughout to indicate that the protein was fluorescently labeled prior to analysis to aid in assay characterization. Labeled proteins and antibodies were stored at 4 °C in the dark until use.

Chip preparation: Optical white soda lime glass (i.e., Crown glass) chips with straight channels were fabricated by Caliper Life Sciences (Hopkinton, MA) using standard wet etching, drilling, and thermal bonding techniques. Patterning of the sieving matrix was performed in-house. Bare channels were first incubated with 1 M NaOH for 10 min followed by flushing with DI water, and then dried by vacuum. In order to prepare the channel for covalent attachment of the polyacrylamide (PA) gel, the channels were incubated with a degassed 2:3:5 mixture of 3-(trimethoxysilyl)-propyl methacrylate, glacial acetic acid and DI water for 30 min. After incubation, the channels were rinsed with methanol and DI water and purged with vacuum.

Fabrication of the pore-size gradient gel: A gradient gel was fabricated in the straight channel through a two-step photopolymerization process. First, degassed 30% T (the concentration of

total acrylamide, w/v), 5% C (ratio of bis-acrylamide and bis-acrylamide + acrylamide, w/w) acrylamide/bis-acrylamide solution was introduced into the surface modified channel by wicking. Then high viscosity 5% 2-hydroxyethyl cellulose (HEC, Sigma, average MW ~720,000) solution was added to terminal wells to yield quiescent fluid conditions in the channels. To establish the small-pore-size end of the gradient gel, a 600 μm membrane (30% T, 5% C) was fabricated near one end of the channel via a UV objective microscope system (Diaphot, Nikon). A mask with a 600 μm x 500 μm window was aligned to the chip using a manual adjust x-y translation stage. UV illumination in the 330-375 nm range was provided by a mercury bulb. Polymerization of the membrane was achieved with a 4 min exposure to UV light (~8 mW/cm^2). After polymerization of the membrane, the HEC solution was removed from the terminal wells. A degassed 3% T, 2.6% C precursor solution was then added to a 200 μl pipette tip press-fit into the via well at the channel terminus furthest from to the membrane. In the well proximal to the membrane, 30% T, 5% C precursor solution was added to prevent dry out of the gel. The chip was equilibrated for 18 hours to establish a diffusion-generated 3% T to 30% T gradient along the channel length. The whole channel was then flood exposed under ~10 mW/cm^2 UV intensity for 8 min using an air cooled mercury lamp (B-100AP lamp, UVP, Upland, CA). The polymerized chip was stored in 1 x Tris/glycine buffer at 4°C until use. After use, chips were regenerated for further use by soaking the glass chips in a 2:1 solution of perchloric acid and hydrogen peroxide overnight at 60°C, thus dissolving the PA gel interiors and leaving the glass intact.

Apparatus and imaging

Ten micro liters of 1 x Tris/glycine or protein samples diluted in Tris/glycine were added to the pipette tips press-fit into the via wells of each channel. Voltage was applied using a custom 8-channel programmable high voltage power supply (current/voltage feedback control with a dynamic range of ~4000 V and +/- 0.01 μA current and ~1 V voltage resolution).

Fluorescence images were collected using an inverted epi-fluorescence microscope (IX-50, Olympus, Melville, NY) equipped with a 1392 x 1040 Peltier-cooled interline CCD camera (CoolSNAP HQ2, Roper Scientific, Trenton, NJ), filter cubes and an automated x-y translation stage (S2000, Applied Scientific Instrument, Eugene, OR). The CCD exposure time was 200 to 800 ms, adjusted depending on the intensity of the fluorescence signal. Fluorescence images of the whole channel were collected at 1 min intervals during PLE-IA. Sets of 400 μm x 60 μm region of interest (ROI) from overlapping images were digitally stitched together to form fluorescence images along the entire separation axis. Background subtraction was performed using identical ROI lying out of the channel. Image analysis was conducted using ImageJ software (NIH, Bethesda, MD). Nonlinear least-squares fitting of the signal was performed using OriginPro 8.0 software (Northampton, MA).

PLE-IA operation

Antibody immobilization: capture antibody from a stock solution of a set concentration (500 nM, labeled with Alexa Fluor 568) was electrophoresed into the PLE-IA channel. During electromigration along the PLE separation axis, antibody was immobilized at the pore limit location through size exclusion by the gel matrix. Henceforth, we refer to capture antibody patterning in the PLE gel as 'pseudo-immobilization' to emphasize that antibody immobilization

arises from pore-limit exclusion and not chemical functionalization of the antibody and subsequent surface/gel attachment. First, the antibody solution was added to the sample reservoir close to the 3% T end. A 3 min loading interval (96 V/cm) was applied to inject the antibody into the PLE channel. Then the antibody solution was replaced with native buffer followed by 10 minute electrophoretic migration of the antibody to its pore limit location (E = 96 V/cm).
Pseudo-heterogeneous IA: after the antibody immobilization, sample solution containing the protein of interest was placed in the sample reservoir. Proteins were injected into the microchannel as either a concentration front or as a plug. For the front-injection method, protein sample was injected into the PLE channel from a sample well for an extended duration (40 min, 96 V/cm), followed by 10 min washing with plain buffer to separate the unbound species from the immune complex. For plug-injection, a 96 V/cm electric field was applied for a short time (30 s) to inject a protein plug into the channel. The sample solution in the reservoir was then replaced with native buffer and the potential was re-applied. This step yielded electrophoretic migration of a protein plug into the PLE channel and past the antibody region.

Measurement of dose response: To study the dose response of the FST PLE-IA, FST* (labeled with Alexa Fluor 488) solutions having a range of known concentrations (5 to 10000 nM for the plug injection or 0.078 nM to 10 nM for the sample front-injection method) were analyzed via the pseudo-heterogeneous IA. For the plug injection method, a mobility and loading control standard (Alexa Fluor 488 labeled TI* at 100 nM) was included. The amount of antibody loaded into the channel was in the range of ± 20% as measured by the red fluorescence signal (peak area) at the capture antibody region. Fluorescence signal from the complex (peak area) was normalized to the measured amount of capture antibody for each run.

2.3 Results and discussion

PLE-IA is an assay that reports both protein identity (via immunoassay) and protein size (via PLE), as illustrated in Figure 2.1. The multi-step assay is conducted in a single straight microchannel housing a decreasing gradient in polyacrylamide gel pore-size. The following section introduces and demonstrates PLE-IA, with the subsequent sections detailing characterization and optimization. The resulting PLE-IA performance is developed with particular focus on measurement of the protein FST.

PLE-IA principle and characterization
To realize PLE-IA, two assays are integrated in a decreasing pore-size gradient PA gel; here housed in a microfluidic channel (Figure 2.1). To achieve the two-step assay, PLE-IA relies on a region of patterned capture antibody at the head of a straight PLE separation channel. The capture antibody region acts as a pseudo-heterogeneous immunoassay. The term "pseudo-heterogeneous" is used, as immobilized capture antibody is not bound to the PA gel through chemical functionalization, but rather through size exclusion in the decreasing PA gel pore-size gradient (Figure 2.1A, Step 1). Consequently, the pseudo-immobilized capture antibody band yields functionality similar to that provided by a true heterogeneous immunoassay. Thus, as species electromigrate through the capture antibody region and along the PLE gradient, proteins with an affinity to the capture antibody form immune-complexes and cease to migrate (Figure 2.1A, Step 2). Analyte transport in PLE-IA is governed by diffusion, electromigration, and

antibody-antigen binding reactions at the site of the pseudo-heterogeneous immunoassay capture antibody. Species that are not bound to the capture antibody region continue to migrate along the separation axis and to the pore limit position of each respective species. Comparison of PLE to PLE-IA of the same protein species yields endpoint information (Figure 2.1A, Step 3) on two physicochemical properties: 1) formation of antibody-antigen complex during PLE-IA allows identification of the target protein present in the sample and 2) the pore-limit location yields information on protein size. Thus, the PLE-IA is designed for species 1) exhibiting the same charge polarity as the antibody (determined by the run buffer pH relative to analyte pI) and 2) with a molecular weight smaller than the capture antibody.

To demonstrate the principle of PLE-IA for FST*, Figure 2.1 B and C compare a time series of fluorescence micrographs from PLE-IA (PLE with capture Ab present) to a PLE time series of fluorescence micrographs (no capture Ab present). Prior to running a PLE-IA for FST*, the PA gel pore-size gradient was fabricated (see Materials and Methods section) and patterned with capture antibody using a 3 min electrophoretic loading interval (500 nM capture antibody solution, 96 V/cm) followed by a 10 min (E = 96 V/cm) compaction interval. The compaction interval was used to transfer the antibody band to its pore limit and to further reduce the bandwidth of the capture antibody as well as increase the local concentration of capture antibody. Bandwidth was reduced by ~70% for the conditions described here (e.g., σ_0 = 1420 μm; $\sigma_{10\ min}$ = 385 μm). During capture antibody patterning, the mobility of the antibody band decreased from 5.4×10^{-5} cm^2/Vs (at 1 min) to 2×10^{-6} cm^2/Vs (at 10 min) and the antibody band was pseudo-immobilized to the $0.3L_{PLE}$ position (i.e., at 3.1 mm from the loading reservoir or at 30% of the total PLE separation length, L_{PLE}, with an inferred 11% T local condition, assuming a linear gradient in PA gel concentration). To initiate the PLE-IA (Figure 2.1B), fluorescently labeled FST was electrophoresed into the PLE-IA channel as an injection plug defined by a 30 s injection interval (96 V/cm). After 10 min of electromigration, 64% of the total FST* signal was detected at its pore limit location ($0.8L_{PLE}$), with the remaining 36% of the FST* signal detected at $0.34L_{PLE}$. This latter position corresponds to the expected location of the 150 kDa anti-FST antibody. Through comparison of PLE results to PLE-IA results, the molecular weight and identity of FST* can be ascertained. As shown in the PLE assay in Figure 2.1C, FST* migrated along the PLE separation axis in the absence of a patterned capture antibody (E = 96 V/cm). During the 10 min electromigration, the FST* mobility decreased from 8.1×10^{-5} cm^2/Vs to 3.2×10^{-6} cm^2/Vs, as the protein neared the pore-limit location on the separation axis. At 10 min, all detectable FST* was immobilized at $0.8L_{PLE}$ (24% T at 8.1 mm). In accordance with expectation, no detectable signal was observed near the head of the PLE separation axis (recall that no antibody was pseudo-immobilized in the PA gel for PLE).

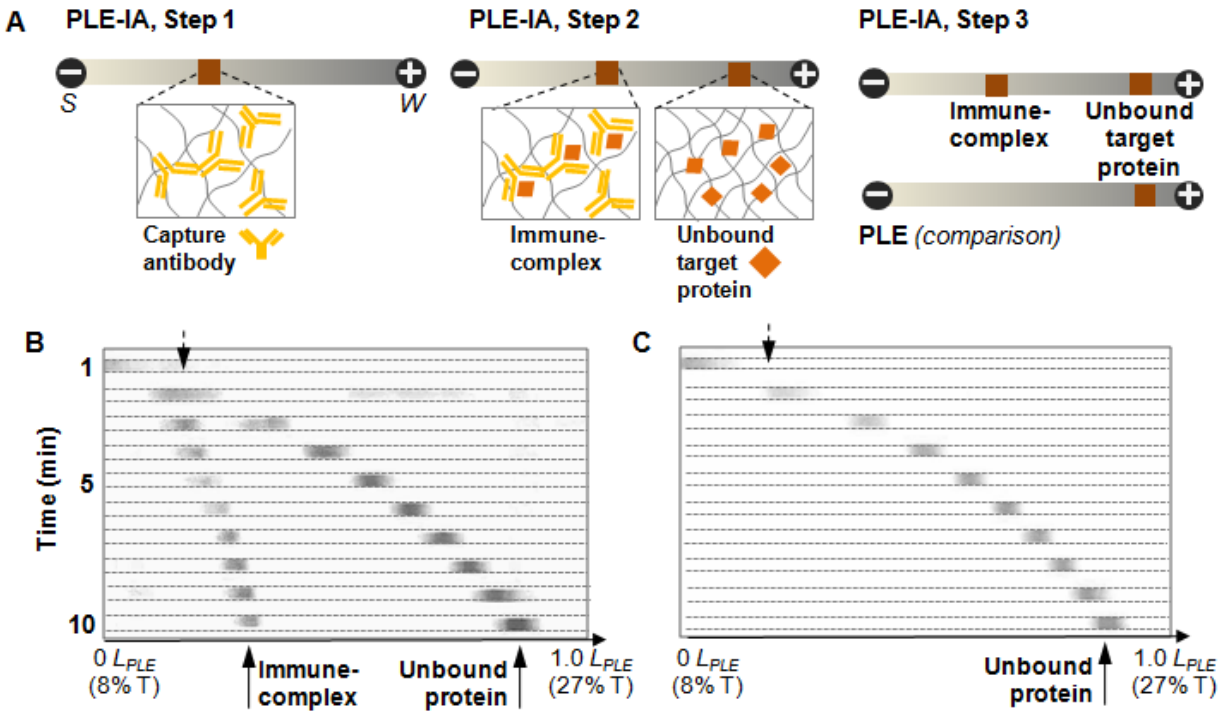

Figure 2.1. PLE-IA reports both protein size and identity. (A) Decreasing pore-size gradient of PA gel (light to dark shading) establishes the separation matrix for the pseudo-heterogeneous immunoassay and PLE. Step 1: Electrophoretic pseudo-immobilization of capture antibody. Step 2: Protein sample electromigrates through the capture antibody region resulting in formation of an immobile immune-complex and, in some operating conditions, an unbound protein band. Step 3: Comparison of PLE results to PLE-IA results yields protein molecular weight and binding affinity information. (B) Inverted grayscale fluorescence images show time evolution of PLE-IA (Ab+) for the fluorescently labeled FST target protein. FST* is detected by binding at the location of the pseudo-heterogeneous immunoassay, as well as at the FST* pore limit location. (C) Inverted grayscale fluorescence images show time evolution of PLE (Ab-) with FST* detected only at the pore limit location. In (B) and (C), channel width = 100 μm, E = 96 V/cm, the FST* and FST antibody concentrations are both at 500 nM.

Figure taken directly from Analytical chemistry, 83(17), 6573-6579.

Characterization of the protein PLE. PLE reports a logarithmic dependence between protein molecular weight and migration distance thus allowing determination of the molecular weight of target proteins, as has been reported on both the macro (i.e., slab gel) [21] and micro (i.e., microfluidic chip) scale.[23] In the present work, PLE is operated in a manner that obviates the need for a defined injection plug of material, as sample fronts are introduced and analyzed (Figure 2.2A, B). Similar on-chip and capillary tube operation has been described for other assays, including as an operational mode for gradient elution moving boundary electrophoresis (GEMBE). During GEMBE, analytes were injected continuously into a microfluidic channel against a counterflow.[24] Here, PLE operation relies on electromigration of a sample concentration front into a single straight microchannel geometry with no injection "cross-t" junction as is commonly used in microfluidic chip electrophoresis. The decreasing PA gel pore-size acts to slow the front and yields enrichment of analyte at the pore limit location as well as the ability to resolve analytes.

To characterize the PLE portion of the PLE-IA (operated in a front-injection mode), a 4 species protein ladder spanning a 21 to 150 kDa molecular weight range was separated in a PLE microchannel (Figure 2.2). As evident in the PLE time course images (10 min) presented in Figure 2.2 A, a concentration front was formed along the separation axis near the pore limit location of each species (TI*, BSA*, CRP*, IgG*) due to the rapidly decreased migration velocity at each respective position. The fluorescence signal along the PLE separation axis at assay completion (10 min) is shown in Figure 2.2 B, with pore-limit positions of the four ladder proteins resolvable. A linear relationship between log molecular weight and migration distance of the concentration front was observed (Figure 2.2 B inset, R^2=0.99), as expected for PLE. Note the increase in fluorescence signal from the 3% T end (PLE axis head) to the IgG peak, which highlights the concentrating effect of PLE. Figure 2.3 shows separation of the same ladder species using a plug injection method as commonly used in microchannel electrophoresis. The PLE assay yielded an estimated average peak capacity of 18 ± 1.3 (assuming SR = 1.0 for baseline separation, reported as SD, n = 4). Also, note that a maximum time for electrophoretic injection of a sample concentration front is limited by the buffering capacity of the solution. Assuming 10 µl of pH 8.3 Tris/glycine buffer in the S and W wells and I = 0.2 µA. A $[H^+]$ production rate of 2 x 10^{-12} mol/s is calculated. Assuming 0.025 M Tris base and 0.175 M glycine in the buffer, the buffer would be titrated in 3750 min at 96 V/cm.

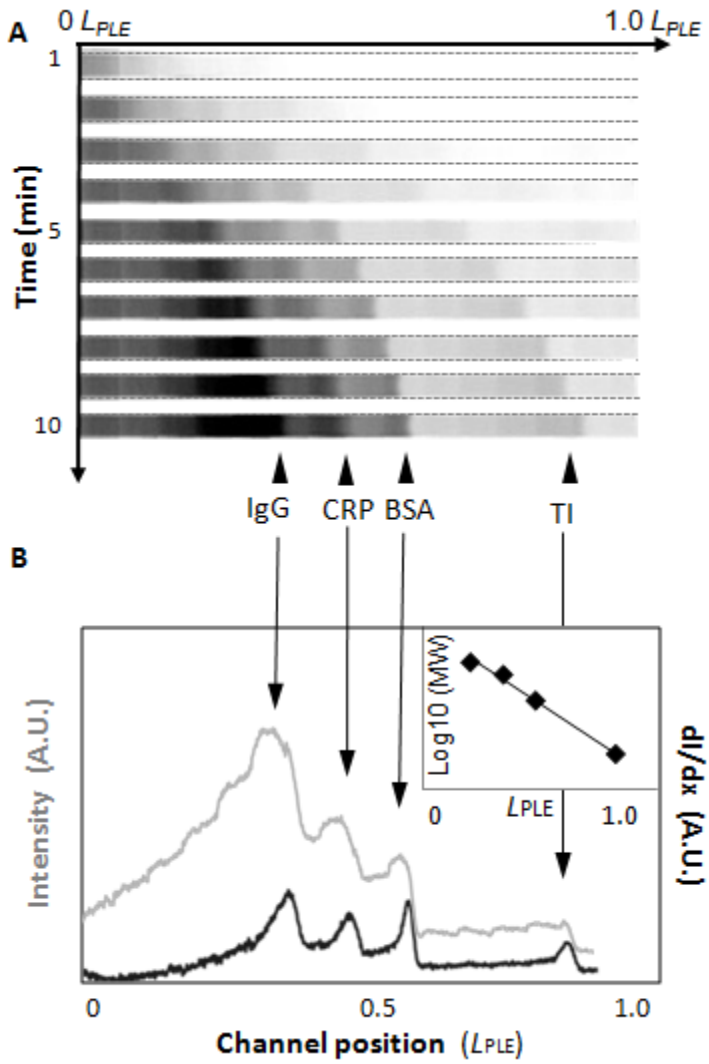

Figure 2.3. PLE implemented on a concentration front yields protein size information while obviating sample plug injection requirements. (A) Time evolution of electrophoretic sample front introduction, as captured using epi-fluorescence imaging. Arrows indicate identify of each concentration front. Width of the channel imaged was 100 μm, with aspect ratio adjusted and dashed channel wall lines added for clarity. (B) Gray trace shows concentration front profile, while black trace shows first spatial derivative of concentration signal, both at assay completion (10 min). Inset shows a log linear relationship was obtained between molecular weight and migration distance of the concentration front. Channel width = 100 μm, E = 96 V/cm, concentration of all species is 20 nM.

Figure taken directly from Analytical chemistry, 83(17), 6573-6579.

Characterization of the pseudo-heterogeneous immunoassay. To characterize both the patterning of the capture antibody and the function of the IA, several fluorescently labeled analytes were studied, including the capture antibody (FST-Ab*, labeled with red Alexa Fluor 568, 500 nM), FST* (labeled with green Alexa Fluor 488, 500 nM), and a calibration size ladder (labeled with Alexa Fluor 488). FigureA shows the spatial overlap between captured FST* and FST-Ab* in PLE-IA. While in PLE (Ab-), free FST* is detectable only at the pore-limit of the protein (0.8 L_{PLE}). PLE-IA shows significant binding of FST* with FST-Ab* (0.45 L_{PLE}). Using a molecular weight ladder (TI at 21.5 kDa, BSA at 66 kDa, CRP at 115 kDa, IgG at 150 kDa with y = -1.05x + 3.2, R^2 = 0.99), the size of FST* was estimated to be 33 ± 3.4 kDa (n=3) and the size of the FST-Ab* was estimated to be 140.0 ± 4.6 kDa (n=3). At assay completion, the capture antibody peak width was estimated at σ = 440 ± 95 μm (occupying 4.3% of the PLE separation axis length), while free FST* had a peak width of σ = 350 ± 40μm (spanning 3.5% of the PLE separation axis length). The local concentration of FST-Ab* is estimated to be 2 μM (132 pg in a volume of 0.44 nL). Similar results are shown for a more complex sample that includes a mixture of TI*, BSA* and FST* (Figure B, 100 nM of each species). By comparing peaks in PLE-IA and PLE channels, the pore limit position of the target protein can be identified. In PLE-IA, the target protein peak has a reduced intensity (smaller area under the curve value) due to target binding to the capture antibody. In FigureB, the middle peak in the Ab- PLE channel is the target protein (FST*). Using this method, the size information of target protein can be obtained from complex mixture containing several protein species.

To characterize the selectivity of the pseudo-heterogeneous IA for FST, FST* (labeled with Alexa Fluor 488, green) and S100* (labeled with Alexa Fluor 568, red) were electrophoretically transported into PLE channels patterned with: 1) no capture antibody (Ab-), 2) on-target antibody (FST-Ab+), or 3) off-target antibody (S100-Ab+). As shown in C, in the absence of capture antibody (Ab-) a green peak and red peak were fully resolved and correspond to FST* and S100*, respectively. In the channel patterned with FST-Ab, FST* (green fluor) was detectable at both the FST-Ab (FST complex), as well as at the free FST pore limit location; S100* (red fluor) yielded no signal at the location of the FST-Ab. Conversely, when the PLE-IA channel was patterned with off target antibody (S100-Ab+), S100* (red fluor) was detectable at both the S100-Ab location (S100 complex), as well as at the free S100* pore limit location; FST* (green fluor) yielded no signal at the location of the S100-Ab. Variation in the absolute location of the free S100* peak (± 3.7% L_{PLE}) is attributed to the variation of the PLE gradient from device to device. These results suggest that antibody affinity for target and not physical size exclusion of antigen governs the PLE-IA assay mechanism, under the conditions used here.

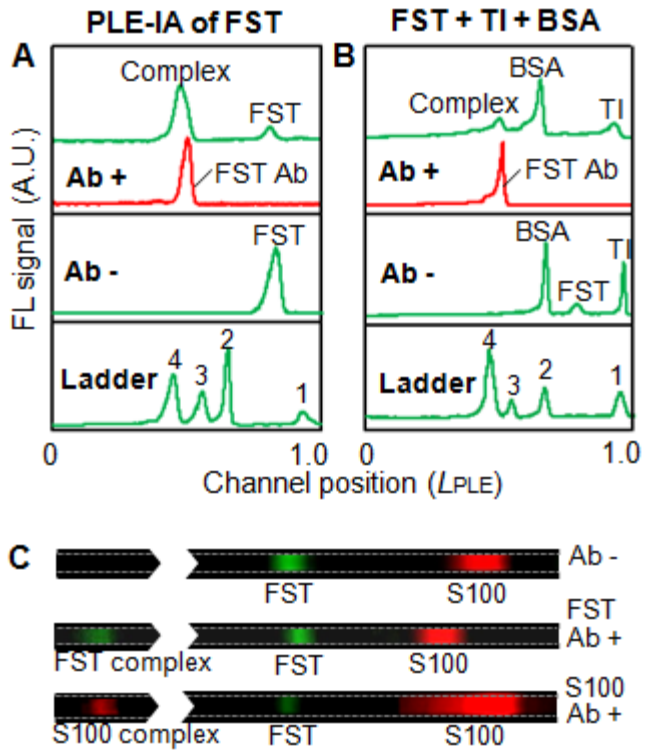

Figure 2.4. Pseudo-heterogeneous IA performance suggests selective capture of FST*. (A) PLE-IA for FST* from pure protein solution. (B) PLE-IA for FST* in a mixture with size ladder protein TI* and BSA*. Ladder protein 1 to 4 are TI (21 kDa), BSA (66 kDa), CRP (115 kDa) and IgG (150 kDa). (C) Selectivity of FST PLE-IA. FST* (green) and S100* (red) were analyzed in PLE (Ab- channel) and immobilized at each respective pore limit location. The FST* and smaller S100* targets were also analyzed in a channel patterned with a single antibody (S100 Ab+ and FST Ab+ channels). Fluorescence micrographs of each assay report no detectable cross-reactivity. E = 96 V/cm. Channel width is 100 μm.

Figure taken directly from Analytical chemistry, 83(17), 6573-6579.

Quantitation capacity of PLE-IA

To maximize the analytical sensitivity and inform optimization of PLE-IA operation, study was undertaken to identify transport regimes relevant to the IA portion of PLE-IA. Comparison of electromigration to IA complex formation timescales were quantified through the Damkohler number, here for binding or Da_{on}. Thus, Da_{on} represents the relative importance of the electromigration timescale to the "on" binding timescale, as given by $Da_{on} = k_{on}L_{ab}b/\mu E$ where k_{on} is the on rate of the binding reaction, L_{ab} is the band width of the capture antibody, b is the concentration of antibody binding sites, μ is the electrophoretic mobility of the complex and E is the applied electric field. Based on a k_{on} of $2x10^6$ ($s^{-1}M^{-1}$) from the literature,[25] Da_{on} of the heterogeneous immunoassay is estimated to be 1000 under 96 V/cm electric field.

A Da >> 1 indicates that the reaction of interest occurs much faster than the rate of mass transfer[26]. Thus, PLE-IA operation as presented here can be classified as a mass transfer limited system where electromigration is slow in comparison to the binding reaction.[27] To obtain high sensitivity detection of target protein, PLE-IA was performed on a front of material introduced via an extended, continuous period of applied electrical potential. In this regime, continuous sample injection acts to replenish the analyte and thus to minimize the depleted analyte concentration near the binding sites. Consequently, assuming a fixed capture antibody concentration (in excess) and low protein target concentration (in comparison to the antibody), PLE-IA operation with extended duration sample loading was hypothesized to achieve more target binding and, consequently, higher sensitivity because the analyte is continuously replenished to the capture antibody. To achieve this design goal, a high electric field was employed to increase the rate of electrophoretic mass transfer. An upper bound on reliable gel performance was observed with an applied electric field in the 150 V/cm range (i.e., PLE gel appears to undergo degradation, possibly due to heat generated at the high gel concentration end). Thus a 96 V/cm electric field was used in this study. Under this lower electric field strength condition, PA gel performed robustly for the duration of both PLE and PLE-IA.

As anticipated, enhanced, high-sensitivity target detection was assessed under extended duration electromigration of the target into the PLE-IA channel. Figure 2.5 shows the fluorescence signal detected at the capture antibody region as the analyte concentration front (FST*, 5 nM) electromigrates into the channel for 40 min (E = 96 V/cm). The loading process was followed by a 10 min electrophoretic "wash" with plain buffer (E = 96 V/cm). An increase in the fluorescence signal at the capture antibody location was observed. Then the fluorescence signal reached a plateau, suggesting equilibrium of the binding reaction. Six minutes after washing, the signal began to decrease, suggesting separation of the unbound FST from the capture antibody and dissociation of the analyte-antibody complex. The unbound protein was removed by electrophoretic exchange of clear buffer into the channel for 10 min at 96 V/cm. Based on these observations, on-going studies in our group are focused on adapting this assay format to quantitative assessment of both k_{on} and k_{off}. Figure B reports a comparison of the dose response behavior between the front-injection (40 min injection, 96 V/cm) and plug-injection (30 s injection of analyte at 96 V/cm) approach. For the plug injection approach, a linear relationship between fluorescence signal and FST concentration was observed from 5nM to 1333nM (R^2 = 0.989) and the detection limit of PLE-IA was 5 nM as indicated by the 2.9 signal to noise ratio. In comparison to the plug injection approach, the front-injection method yields a linear dose response range from 0.078 nM (2.5 ng/mL) to 10 nM (R^2 = 0.985). Use of the front-injection

method enhances the sensitivity of PLE-IA by lowering the detection limit to 0.078 nM (SNR ~ 2.7). In addition, SNR for an analyte concentration of 5 nM was increased to 124 with the front-injection method, compared to 2.9 for plug injection (see Table 2.1). As is pertinent to development of the assay, FST expression levels are relevant to polycystic ovary syndrome (PCOS, related to infertility) with the role of FST in PCOS not completely understood.[28] Using conventional assays, FST has been determined to be in the range of several hundred ng/ml in the female follicular fluid.[29] While our present assay yields analytical sensitivity on par with FST measurement in the follicular fluid, enhanced sensitivity may be realized using enzyme based chemiluminescence, which yielded zmol level limits of detection in our previous PLE studies.[22] As with all assays, optimization of conditions is needed for the specific sample matrix (e.g., pH, ionic strength, protein and lipid concentrations, non-specific adsorption) and antigen target and antibody pair employed.[30]

Using fluorescence alone, the sensitivity increase with the front-injection method is attributed to the extended, continuous replenishment of the analyte to the capture antibody. In comparison to the plug injection approach, the front-injection approach yields an increased signal until the point of equilibrium where a balance between electromigration and reaction is established (See Figure A). With the plug injection approach, the reaction time (duration that the antibody is exposed to analyte) is limited by the length of the plug as given by $t = (l_1 + l_2)/U_c$, where l_1 is the band width of the pseudo-immobilized antibody (~400 μm), l_2 is the band width of the analyte plug (~300 μm), and U_c is the average velocity of the analyte plug at the position of the antibody. The estimated reaction time for the plug injection method is ~14 s. After migrating analyte band sweeps past the immobilized capture antibody site, the concentration of the free analyte at the binding site drops to 0 (neglect analyte dissociation) and no more analyte is available to the capture antibody. In addition to enhanced sensitivity, the front-injection method is compatible with the single microchannel (2 terminal reservoirs) architecture. An assay conducted in a single, straight microchannel lends towards facile multiplexed systems design and may advance experimental design strategies relevant to systems biology based inquiry.

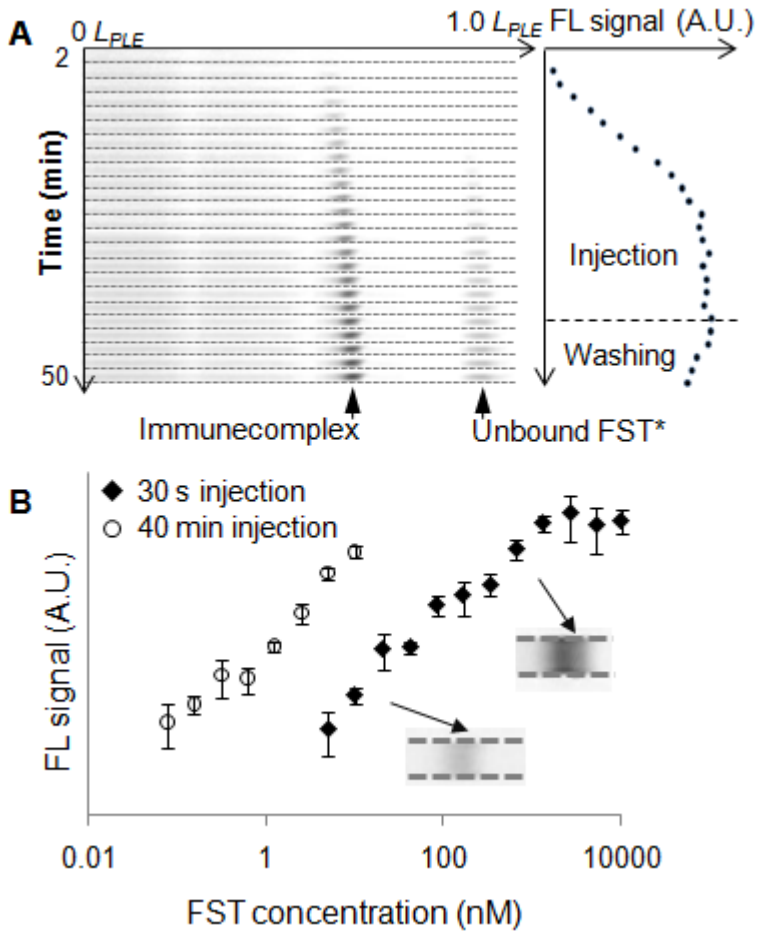

Figure 2.5. Sensitivity of PLE-IA was improved with the front-injection method. (A) Continuous formation of complex at the capture antibody region is observed when the target protein (FST*, 5 nM) is injected continuously for 40 min (96 V/cm). The fluorescence intensity of the complex is shown on the right. (B) Dose-response of PLE-IA operated under plug injection (30 s) and front-injection method (40 min).

Figure taken directly from Analytical chemistry, 83(17), 6573-6579.

2. 4 Conclusions

We introduce an integrated multi-stage assay reporting both protein identity and size information. The PLE-IA assay was performed in a single straight microfluidic channel housing a gradient PA gel. A heterogeneous immunoassay employing a pseudo-immobilized antibody at the head of a pore-size gradient PA gel allows identification as well as quantification of the target protein. Subsequent PLE-based separation of unbound species yields information on protein size upon comparison with PLE (no capture antibody) of the same species. Initial characterization of the heterogeneous immunoassay indicates that PLE-IA is a highly specific method. By using a "front-injection" method a detection limit of 78 pM was achieved. These results suggest that PLE-IA is well suited to automated detection of diluted heterogeneous samples. The PLE-IA is also a user friendly platform since the capture antibody can be patterned by the end user using very simple electrophoresis steps. The seamless microfluidic integration of multiple steps (immunoassay and separation) yields a streamlined work flow with potential for "hands free" and multiplexed operation.

Table 2.1: Increased sensitivity with continuous sample injection

Time of injection	30 s	15 min	40 min
Limit of detection	5 nM	0.2 nM	0.078 nM
SNR at 5 nM	2.87	36.42	123.76

Chapter 3: Kinetic Pore Limiting Electrophoresis Immunoassay (KPLE-IA): Binding Kinetics & Quantitativ Capacity performed in a single-microchannel, multi-step assay that reports protein size and immunoaffinity

Based on published masters report in mechanical engineering from University of California Berkeley, Berkeley, May 2011.

3. 0 Abstract

Kinetic pore limit electrophoresis (PLE) with a heterogeneous immunoassay in a single microchannel (KPLE-IA) is reported here as method to measure association and dissociation rates (k_{on} and k_{off}) directly without the use of invasive chemicals for surface immobilization or complex mathematical manipulations to extract rate information. The KPLE-IA assay was applied in a study of follistatin, a 31.5 kDa glycoprotein regulating mammalian cell proliferation and differentiation. In this multistep assay, target species were electrophoretically introduced into an antibody-patterned PLE channel via an "injectorless method". Species having an affinity for the pseudo-immobilized antibody were detected via heterogeneous immunoassay and accumulated at the antibody location. A subsequent buffer wash was then introduced in order to stop further association and a decay of complex was observed. The k_{on} and k_{off} for FST using KPLE-IA were found to be 4.44E+05$M^{-1}s^{-1}$, and .0083$s^{-1.}$ In order to optimize operational parameters of this assay and maximize the analytical sensitivity, the interplay between reaction, diffusion, and convection were modeled. KPLE-IA was found to operate in the mass transfer limited regime by studying the time to reach equilibrium under different electric fields. Equilibrium time decreased from 27 minutes to 22 minutes under higher electric fields ranging from 50-150V/cm.

3. 1 Introduction

Quantitative measurements of noncovalent interactions are important for understanding protein-protein interactions for cellular signaling, therapeutic antibodies, drug interactions, and biomarkers for disease diagnostics [31-34]. The binding kinetic association and dissociation rate constants, k_{on} and $k_{off,}$ are parameters that provide a more complete characterization of immunocomplexes formation and dissociation. There are a number of conventional techniques that exist that can measure binding kinetics including surface plasmon resonance (SPR) and backscattering interferometer (BSI). SPR spectroscopy, the most widely used binding kinetics technique, facilitates real-time detection of antigen binding to surface-immobilized antibodies by detecting refractive index changes at the binding surface using a gold substrate. Since refractive index changes are proportional to the mass bound to the sensor surface, SPR measurements are poorly suited to the detection of low molecular mass molecules (<200 Da) and is not optimal for extremely fast reaction rate measurements due to diffusion limitations [34]. In addition, SPR is used only for direct measurements of k_{off} and the equilibrium dissociation constant (K_d), which describes the dynamic equilibrium between binding and unbinding events and requires the study over a vast array of concentrations**.** Backscattering interferometry (BSI) is an alternative technique capable of measuring binding, however, as a solution-phase method, BSI does not enable direct measurement of dissociation kinetics [34]. In addition, both SPR and BSI are surface based sensors that require immobilization of one of the binding partners onto the sensor surface using various binding agents such as a carboxylated dextran matrix which may cause conformational change and can interfere with accurate kinetic parameter measurements.

In more recent studies, the use of a microfluidic fluorescence bead assay was developed for measuring antibody-antigen binding kinetics using time-course fluorescence microscopy of antibody-conjugated beads immobilized in microfluidic traps. k_{on} and k_{off} rates of low-abundance samples were measured by subsequent series of wash cycles with fluorescently labeled antigen and buffer [34]. In another study, the use of plug-plug kinetic capillary electrophoresis (ppKCE)

was implemented, where the use of short plugs of antigen (A) and antibody (B) were injected into a capillary. The sample with the lower mobility (B) was injected first and electrophoresis was then used to migrate the faster component (A) past (B) forming immunocomplex (C). With time, the complex was subsequently separated based on difference in mobility and k_{on} and k_{off} was calculated from a single ppKCE electropherogram using the area of the peak, smears, and migration time scales [33]. In another study, in a similar approach an equilibrium mixture (EM) of L and T was separated in a capillary reactor filled with T. An electric field was then applied and the difference in mobility of the reactants and their interactions with the reactor lead to a change in the EM peak position and shape [32]. The association and dissociation rates were extracted from the electropherogram using advanced mathematical manipulation from the change in peak shape (smear) with time**.** Unlike SPR and BSI, the microfluidic fluorescence bead assay allows for direct measurements of k_{on} and k_{off} however, it requires one immobilization of the antibody to the bead surface which can interfere with accurate measurements of reaction rates. Although kinetic capillary electrophoresis methods do not require species to be immobilized on the surface, their measurements of k_{on} and k_{off} can only be made after extracting the rates from their electropherograms using complex mathematical manipulations and several iterations.

In addition to measuring on and off rates of protein-protein interactions, robust analytical measurements linking protein identity to function is a persistent challenge in the field of proteomics. High throughput protein analyses that can yield information on multiple physicochemical properties are greatly needed for clinical diagnostics and fundamental life science investigations. Immunoaffinity methods coupled with electrophoreses can be used for immuno-identity of proteins in addition to protein sizing. Chip based polyacrylamide gel (PA) electrophoresis integrated with immunoassay provide a promising platform for integrated protein analysis in conjunction with electrokinetic fluid manipulation, rapid electrophoretic separation and the potential for multiplexing. While uniform PA gel has been demonstrated for protein sizing and immunoassay[35], the fabrication of a stacking gel (which has a smaller pore-size than the loading gel) resulted in sharpen bands, shorter required separation distance and higher separation resolution of homogenous immnoassays [36]. However, these methods do not obtain size information under native conditions and required the use of surfactants such as sodium dodecyl sulfate (SDS) to create a uniform charge to mass ratio across most protein species. Surfactants such as SDS can interfere with immunoassay performance as the 3D protein structure is destroyed, disrupting protein binding with antibody. Thus an electrophoretic technique that can obtain size information under native conditions is ideal for integration with immunoassays.

Pore limit electrophoresis (PLE) was introduced in the 1960's as a separation technique whereby a mixture of proteins was separated in slab gel with a decreasing gradient in pore-size. The polyacrylamide pore-size gradient extends to pore-sizes much smaller than those typically used in slab-gel electrophoresis [21]. In PLE, protein mobility is reduced with decreasing pore-size until electromigration reaches a near stop where the pore-size is smaller than the effective dimension of the analyte. PLE typically yields a logarithmic relationship between migration distance and protein size, which is useful in determining analyte molecular weight. In addition to protein sizing information, PLE has been developed as a multri-stage immunoassay (PLE-IA) that integrates a quantitative pseudo-heterogeneous immunoassay and protein sizing into a single microchannel without the use of surfactants such as SDS [30].

In this study, PLE-IA is reported here as method to obtain kinetic information (KPLE-IA) through the measurement of association and dissociation rates (k_{on} and k_{off}) in addition to identifying proteins and protein sizing. To maximize the analytical sensitivity and inform

optimization of PLE-IA operation, study was undertaken to identify transport regimes relevant to the IA portion of PLE-IA.

3. 2 Materials and Methods

Reagents

The UV photoinitiator 2,2-azobis[2-methyl-N-(2-hydroxyethyl) propionamide] (VA-086) was purchased from Wako Chemicals (Richmond, VA). 3-(Trimethoxysilyl)-propyl methacrylate (98%), glacial acetic acid (ACS grade), methanol (ACS grade), 2-hydroxyethyl cellulose (HEC), acrylamide, bis-acrylamide were all purchased from Sigma. Premixed 10x Tris/glycine native electrophoresis buffer (25 mM Tris, 192 mM glycine in 1x buffer, pH 8.3) was purchased from Bio-Rad (Hercules, CA). Alexa Fluor 488 labeled trypsin inhibitor (TI) , bovine serum albumin (BSA), and ovalbumin (OVA) were purchased from Invitrogen (Carlsbad, CA). Recombinant human FST protein, and mouse monoclonal antibody to FST were all purchased from Abcam (Cambridge, MA). All proteins and antibodies were fluorescently labeled in-house using Alexa Fluor 488 and 568 labeling kits from Invitrogen per the supplier's instruction and purified by P-6 and P-30 Bio-Gel columns (Bio-Rad, Hercules, CA). Labeled proteins and antibodies were stored at 4 °C in the dark until use.

Chip Preparation

Glass chips with straight channels were fabricated by Caliper Life Sciences (Hopkinton, MA) using standard wet etching, drilling, and thermal bonding techniques. Bare channels were first incubated with 1 M NaOH for 10 min followed by flushing with DI water, and then dried by vacuum. In order to prepare the channel for covalent attachment of the polyacrylamide gel, the channels were incubated with a degassed 2:3:5 mixture of 3-(trimethoxysilyl)-proply methacrylate, glacial acetic acid and DI water for 30 min. After incubation, the channels were rinsed with methanol and DI water and purged with vacuum.

Fabrication of the Pore-Size Gradient Gel

A gradient gel was fabricated in the straight channel through a two-step photopolymerization process. First, degassed 30% T (the concentration of total acrylamide, w/v), 8% C (ratio of bis-acrylamide and bis-acrylamide + acrylamide, w/w) acrylamide/bis-acrylamide solution was introduced into the surface modified channel by capillary flow. Then high viscosity 5% 2-hydroxyethyl cellulose (HEC, Sigma, average MW ~720,000) solution was added to terminal wells to stop hydrodynamic flow. To establish the small-pore-size end of the gradient gel, a 600 μm membrane (30% T, 8% C) was fabricated near one end of the channel via a UV objective microscope system (Diaphot, Nikon). A mask with a 600 μm x 500 μm window was aligned to the chip using a manual adjust x-y translation stage. UV illumination in the 330-375 nm range was provided by a mercury bulb. Polymerization of the membrane was achieved with a 3 min exposure to UV light (~8 mW/cm^2). After polymerization of the membrane, the HEC solution was removed from the terminal wells. A degassed 3% T, 3.3% C precursor solution was then added to a 200 μl pipette tip press-fit into the well at the channel terminus furthest from to the membrane. In the well proximal to the membrane, 30% T, 8% C precursor solution was added to prevent dry out of the gel. The chip was equilibrated for 18 hours to establish a diffusion-

generated 3% T to 30% T gradient along the channel length. The whole channel was then flood exposed under ~10 mW/cm^2 UV intensity for 8 min using an air cooled mercury lamp (B-100AP lamp, UVP, Upland, CA). The polymerized chip was stored in 1 x Tris/glycine buffer at 4°C until use. After use, chips were regenerated for further use by soaking the glass chips in a 2:1 solution of perchloric acid and hydrogen peroxide overnight at 60°C, thus dissolving the PA gel interiors and leaving the glass intact.

Apparatus and Imaging

Twenty micro liters of 1 x tris/glycine or protein samples diluted in tris/glycine were added to the pipette tips press-fit into the via wells of each channel. Voltage was applied using a custom 8-channel programmable high voltage power supply (current/voltage feedback control with a dynamic range of ~4000 V and +/- 0.01 μA current and ~1 V voltage resolution). Fluorescence images were collected using an inverted epi-fluorescence microscope (IX-50, Olympus, Melville, NY) equipped with a 1392 x 1040 Peltier-cooled interline CCD camera (CoolSNAP HQ2, Roper Scientific, Trenton, NJ), filter cubes and an automated x-y translation stage (S2000, Applied Scientific Instrument, Eugene, OR). MetaMorph software Version 7.1 (Molecular Devices) was used for all data acquisition. The CCD exposure time was 100 ms. Fluorescence images of the whole channel were collected at 1 min intervals during KPLE-IA. Sets of 400 μm x 60 μm region of interest (ROI) from overlapping images were digitally stitched together to form fluorescence images along the entire separation axis. Background subtraction was performed using identical ROI lying out of the channel. Image analysis was conducted using ImageJ software (NIH, Bethesda, MD).

Antibody Immobilization

Antibody labeled with Alexa Fluor 568 was first diluted from a stock solution to a set concentration of 500 nM . The labeled antibody solution was then added to the sample reservoir in the low %T side (3%T loading gradient) and was injected for 3 min at 100V/cm. After a 3 min loading, the antibody solution was replaced with native buffer followed by 10 minute electrophoretic migration of the antibody to its pore limit location (E=100V/cm) Figure 3.1 Step 1.

Quantitation capacity of PLE-IA Pseudo-Homogenous Immuno –assay

After the antibody immobilization, sample solution containing the protein of interest was placed in the sample reservoir. Proteins were injected into the microchannel through an “injectorless” method. This method is where the protein sample is injected continuously for an extended duration (40 min, 100 V/cm), where proteins that have an affinity to the antibody accumulated at the antibody location and complex formation increases with time. Followed by the continuous injection, a 20 min washing with plain buffer is used to separate the unbound species from the immune complex. In essence, the injectorless method yields electromigration of a protein concentration front (not plug) into the PLE-IA channel. In addition to the injectorless method, an injection method using 30s injection can be used. With the injection method proteins with an affinity to the antibody form a complex and subsequent unbound proteins electromigrate to their pore limit Figure 3.1 step 2.

PLE-IA for immuneidentity and sizing

PLE-IA is an assay that reports both protein identity (via immunoassay) and protein size (via PLE), as illustrated in Figure 3.1 and 3.2. The multi-step assay is conducted in simple single straight channel using a large to small pore size gradient. The work conducted in regards to PLE-IA performance is developed with the measurement of the protein FST, a 31.5 kDa autocrine glycoprotein expressed in almost all tissues of mammals and used in studies for its role in regulation of muscle growth in mice [37].

PLE-IA Principle and Characterization

PLE-IA uses a decreasing pore-size gradient PA gel; here housed in a glass microfluidic channel. To achieve the two-step assay, PLE-IA requires a region of patterned capture antibody (Figure 3.1, Step 1). The pseudo-immobilized capture antibody band yields functionality similar to that provided a heterogeneous immunoassay without the use of chemical functionalization. Thus, as species electromigrate through the capture antibody region and along the PLE gradient, proteins with an affinity to the capture antibody form immune-complexes (figure 3.1, Step 2). PLE-IA can yield information of two physicochemical properties including protein identity via the formation of antibody-antigen complex and protein sizing via the protein immobilization at its pore-limit location (figrure 3). Thus, the PLE-IA is designed for species exhibiting the same charge polarity as the antibody determined by the run buffer pH relative to analyte isoelecric point and a molecular weight smaller than the capture antibody.

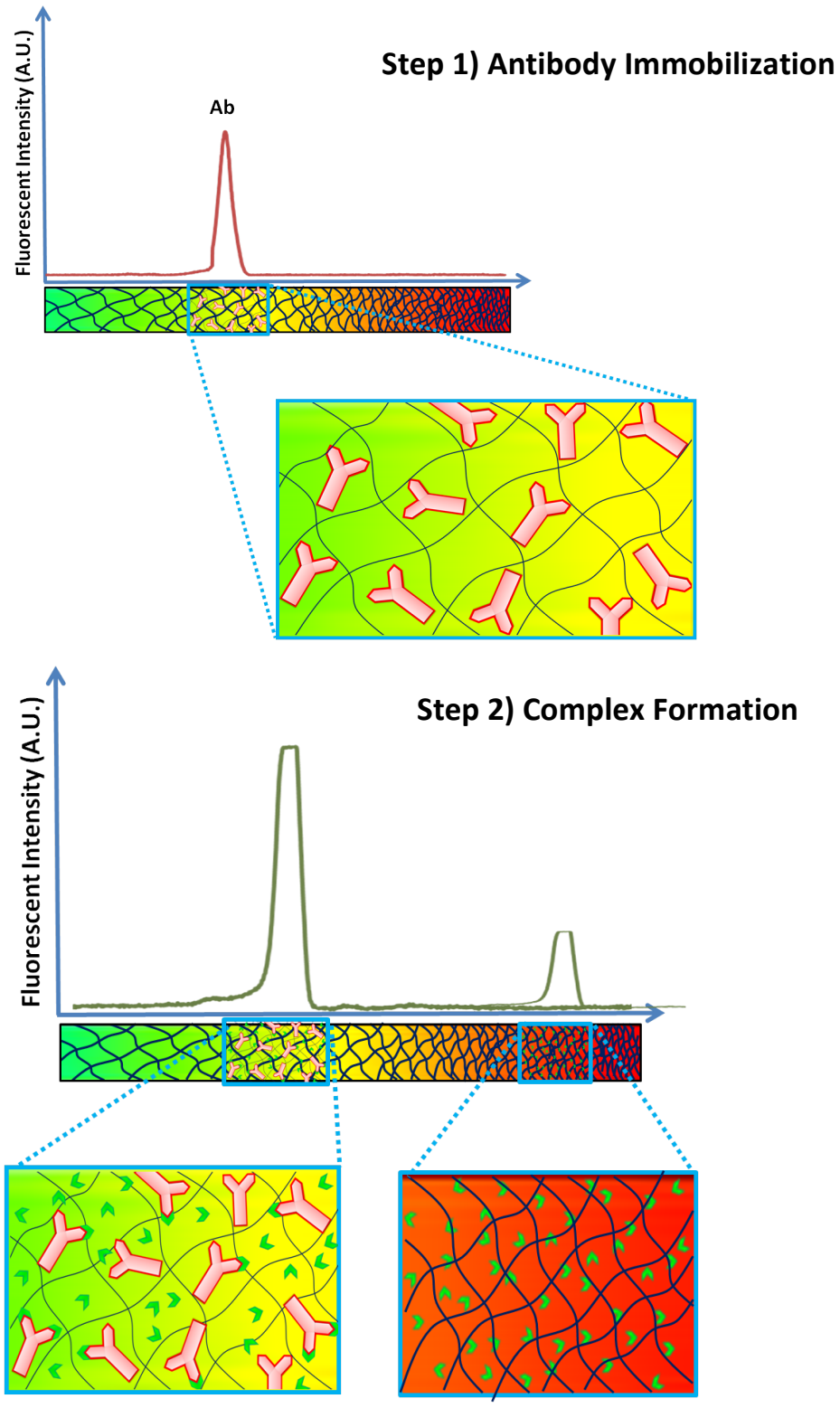

Figure 3.1 PLE-IA Principle and Characterization **Step 1**: Electrophoretic pseudo-immobilization of capture antibody. **Step 2**: Protein sample electromigrates through the capture

antibody region resulting in formation of an immune-complex and, in some operating conditions, an unbound protein band.

To demonstrate the principle of PLE-IA for FST*, the PA gel pore-size gradient was fabricated (see Materials and Methods section) and patterned with capture antibody using a 3 min electrophoretic loading interval (500 nM capture antibody solution, 100 V/cm) followed by a 10 min (E = 100 V/cm) compaction interval used to transfer the antibody band to its pore limit. To initiate the PLE-IA (figure 3.1, Step 2), a plug of fluorescently labeled FST was electrophoresed into the PLE-IA channel for 30 s (100 V/cm) and unbound protein can be observed at its pore limit.

PLE reports a logarithmic dependence between protein molecular weight and migration distance thus allowing determination of the molecular weight of target proteins, as has been reported on both the macro (i.e., slab gel) [21] and micro (i.e., microfluidic chip) scale.[23] In figure 3.2 a molecular weight ladder of proteins consisting of BSA (66kDa), OVA (45kDa) and TI (21.5kDa) (200 nM) were injected for 30 s followed by a 10 min (E = 100 V/cm) compaction interval and a time lapse image of the migration of proteins is shown. In figure 3.2, the electropherogram of the protein ladder is presented. A schematic illustrating the linear gradient of polyacrylamide monomer %T in shown and going from left to right in the figure 3.2, the pore size decreases from large pore size (low %T) to small pore size (high%T). Within the channel, the proteins are pseudo-immobilized at their respective pore limit due to size exclusion. Figure 3.2 C plots the log linear molecular weight relationship to migration distance that can be used for subsequent protein sizing [23]. In Figure 3.2 C has a log linear dependence of molecular weight and distance can be described with the following equation, $y = -0.0224x + 166.54$, $R^2 = 0.99$. The molecular weight and identity of FST* can then be ascertained from a log linear dependence found by obtaining the location of the unbound free FST*. The size of FST* was estimated to be 30.6 ± 3 kDa (n=3) and the size of the FST-Ab* was estimated to be 144 ± 4.6 kDa (n=3).

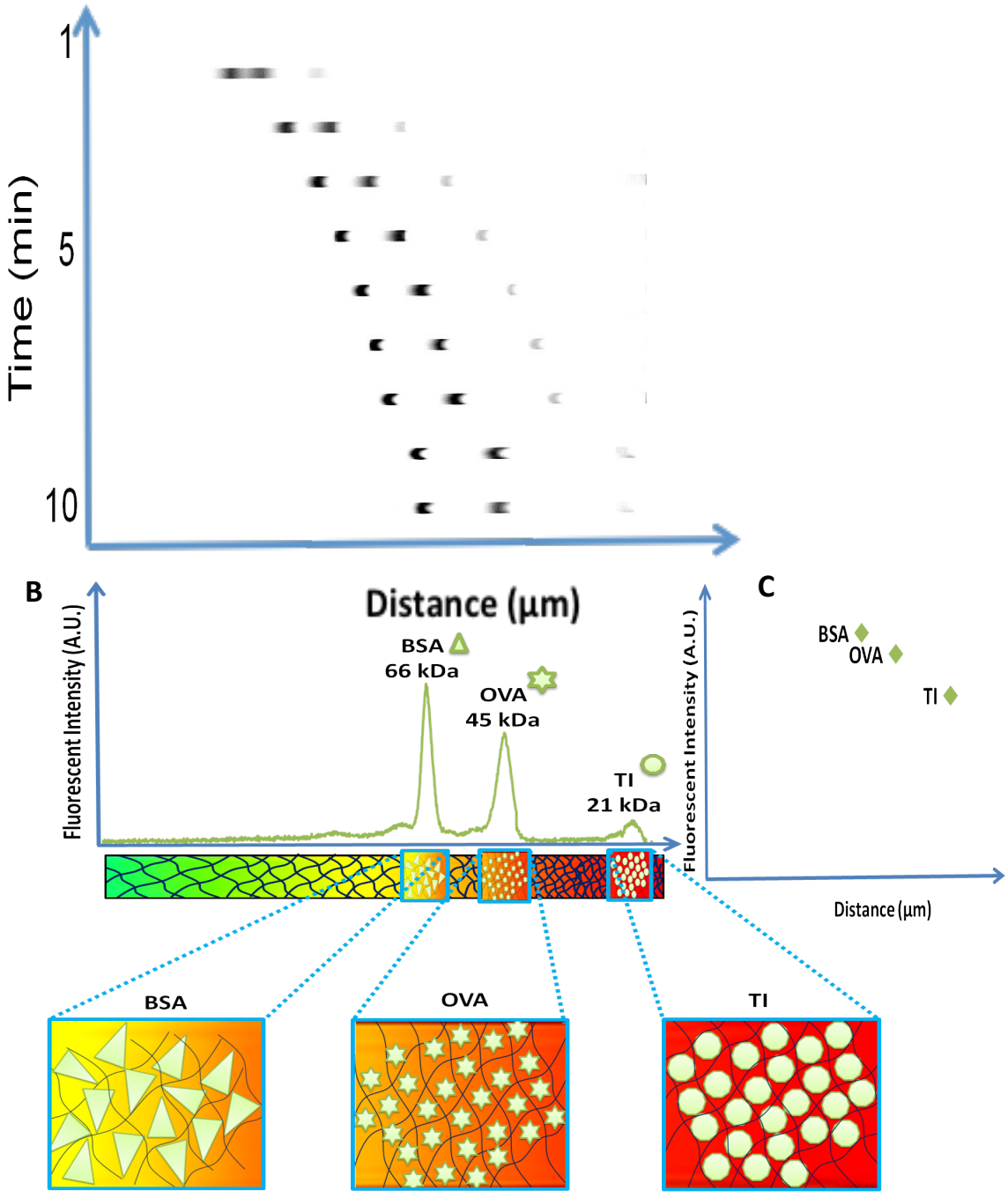

Figure 3.2 PLE- Protein Sizing Characterization **A)** A time lapse montage of the migration of fluorescently labeled proteins consisting of BSA (66kDa), OVA (45kDa), and TI (21.5kDa) is shown. **B)** Shows the respective electropherogream of the **A)** in addition to a to schematic representing the linear gradient of polyacrylamide monomer %T in the channel going from large pore size (low %T) to small pore size (high%T) (from left to right). Within the channel, the proteins (BSA, OVA and TI) are pseudo-immobilized at their respective pore limit due to

3. 3 Kinetic PLE-IA

Binding kinetic theory

Kinetic rate constants provide invaluable quantitative information about how fast a reaction takes place or how slow dissociation occurs in regards to the concentration of the biomolecules involved in the reaction. Kinetic studies have the potential to provide deep insight onto the mechanisms of the reaction itself as well as temporal regulation processes. Consider the expression below, where Ab represents an antibody and Ag* is the antigen as seen in equation 1. The top arrow of equation 1 represents the forward reaction rate, also known as k_{on} and the bottom arrow indicates the reverse reaction rate, k_{off}. The rate of the reaction is defined as the change in concentration of the reactants (Ab+Ag*) and products (Ab•Ag*) over time (equation 13). Product accumulation as equilibrium is approached (where equilibrium is defined as no net change in reactant or product where $k_{on} = k_{off}$) must take into account both forward and reverse rates, however, when $k_{on} >> k_{off}$, the product is far greater than the reactants, the rate of product decay is negligible and can be assumed as just k_{on}. This can also be assumed for the rate of product decay, where the rate of product decay = k_{off}. To determine k_{on} and k_{off}, the fraction of product formed and decayed over time is required (equations 3 and 4). Figure 3.3 A-B are theoretical plots of the exponential progression and decay of a product at a given time point, t, over the maximum or initial product. The reaction times for association and dissociation can then be extracted from these plots. In both cases the rate constant are equivalent to the inverse of the time point at which the reaction is 63% complete. This is because the rate constant k =1/t, e^{-kt}=0.37 [31]. k_{on} occurs at 63% of the product formed at equilibrium and k_{off} occurs at 37% from the initial concentration of the decay figure 3.3.

$$Ab + Ag* \underset{koff}{\overset{kon}{\rightleftharpoons}} Ab \bullet Ag* \quad \textbf{(1)}$$

$$\frac{\partial[Ab \cdot Ag*]}{\partial t} = k_1[Ab][Ag*] - k_{-1}[Ab \cdot Ag*] \quad \textbf{(2)}$$

$$\frac{[Ab \cdot Ag*]_t}{[Ab \cdot Ag*]_f} = 1 - e^{-k_1 t} \quad \textbf{(3)}$$

$$\frac{[Ab \cdot Ag*]_t}{[Ab \cdot Ag*]_i} = e^{-k_1 t} \quad \textbf{(4)}$$

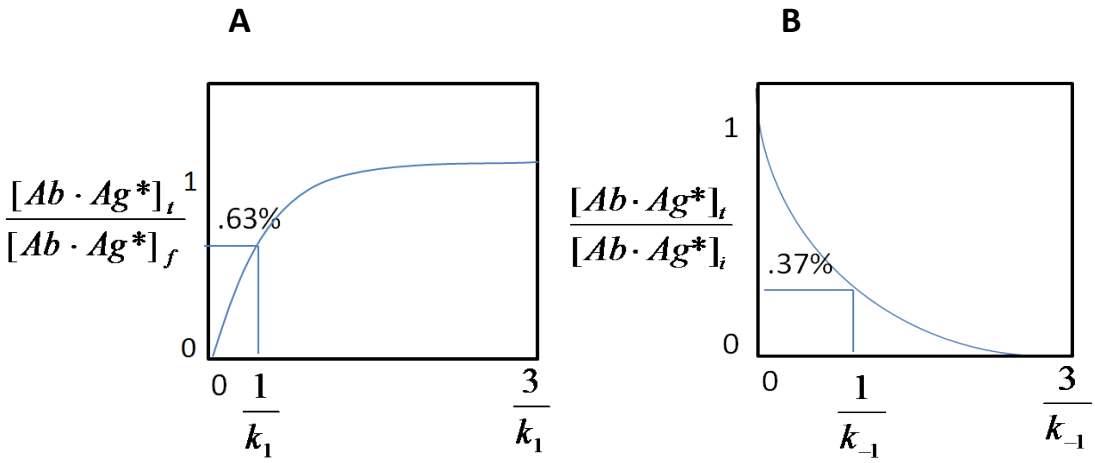

Figure 3.3 A and B Product accumulation and degradation with time and their respective on and off rates found at 63% and 37%

PLE-IA as a method of measuring k_{on} and k_{off} Rates

PLE-IA presented here is used as a method of reporting binding kinetic information KPLE-IA. The amount of product (complex) at a given time point can easily be acquired over the pseudo-immobilized antibody location with the injectorless method. In figure 3.4 A-B, the Complex (product) accumulation and decay with time can be observed using first an injectorless method approach for the accumulation (k_{on} measurement) and a subsequent buffer wash for the decay (k_{off} measurement). To determine k_{on} and k_{off} rates, a plug of FST* antibody was injected for 3 minutes at 100V/cm and was then replaced with clear run buffer for 10 min to push antibody to its pore limit. FST* antigen was then injected for 40 min followed by 20 min wash with plain buffer to separate the unbound species from the immune complex. The association of FST* accumulates with time until equilibrium is reached as seen figure 3.4 Awhere the change in fluorescent intensity remains constant at t=27±1min to (n=3) t=40min for an antibody concentration of 500nM and FST* concentration of 20nM (E=50V/cm) . The maximum florescent intensity for each time point versus time is plotted in figure 3.4 A. k_{on} can then be determined at 63% of the equilibrium time and was found to be 15±1.7 (n=9) min. The association rate, k_{on} can then be the calculated by multiplying the equilibrium time by the concentration at that time point. In order to extract the concentration at time t=15 min from the fluorescent intensity output collected, a dose response curve was generated in order to correlate fluorescent intensity output to concentration. In this study, the k_{on} for FST* was determined to be 4.44E+05$M^{-1}s^{-1}$. In order to obtain k_{off} a subsequent buffer wash was then administered to dilute the complex region and remove any further association. Dissociation can then be observed from the decay of fluorescent intensity at a given time point. The complex degradation with time is seen in figure 3.4B, where the complex decay with time can be observed upon a buffer wash from t=0 to t=10. The k_{off} for FST* was found to be 0.00833 s^{-1} (2 min) as seen in figure 3.4 C.

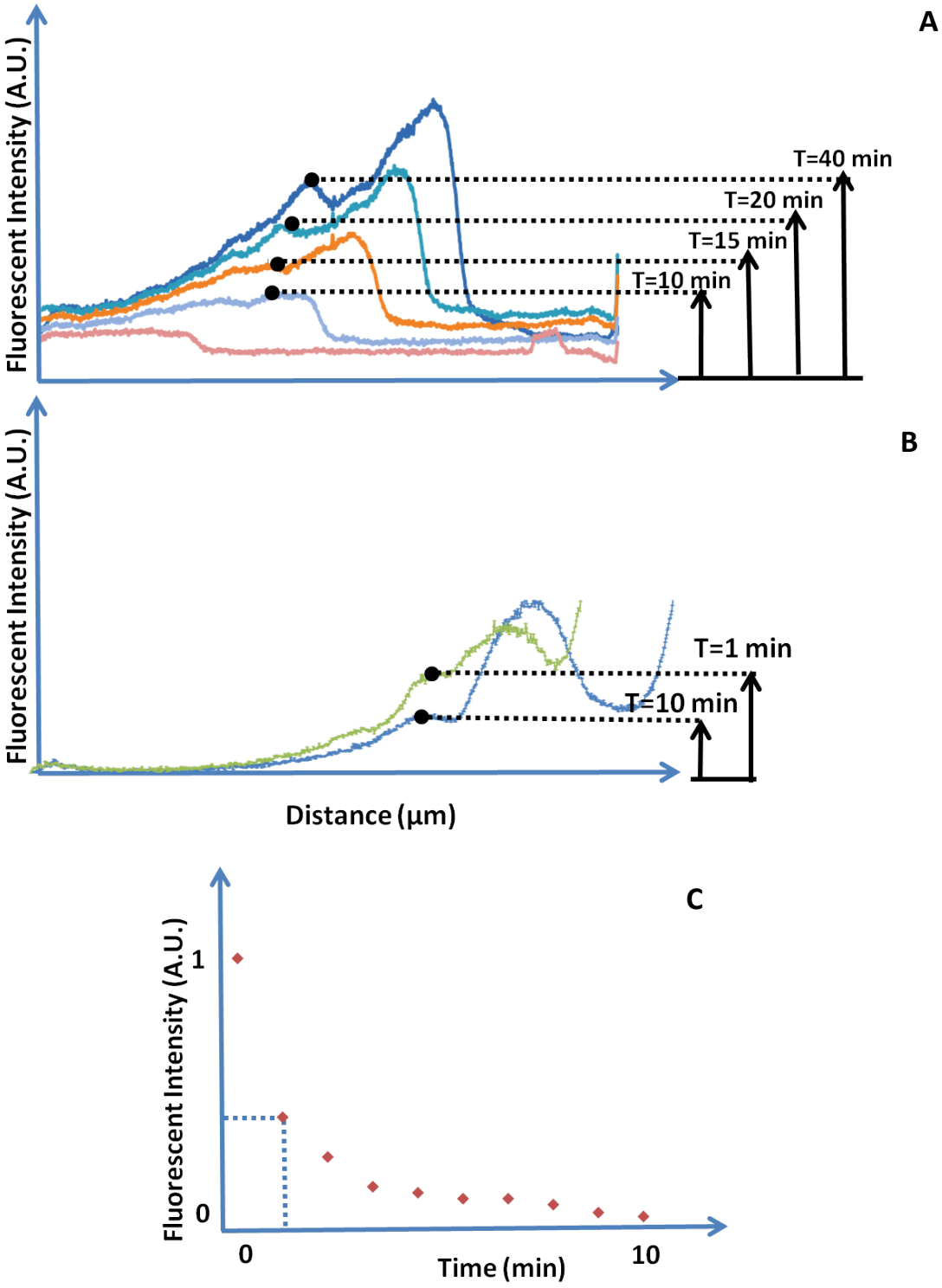

Figure 3.4 Complex Accumulation and Degradation with Time A) shows the complex increasing with time at the antibody location **B)** shows the complex decay with time with the buffer wash and **C)** shows that k_{off} occurs in 2 min.

3. 4 Mathematic model of Kinetic PLE-IA

Surface binding kinetics

To describe antibody and analyte reactions, we begin with first order Langmuir kinetics,

$$c + (b - C_c) \underset{k_{off}}{\overset{k_{on}}{\rightleftharpoons}} C_c \quad \textbf{(5)}$$

$$\frac{\partial C_c}{\partial t} = k_{on} c(b - C_c) - k_{off} C_c \quad \textbf{(6)}$$

Where C_c is the local concentration of the complex, t is time, c is the bulk concentration of the analyte, b is the initial concentration of antibody, and k_{on} and k_{off} are the association and dissociation rate constants.

Mass transport: Convection and diffusion

Diffusion and convection also play a role in how well complex is formed. Target molecules diffuse randomly within the solution. The diffusion of analytes can be described by ficks second law of diffusion, which predicts how diffusion causes the concentration field to change with time t, where D is the diffusion coefficient, and x is the position within the channel.

$$\frac{\partial C_c}{\partial t} = D \frac{\partial^2 C_c}{\partial x^2} \quad \textbf{(7)}$$

In addition to diffusion, the analytes move through a porous gel gradient via electrophoresis and experience a hindrance in convection due to the decrease in pore size from the gradient gel . The Ferguson relationship can be used to approximate electrophoretic mobility of a protein based on the gel's concentration parameters as seen in equation 8 and 9, where μ is the electrophoretic mobility, E is the applied electric filed, R is a retardation coefficient, G_0 and G_0 are the gel concentration of acrylamide (%T) at x=0 and x=L_{ab}, where L_{ab} is the length of the antibody plug [38].

$$u = \frac{dx}{dt} = E(x)\mu e^{-RG(x)} \quad \textbf{(8)}$$

$$G(x) = \frac{G_L - G_0}{L_{ab}} x + G_0 \quad \textbf{(9)}$$

Mass transport: Convection, diffusion and Reaction

The sensitivity of this assay in regards to complex concentration over time can be described by these three parameters put together (equations 6, 7, and 8) in one partial differential equation that describes the complex formation with time.

$$\frac{\partial C_c}{\partial t} = D \frac{\partial^2 C_c}{\partial x^2} - E(x)\mu e^{-RG(x)} \frac{\partial C_c}{\partial x} + k_{on} c(b - C_c) - k_{off} C_c \quad \textbf{(10)}$$

If we then define the following dimensionless parameters numbers where $\bar{X}$=x/L_{ab} where L_{ab} is the length of the antibody plug and and $\bar{C}$=C_c/c and $\bar{t}$=tu/L_{ab} we can then extract three non

dimensionless parameters that help us determine what regimes we are operating in order to optimize complex formation.

$$Pe = \frac{\mu E L_{ab}}{D} \textbf{(11)} \qquad Da_{off} = \frac{k_{off} L_{ab}}{\mu E} \textbf{(12)} \qquad Da_{on} = \frac{k_{on} L_{ab}}{\mu E}(b) \textbf{ (13)}$$

The Peclet (Pe) number is the ratio of convective and diffusive time scales. As the peclet number increases, convective mass transport due to electromigration becomes dominate and diffusion is considered negligible. The Damkohler numbers (Da) provides a comparison of reaction times scales and mass transport due to electectromigration. When Da<<1 the system is in the reaction limited regime where convective forces dominate and increase the binding of analytes to the pseudo-immobilized antibody faster than the reaction kinetics can. A Da >> 1 indicates that the reaction of interest occurs much faster than the rate of mass transfer [26].

The concentrations of the antibody and analyte dictate how much time is needed to reach equilibrium. If convection and diffusion bind analytes to the pseudo-immobilized antibody faster than the surface binding kinetics can, the system is reaction limited and the concentration of the antibody b can be assumed equal to the antigen at the region of the sensor where b=c. Equation 14 can be solved where the concentration of complex at any given time is

$$C(t) = \frac{cb}{c+K_D}\left[1 - e^{-(k_{on}c + k_{off})t}\right] \textbf{(14)}$$

where $K_D = k_{off}/k_{on}$. The time required for the reaction to reach equilibrium under reaction limited condition (where convection transports the analytes to the pseudo-immobilized antibody at a much higher rate than the reaction can take place) is $\tau = (k_{on}c + k_{off})^{-1}$. Equation 15 represents the time to reach equilibrium in the mass transport limited regime [39].

$$\tau = (k_{on}c + k_{off})^{-1} * Da_{on} \textbf{(15)}$$

3. 5 Results and discussion - Quantitation Capacity of PLE-IA

Comparison of Peclet and Damkohler:

To maximize the analytical sensitivity and inform optimization of the PLE-IA operation, study was undertaken to identify what transport regimes are relevant to the IA portion of PLE-IA. Comparison of electromigration to IA complex formation timescales were quantified through the Peclet number and Damkohler number. In this system, the length of the antibody plug is $L_{ab} = 500\mu M$, the electrophoretic mobility is $\mu = 8.3\text{E-}6\ \text{cm/Vs}$, the operating voltage E=100 V, and the antibody concentration is $b = 500nM$.

Table **3.** shows the theoretical values of the Peclet and Damkohler numbers for this system calculated from various antibody-antigen pairs with their respective association and dissociation rates (k_{on} and k_{off}) [34,40]. For this system the theoretical Peclet number ranged from 40-400, where convective mass transport due to electromigration is dominant and diffusion can be considered negligible. The Damkohler number ranges from 1.5 to 173, and is in the mass transport limited regime, where the reaction happens much faster than analytes transport. The k_{on} and k_{off} rates found in literature range from 2.00E+06 to 5.00E+04 [$M^{-1}s^{-1}$] and 10-3 min (generated via various methods including SPR and single bead assay) [34,40]. The on and off rates found for FST* using KPLE-IA are comparable to the antibody antigen pairs reported in literature (4.44E+05$M^{-1}s^{-1,}$ and 2 min).

Constants	Ovarian Cancer CA125	LGB-1 mAb/EGFP	HyHEL-5 mAb/HEL - Dylight488	D1.3 mAb/HEL Dylight633	D1.3 mAb/HEL Dylight488
Diffusivity (m^2/s)	1E-10	1.00E-10	1.00E-11	1.00E-11	1.00E-10
k_{on} **($M^{-1}s^{-1}$)**	2.00E+06	5.00E+04	5.75E+06	1.27E+06	1.87E+06
k_{off} **(s^{-1})**	2.00E-03	5.00E-03	5.15E-03	1.69E-03	2.00E-03
Kd (nM)	1	100	0.90	1.3	1.1
k_{off} **(mins)**	8	3	3	10	8
Pe	42	41.7	417	417	41.7
Da_{on}	60	1.5	173	38.1	56.1
T_{eq} (mins) reaction limited	0.397	3333	0.1	0.615	0.4
T_{eq} (mins) mass transport limited	24	5000	24	23	24

Table 3.1 Comparison of Peclet and Damkohler numbers for this system calculated from various antibody-antigen pairs with their respective diffusivities, association, and dissociation rates [34,40].

For this system, it was experimentally determined that the maximum operating voltage that can be used before gel degradation was 150V/cm where the Da>>1. Based on figure 3.5, all antibody- antigen pairs below 150V/cm have a Da>>1 and indicates that the reaction of interest occurs much faster than the rate of mass transfer and this system is in the mass transfer limited regime [26].

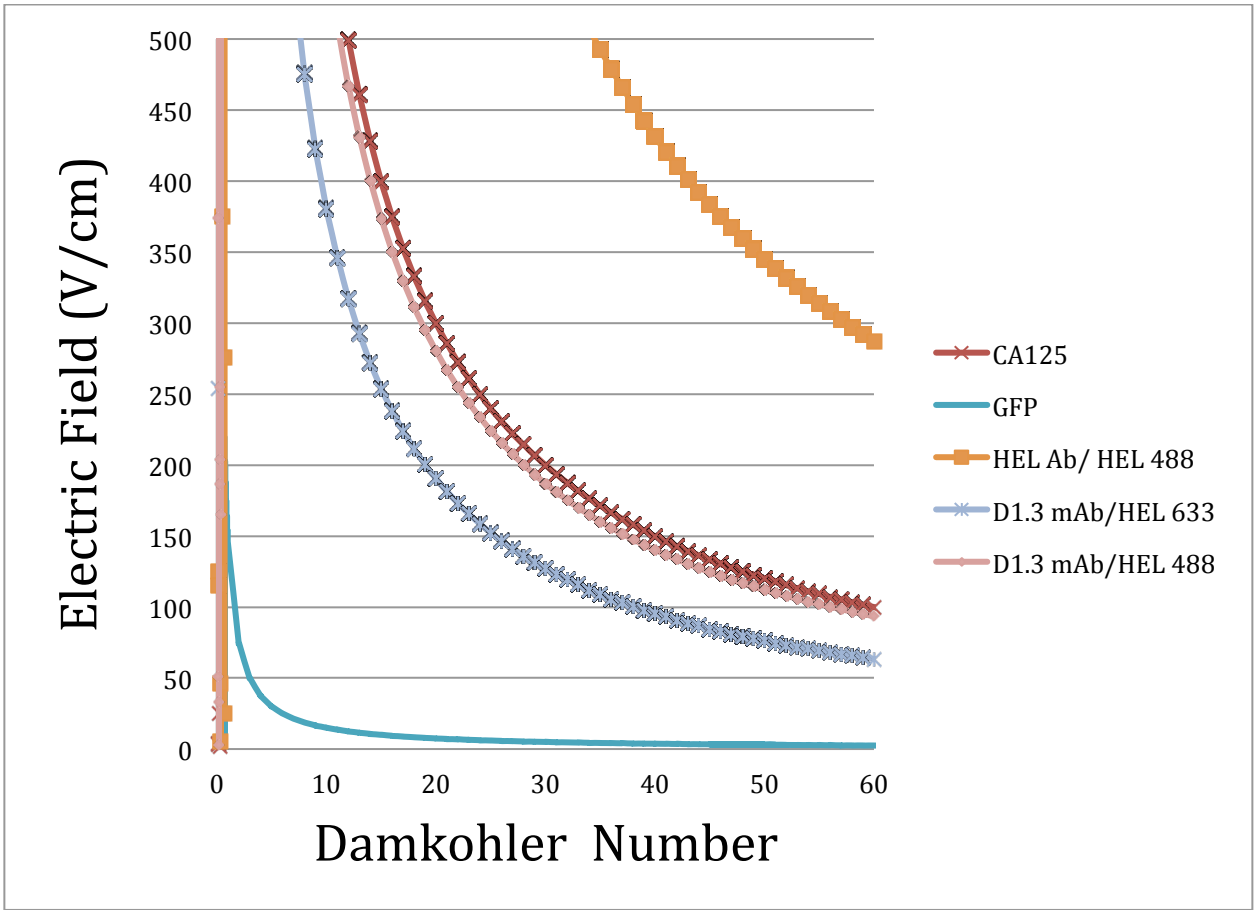

Figure 3.5 Comparison of various antibody-antigen pairs taken from literature and their respective Damkohler number in relation to operating voltage for this system. The antibody-antigen pairs below 150V/cm have a Da>>1 which indicates that the reaction of interest occurs much faster than the rate of mass transfer.

PLE-IA Transport Regimes

In order to experimentally validate if our system was in the mass transport limited regime or reaction limited regime, study was taken to look at the equilibrium times at different electromigration speeds. The time to reach equilibrium in the mass transport limited case is inversely proportional to concentrations of antigen, the on and off rates of the reaction, and electric field strength. To study this, the electric fields were varied from 50V/cm to 150V/cm and the time to reach equilibrium was observed. Similar to the on and off rate studies presented earlier, a plug of FST* antibody was injected for 3 minutes and compacted with clear run buffer for 10 min. Following antibody immobilization, FST* antigen was injected for 40 min followed by 20 min wash with plain buffer to separate the unbound species from the immune complex. The complex formation increases with time at the antibody location as seen in Figure 3.6 A. As the front moves in over a duration of 40 min, the antibody also continues to migrate over the channel with time and shifts 0.7 mm after 40 min as seen in Figure 3.6 B, hence the term pseudo-immobilized. Consequently, the complex also shifts with time as the antibody migrates through the channel at a rate of 17μm per minute. Assuming a fixed capture antibody concentration b and protein target concentration c , PLE-IA operation at higher electric fields require shorter time to reach equilibrium according to the theory from equation 15. To confirm this we looked at the time needed to reach equilibrium for a set antibody and protein concentrations ([Ab] = 500nM, [FST*] = 20 nM). By varying the electric fields from 50V/cm - 150V/cm and accounting for the offset time necessary for the analyte to reach the antibody location, the respective equilibrium times for the 50, 100, and 150 V/cm decrease with increasing voltage to 27±1, 24.3±0.58, and 22.7±1.53 (n=3) minutes as seen in Figure 3.7 A-C. Thus, PLE-IA operation as presented here can be classified as a mass transfer limited system where the reaction occurs at a much faster rate than electromigration.

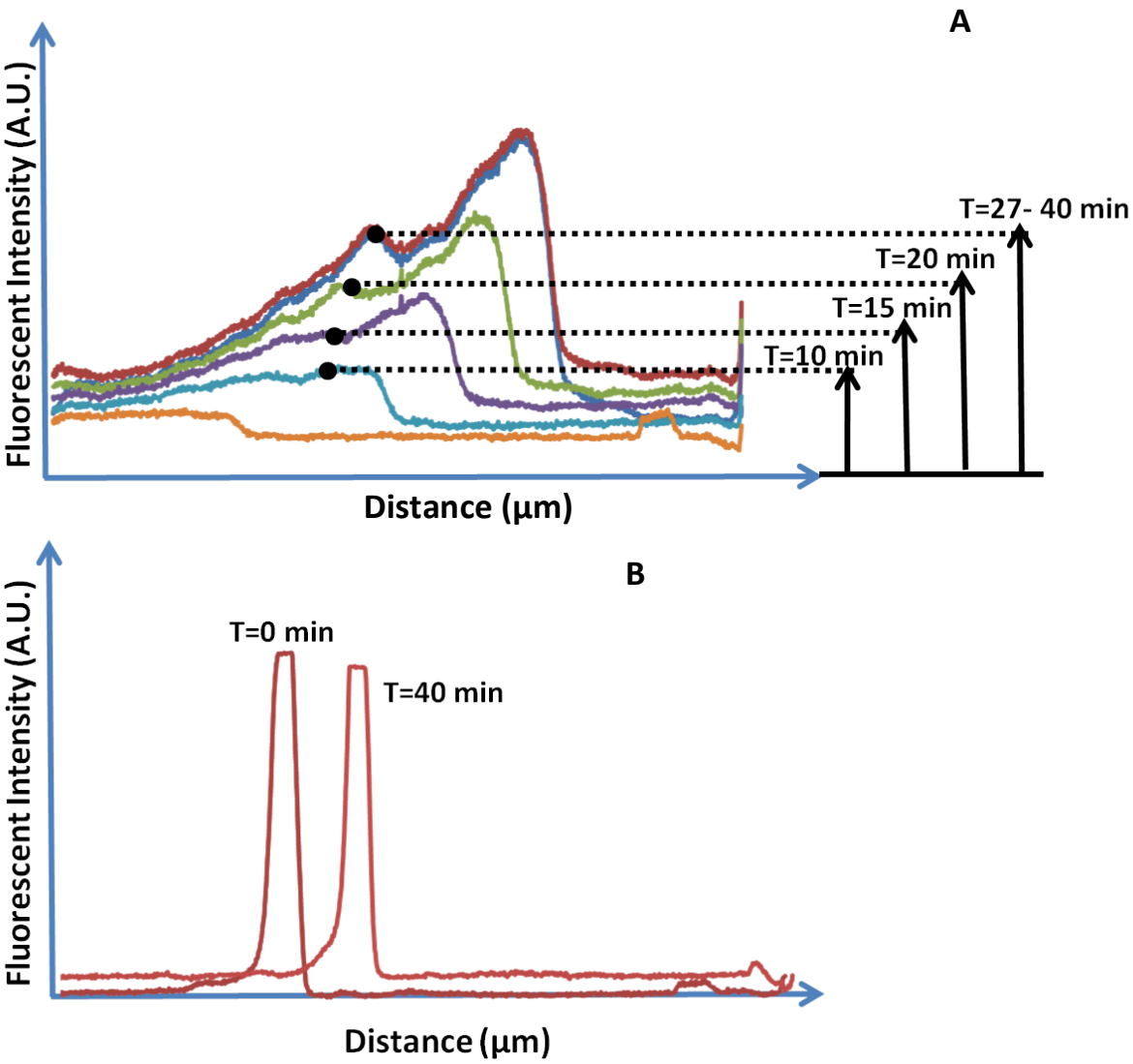

Figure 3.6 A) shows the fluorescent output versus distance of the complex formation as time increases from T=0 to T=40 min. From T=27 to T=40 min there is no difference in fluorescent intensity which signifies that the complex has reached equilibrium**. B)** Shows the antibody location at T=0 and after the 40 min wash at T=40. As the antigen in electrophoresed in channel over duration of 40 mins the antibody continues to migrate over the channel with time and shifts 0.7 mm at a rate of 17µm per minute and hence the complex shifts. The operating voltage used in this study was 50V/cm.

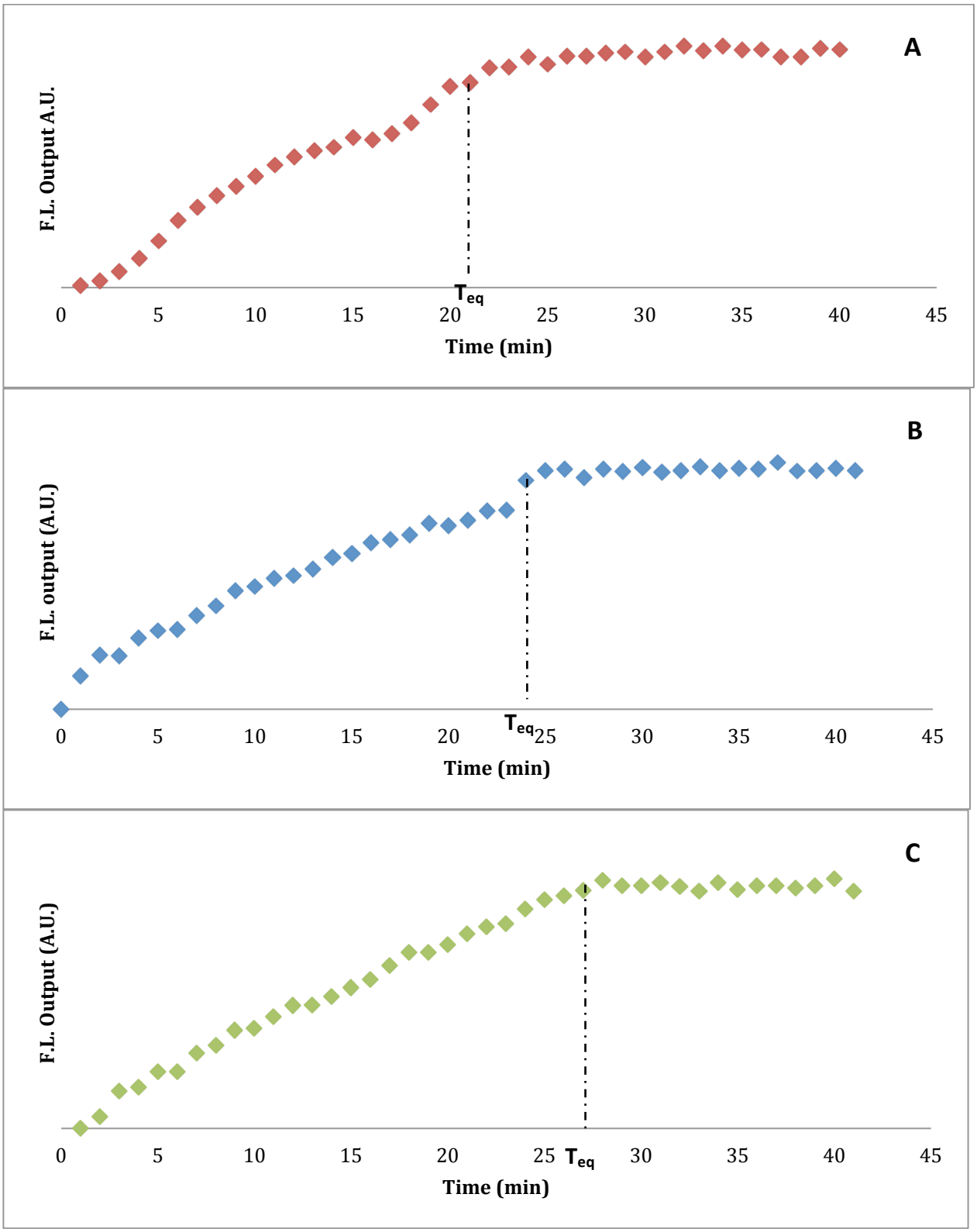

Figure 3.7 A-C Time to reach equilibrium with varying electric fields is shown above by plotting the maximum fluorescent intensity at each time point from their respective complex electropherogram. **A)** plots 150V/cm **B)** plots 100V/cm and **C)** at 50V/cm. Their respective equilibrium times are 22.7±1.53, 24.3±0.58, and 27±1 min (n=3).

PLE-IA operation strategy and increased sensitivity

In order to obtain high sensitivity detection of target protein, a PLE-IA operation strategy of continues sample injection (injectorless method) at high electric field was employed in an effort to drive the reaction to equilibrium. Higher electrical fields for long times yield more efficient mass transfer of the analyte to the capture antibody which act to minimize depleted concentration near the binding sites. To achieve this design goal, a high electric field was employed to increase the rate of electrophoretic mass transfer to the antibody location. Thus a 100 V/cm electric field was used.

In recent work by our group in a [30], enhanced, high-sensitivity target detection was assessed under extended duration electromigration of the target into the PLE-IA. The detection limit of PLE-IA using the plug injection approach was was 5 nM and the use of the injectorless method enhanced the sensitivity of PLE-IA by lowering the detection limit to 0.078 nM. In addition, the signal to noise ratio for an analyte concentration of 5 nM was increased to 124 with the injectorless method in comparison to 2.9 for the plug injection.

The sensitivity increases with the injectorless method and is attributed to the extended, continuous replenishment of the analyte to the capture antibody. In comparison to the plug injection approach, the injectorless approach yields an increased signal until the point of equilibrium where a balance between electromigration and reaction is established. With the plug injection approach, the reaction time (duration that the antibody is exposed to analyte) is limited by the length of the plug, concentration and interaction time. With the plug injection approach, the migrating analyte band sweeps past the immobilized capture antibody site for approximately 14s. This amount of interaction time with the antibody is not sufficient to reach maximum signal at equilibrium. In addition to enhanced sensitivity, the injectorless method is compatible with the single microchannel (2 terminal reservoirs) architecture. An assay conducted in a single, straight microchannel creates a facile avenue for multiplexed systems design and can advance experimental design strategies relevant to systems biology based inquiry.

3. 6 Conclusion

KPLE-IA is reported here as a method to measure association and dissociation rates (k_{on} and k_{off}) directly without the use of functionalized chemicals for surface immobilization of biomolecules or complex mathematical manipulations to extract rate information. The k_{on} and k_{off} rates found for FST* using KPLE-IA were found to be 4.44E+05$M^{-1}s^{-1,}$ and 0.00833 s^{-1} (2 min). In addition, in order to inform on optimization and operational parameters as well as maximize the analytical sensitivity of this assay, the interplay between different competing factors such as reaction, diffusion, and convection were assessed. PLE-IA was theoretically found to operate in the mass transfer limited regime. To experimentally validate , the respective equilibrium times for the 50, 100, and 150 V/cm were determined and found to decrease with increasing voltage to 27±1, 24.3±0.58, and 22.7±1.53 (n=3) minutes as expected from theory. Extended duration of sample loading was used to drive the assay to equilibrium and achieve higher sensitivity by replenishing analyte to binding sites via continuous electromigration, minimizing local depleted concentrations. To increase the rate of replenishment and provide efficient mass transfer, high electric fields at 100V/cm were used.

Chapter 4: Kinetic polyacrylamide gel electrophoresis (KPAGE) microfluidic assay: Binding Kinetic Rates Measured via Electrophoretic Band Crossing ia a Pseudohomogeneous Format

Based on Published article in Analytical chemistry by Kapil, M. A., & Herr, A. E. (2014). Binding Kinetic Rates Measured via Electrophoretic Band Crossing in a Pseudohomogeneous Format. Analytical chemistry, 86(5), 2601-2609.

4.0 Abstract

With relevance spanning from immunohistochemistry to immunoassays and therapeutics, antibody reagents play critical roles in the life sciences, clinical chemistry, and clinical medicine. Nevertheless, non-specific interactions and performance reproducibility remain problematic. Consequently, scalable and efficient analytical tools for informed selection of reliable antibody reagents would have wide impact. Therefore, we introduce a Kinetic Polyacrylamide Gel Electrophoresis (KPAGE) microfluidic assay that directly measures antibody-antigen association and dissociation rate constants, k_{on} and k_{off}. To study antibody-antigen association, an antigen zone is electrophoresed through a zone of immobilized antibody. Upon crossing, the interaction yields a zone of immobilized immunocomplex. To quantify $k_{on,}$ we assess immunocomplex formation for a range of antigen-antibody interaction times. Here, interaction time is controlled by the velocity of the electromigrating antigen zone, which is determined by the strength of the applied electric field. All species are fluorescently labeled. To quantify k_{off}, an immobilized zone of immunocomplex is subjected to *in-situ* buffer dilution, while measuring the decay in immunocomplex concentration. Two approaches for antibody immobilization are detailed: (i) size-exclusion based antibody immobilization via a molecular weight cut off (MWCO) filter fabricated using polyacrylamide gel and (ii) covalent antibody immobilization realized using a photoactive benzophenone methacrylamide polyacrylamide gel. We determine k_{on} and k_{off} for prostate specific antigen (PSA) and compare to gold-standard values. The KPAGE assay completes in 90 minutes, requiring 45 ng of often limited antibody material, thus offering a quantitative antibody screening platform relevant to important but difficult to characterize interaction kinetics.

4.1 Introduction

For assays that rely on antibody-based detection, selection of an antibody reagent presents a critical challenge[41,42]. Non-specific binding and reproducibility remain problematic [41,43,44.]. Typical immunoreagent selection criteria include affinity determination for an antibody-antigen interaction quantified by the equilibrium constant (K_d). The K_d describes the dynamic equilibrium between association (binding) and dissociation (unbinding). Although K_d is widely used for antibody selection[45,46] – and can be related to kinetic association and dissociation rate constants (k_{on} and k_{off}) – the direct measurement of k_{on} and k_{off} provides more specific information on binding and dissociation, both of which are useful as selection criteria[47,48,49]. In other words, two antibodies with identical K_d values may have dramatically different binding kinetics, making performance for a specific application difficult to predict. For example, identification of an antibody-antigen pair possessing a high association rate but low dissociation rate will result in appreciable binding with persisting immunocomplex, as may be desired in immunohistochemistry. Such considerations are also important in assays that involve advection or diffusion (e.g., washing or incubation steps, separation steps).

Gold standard immunoreagent screening and selection assays, such as enzyme linked immunosorbent assays (ELISAs) and surface plasmon resonance (SPR) do not report both k_{on} and k_{off} directly[45,50] yielding instead a measurement of K_d. In ELISA, an antigen is immobilized to a solid surface (96 well plate) and then complexed with an antibody linked to an enzyme. Through a series of equilibrium experiments the K_d can be quantified, however these measurements rarely yield values reflecting reliable equilibrium constants due to mass transport limitations[51]. These mass transport limitations increase the time needed for the antibody to reach the immobilized antigen. The time and concentrations needed for the reaction to reach equilibrium are often unknown and underestimated. In fact, the reaction may never reach equilibrium, thus ELISA provides a qualitative measurement of relative binding, rather than a quantitative assessment[52,53]. In addition, ELISA is time consuming, taking up to 4 hours to overnight to complete equilibrium and extract the K_d.

Like ELISA, SPR facilitates the measurement of K_d via label-free detection of antigen binding to chemically surface-immobilized antibodies by detecting refractive index changes at the binding surface. Due to the heterogeneous SPR format and the poorly defined surface density of the immobilized antibody, SPR cannot make direct measurement of k_{on} [54]. k_{on} can be calculated, however, via the relationship: $k_{on} = k_{off}/K_d$, when k_{off} is known. Further SPR measurement limitations stem from challenges in supplying sufficient analyte transport to the sensor surface and chemical immobilization of the antibody[54]. Both factors hinder binding and introduce mass transport limitations[55, 56,57,58]. Consequently, 10-100x slower direct measurements of k_{on} values are reported in comparison to SPR calculated k_{on} values[59]. Finally, the SPR immobilization procedure can be time-consuming, labor-intensive, and expensive[60].

Kinetic capillary electrophoresis (KCE) is a powerful alternate technique for making direct measurements of k_{on} and k_{off} [61, 61,62, 63, 64]. In plug-plug kinetic capillary electrophoresis (ppKCE)

short plugs (zones) of antigen and antibody are injected into a 20-40 cm long capillary. The sample zone with the lower mobility is injected first, followed by injection of the high mobility species. During the assay, the trailing species zone overruns the slower leading species zone. As both species are in solution, the assay benefits from reaction characteristics of a homogeneous (not heterogeneous) format, thus eliminating concerns associated with concentration depletion boundary layers that can form in heterogeneous reactions. The over-speeding duration sets the interaction time and yields formation of a third species zone, the immunocomplex. The immunocomplex subsequently resolves from the two reactant zones. k_{on} and k_{off} are calculated from a single ppKCE electropherogram using the area of the peak, signal 'tailing' and 'fronting', and migration time scales. Owing to high separation efficiency, fast speed, and minute sample consumption, KCE has been intensively studied for measurement of the binding constants and binding stoichiometry of various affinity interactions[65,66,67]. Although kinetic capillary electrophoresis methods do not require the surface immobilization needed for SPR and ELISA, measurements of k_{on} and k_{off} require fairly complex and iterative mathematical manipulations of resultant electropherograms and, of course, sufficient mobility difference between species zones for reasonable resolution of the formed complex and free antigen[68].

Taken together, characterization of antibody reagents in a rapid, facile, and low reagent-consuming format suitable for screening would have wide impact. Here we introduce an electrophoretic microfluidic assay, termed Kinetic Polyacrylamide Gel Electrophoresis (KPAGE), which directly quantifies both association and dissociation rates, k_{on} and k_{off}, and the dissociation constant K_d. Association is determined by observing a fluorescently labeled antigen zone electromigrate through an immobilized antibody zone. The k_{off} is quantified by observing dissociation of immunocomplex as clear buffer (i.e., antigen not present) is electrophoresed through the antibody-immobilized zone of immunocomplex. Two approaches to *in-situ* antibody immobilization are investigated, including immobilization of an antibody zone at a microscale size exclusion filter (step change in pore-size) and covalent immobilization of an antibody zone on a photoactive polyacrylamide gel (uniform pore-size). Using both approaches, we apply the KPAGE assay to study of a well-validated system of prostate specific antigen (PSA) and a cognate monoclonal antibody. Results suggest this low-infrastructure microfluidic KPAGE assay is a feasible means to realize rapid, quantitative, and scalable antibody screening tools, without the need for complex data interpretation or immobilization schemes.

4.2 Materials and methods

Apparatus and imaging

Fluorescence images were collected using an inverted epi-fluorescence microscope equipped with CCD camera, filter cubes and an automated *x-y* stage. The CCD exposure time was 10 – 100 ms depending on the intensity of the fluorescence signal. Image analysis was conducted using ImageJ software (NIH, Bethesda, MD). The inverted epi-fluorescence microscope used was an IX-50 (Olympus, Melville, NY) equipped with a 1392 x 1040 Peltier-cooled interline CCD camera (CoolSNAP HQ2, Roper Scientific, Trenton, NJ). Automated x-y stage used was S2000, Applied Scientific Instrument. The CCD exposure time was 10 - 100ms depending on the intensity of the fluorescence signal.

Reagents

Silane, glacial acetic acid, methanol, acrylamide, bis-acrylamide and the chemical initiators, such as ammonium persulfate (APS) and tetramethylethylenediamine (TEMED) were all purchased from Sigma-Aldrich. UV photoinitiator was purchased from Wako Chemicals. 10x Tris/glycine native electrophoresis buffer (25 mM Tris, 192 mM glycine, pH 8.4) was purchased from Bio-Rad. Benzophenone methacrylamide monomer (BPMA, (N-[3-[(4-benzoylphenyl) formamido]propyl] methacrylamide) was synthesized and characterized by PharamAgra Labs Inc. Proteins and antibodies were fluorescently labeled in-house using Alexa Fluor 488 and 568 protein labeling kits from Invitrogen and purified by Bio-Gel columns from Bio-Rad. Purified prostate specific antigen (PSA) and Anti-Prostate Specific Antigen antibody were purchased from Abcam. Alexa Fluor 568 Goat Anti-Mouse IgG (H+L) antibody was purchased from Life Technologies Corporation. 3-(Trimethoxysilyl)-propyl methacrylate (98%), glacial acetic acid and methanol (ACS grade), acrylamide, bis-acrylamide were all purchased from Sigma (St. Louis, MO). The UV photoinitiator 2,2-azobis[2-methyl-N-(2-hydroxyethyl) propionamide] (VA-086) was purchased from Wako Chemicals (Richmond, VA). The initiators ammonium persulfate (APS, 0.015%; A3678, Sigma-Aldrich),N,N,N′ ,N′ -tetramethylethylenediamine [TEMED, 0.05% (vol/vol); T9281 was purchased from Sigma-Aldrich]10x Tris/glycine native electrophoresis buffer (25 mM Tris, 192 mM glycine, pH 8.3) was purchased from Bio-Rad (Hercules, CA). Benzophenone methacrylamide (BPMA) monomer (N-[3-[(4-benzoylphenyl) formamido]propyl] methacrylamide was synthesized by PharamAgra Labs Inc (Brevard, NC). Proteins and antibodies were fluorescently labeled in-house using Alexa Fluor 488 and 568 protein labeling kits from Invitrogen per the supplier's instructions and purified by P-6 Bio-Gel columns (Bio-Rad). Purified prostate specific antigen (PSA) (from human seminal fluid; ab78528) and Anti-Prostate Specific Antigen antibody (ab403) were purchased from Abcam (Cambridge, MA). Alexa Fluor 568 Goat Anti-Mouse IgG (H+L) (A-11004) antibody was purchased from Life Technologies Corporation. Labeled proteins and antibodies were stored at 4 °C in the dark until use.

Chip preparation

Glass microfluidic chips with double cross T-junction channels were designed in-house using AutoCAD 2012. Three parallel channels, each with a depth of 20 μm and a width of 70 μm were fabricated using a standard wet etching[69] process (Caliper Life Sciences, Hopkinton, MA). Chip surface preparation prior to gel polymerization was performed as described in previously[70] Two fabrication approaches were developed for realizing an immobilized zone of antibody.

Immobilization Approach 1: Size-exclusion antibody immobilization via a molecular weight cut-off (MWCO) filter

The MWCO filter was fabricated using a two-step mask-based photopolymerization process as described previously[70] using a precursor solution of 10%*T* (*T*, the concentration of total acrylamide, w/v), 5.5%*C* (*C*, ratio of bisacrylamide and bisacrylamide + acrylamide, *w*/*w*) for the filter and 3%*T,* 3.3%*C* for the loading gel. For more details see Supporting Information, Methods. After use, polyacrylamide was removed from the microchannel network (allowing glass chip reuse) by soaking the chips in a 2:1 solution of 70% perchloric acid and 30% hydrogen peroxide overnight at 60°C as described previously[71]. Proper precautions should be carefully observed.

To conduct KPAGE using the MWCO filter, 10 μL of 1x Tris/glycine or protein sample diluted in Tris/glycine was added to channel termini reservoirs (i.e., pipette tip press-fit into the termini wells). In step (1) Figure 4.1, antibody (Ab, 20nM) was electrophoretically loaded from the top T-junction (wells 1 and 5), a plug of Ab was injected and immobilized at the MWCO filter (wells 4 and 3), by physical exclusion of large molecular mass Ab at the filter pore-size discontinuity (interface). Owing to the physical exclusion from the filter, the local Ab concentration enriched 5X (100nM ± 20%). In step (2), a plug of antigen (Ag) (10 uM) was electrophoretically loaded at the bottom T-junction (wells 2 and 6) and electrophoretically injected into the reaction channel (wells 4 and 3). The applied potential was adjusted to control the band-crossing interaction time (t_c) allowing interactions times in the range 1 s < t_c < 60 s. As a corollary consideration, to obtain different interaction times, the electric field is adjusted. Different field strengths should yield different channel transit times for each antigen zone, thus the peak width and maximum concentration of the antigen zone should be different upon arrival at the immobilized antibody zone **(Figure 4.2).** Consequently to expose each immobilized Ab zone to a similar antigen plug concentration, regardless of t_c, we implemented a two-step injection process. First, antigen was injected and electrophoresed to the 1 mm point at a high *E*. Second, upon reaching the 1 mm mark, *E* was decreased to provide the desired t_c. The maximum antigen concentration was 7 μM ± 500nM. In step (3), epi-fluorescence micrographs were collected continually at the immobilized Ab zone enabling monitoring of the immunocomplex formation and direct measurement of the electric field-controlled t_c. To reset the assay in step (4), after immunocomplex (C) measurement was made, field polarity was reversed across the filter to electrophorese away C, Ab, and Ag. Steps (1) through (4) were repeated for the series of t_c. In step (5) to determine the dissociation rate constant, equilibrium mixtures of C were incubated overnight. A plug of C was electrophoretically loaded to wells 2-6 and injected into the MWCO filter (wells 4 and 3). The complex was subjected to buffer dilution for a dilution time (t_d) of 60 min while monitored *via* epi-fluorescence imaging.

The MWCO filter was fabricated using a two-step mask-based photopolymerization process. First, degassed acrylamide/bisacrylamide precursor solution was introduced into the surface modified channel by capillary effect. The precursor was a solution of 10%T (T, the concentration of total acrylamide, w/v), 5.5%C (C, ratio of bisacrylamide and bisacrylamide + acrylamide, w/w) containing 2 mg/mL of the azo-initiator, VA-086. Next, a clear round cover glass slide (0.13–0.17 mm thickness), 18-mm diameter (VWR Scientific, Boston, MA, Catalog number 48380–046) was placed on top of the chip to cover all wells and yield quiescent conditions inside the channel network. To photopattern a 500 μm long, channel-filling MWCO filter 1 mm downstream of the second T-junction, a UV objective microscope system (Diaphot, Nikon) was used in conjunction with a AutoCAD-designed chrome-glass photo mask (Photo Sciences) having a 1000 μm x 500 μm window. The mask was aligned to the chip using a manual adjust x-y stage. A Hamamatsu LightningCure LC5 (Hamamatsu City, Japan) with intensity control with its UV beam with UV illumination in the 350-365 nm range directed through the light path of a Nikon Diaphot 200 (Tokyo, Japan) inverted microscope with a UV-transmission objective lens (UPLANS-APO 4X, Olympus, Melville, NY). UV intensities ranging from 5-6 mW/cm^2 measured with a pocket UV light meter (Lutron, Taipei, Taiwan), and 5 min exposure times were used. After polymerization of the MWCO filter, covering glass slide was removed and a solution of degassed 3% T, 3.3% C precursor was added each well. The 10%T precursor solution was evacuated from the channels. The entire channel network was then flood exposed to UV light at ~10 mW/cm^2 UV intensity for 8 min using a fan-cooled mercury lamp (B-100AP lamp, UVP, Upland, CA). The chip, now containing polymerized gel, was stored fully submerged in 1x Tris/glycine buffer at 4°C until use.

MWCO filter method Steps	**Wells**	**Applied Electric Field (Vcm^{-1})**	**Time (s)**
Antibody Loading	1 and 5	753	30
Antibody Injection	4 and 3	718	120
Antigen Loading	2 and 6	753	30
Antigen Injection	4 and 3	1739 < E < 38	120
Buffer Wash	4 and 3	718	3600

Table 1. Voltage protocol for KPAGE assay MWCO filter method. Chip layout as shown in figure 4.1.

Immobilization Approach 2: Covalent antibody immobilization via a photoactive polyacrylamide gel

The photoactive polyacrylamide gel was fabricated using a precursor solution of 4%*T*, 3.3%*C*. BPMA monomer was added to precursor solutions at 1.1 mM from a 100 mM stock in DMSO. Gels were chemically initiated by 0.08% each of APS and TEMED in buffer of 1x Tris/glycine. Degassed precursor was introduced to channels by capillary action. 4μL of precursor was added to each well. To avoid diffusion of oxygen into the channel and, thus, inhibition of acrylamide polymerization, a cover glass slide was placed on top of the glass chips to cap the wells at the channel termini. Chips were incubated for ~10 min until gelation of excess precursor on top of the chip was observed.

To conduct KPAGE using the photoactive gel immobilization method, we developed a protocol similar to the MWCO filter method; the major difference being the method of Ab immobilization. In Approach 2, covalent attachment of Ab to the benzophenone containing polyacrylamide gel through UV photopatterning was used, not physical exclusion as in the MWCO in Approach 1. To immobilize a plug of Ab (step 1), Ab (2μM) was first loaded into the reaction channel (wells 4-3). A photomask with a 20 μm slit was designed and fabricated in-house. The slit was cut in stainless steel using a laser cutter (Universal Laser Systems, PLS6MW Multi-Wavelength Laser Platform (30W fiber laser cartridge) (Scottsdale, AZ)). The mask was placed on top of the glass chip, with the slit 1mm downstream from the second double cross T-junction. Flood UV (350–365 nm) light was provided by a Hamamatsu Lightningcure LC5 directed through a liquid light guide (Newport Corporation, 77566 Liquid Light Guide) for 5 s at 20% intensity. Contact masking was used, with the liquid light guide pressed directly onto the mask surface. After UV exposure, electrophoresis was resumed to remove free Ab from the channel (wells 4-3). The Ab capture efficiency was defined as the fraction of antibody that was retained in the channel after UV exposure and washout to the antibody initially loaded into the channel before UV exposure. UV capture efficiencies depend on the benzophenone concentration within the gel, UV exposure times, and the amount of available C–H bonds in target polypeptides and proteins. In addition, we have observed sample preparation to be an important factor in binding efficiency of protein to gel scaffold. For example, we have observed native proteins to immobilized with notably less efficiency (1.5%, under IEF conditions)[72] than fully reduced/denatured proteins (>85%)[73]. In line with the native protein immobilization efficiencies previously observed, KPAGE reports antibody capture efficiencies of 8.8% ± 2%. Steps (2-4) follow the MWCO filter method as described above. For step (5), Ab was immobilized as stated in step (1) and antigen was electrophoretically loaded through the reaction channel (wells 4-3) until the complex reached equilibrium. The complex was then subjected to buffer dilution via electrophoresis for a t_d of 60 min, with imaging conducted every 10 min using a 100 ms exposure time. Replicates were performed using a new channel and photo immobilized plug of antibody for each interaction and dilution. After loading and photocapture of antibody, residual background signal was observed with an SNR >3.3.

Photoactive gel method Steps	**Wells**	**Applied Electric Field (Vcm^{-1})**	**Time (s)**
Antibody Loading	1-3	753	120
Antibody washout	4-3	718	120
Antigen Loading	2-6	753	30
Antigen Injection	4-3	1739 < E < 38)	120
Buffer Wash	4-3	718	3600

Table 2. Voltage protocol for KPAGE assay Photoactive gel method method. Chip layout as shown in figure 4.1.

Fluorescence signal calibration: To quantify the local antigen and Ab concentrations, images of analytes with concentrations ranging from 1.0 - 0.125 μM in free solution were acquired using the same channel dimensions and imaging settings as used for the KPAGE studies. We observed that as the antigen and antibody concentrations increased, the image intensity increased linearly ($y_{Ag} = 0.4x$, $R^2 = 0.99$; $y_{Ab} = 9.0x$, $R^2 = 0.97$). Calibration was conducted before each KPAGE

experiment. Photo bleaching studies (**Figure 4.3**) show minimal decrease (-4.4 ± 3%, n = 3) in fluorescence signal intensity for AF488 labeled PSA when imaged continuously for 600 s (100 ms exposure time, 30 nM PSA).

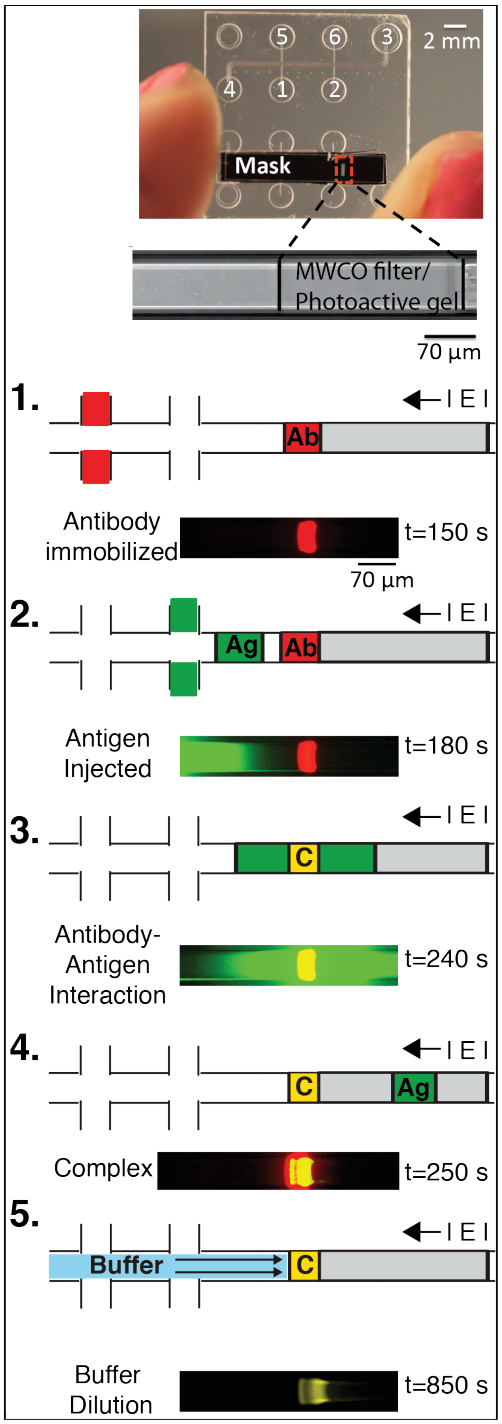

Figure 4.3 Direct measurement of binding kinetic constants k_{on} and k_{off} via KPAGE relies on an immobilized antibody zone and a freely electromigrating antigen zone. The microchannel assay is comprised of 5 steps: (Step 1) antibody (Ab) immobilization (MWCO filter and photoactive gel methods), (Step 2) antigen (Ag) sample injection, (Step 3) antibody-antigen interaction (Step 4) complex (C) formation and (Step 5) buffer dilution where the '|E|' for each step represents the direction of the electric field.

Estimation of interaction time, t_c

For k_{on} measurements, the t_c was defined as the time required for a zone of antigen (at a known concentration) to traverse the zone of immobilized Ab. As fluorescent antigen electromigrated through the immobilized Ab zone, fluorescence signal was collected and integrated from the Ab region (axial length of 10-170 μm, transverse width of 70μm) as a function of time. This capture region was designed such that we could obtain interaction times before the reaction reached equilibrium as discussed in the Results and Discussion section. The signal was fitted to Gaussian distributions numerically (MATLAB R2010b), with the full width half maximum (FWHM) computed and used as the t_c. The antigen distributions used to determine t_c were asymmetrical for the MWCO filter as the immobilized Ab region was located at the sharp MWCO filter interface. As antigen enters the immobilized Ab region, the zone enters a small pore-size gel and slows, accelerating again when the zone exits the filter into a higher pore-size gel. Antibody-antigen interaction times were controlled by varying the electric fields from 1739V/cm – 38 V/cm yielding analyte velocities from 500 - 10 μm/s and interaction times from 2-60 s with standard deviations for each interaction time up to 0.25 s for a given applied field.

Estimation of kinetic rate constants k_{on} and k_{off}

Epi-fluorescence micrographs of the immobilized Ab and (bound antigen) immunocomplex signals for each t_c and t_d were fitted to Gaussian distributions numerically (MATLAB R2010b). The area under the curve (AUC) of the antibody and immunocomplex signal was determined by integrating the Gaussian distribution. The antibody and immunocomplex concentration in (nM) was obtained using calibration curves developed as described above. For k_{on} measurements, the percent bound (%Bound) for each immunocomplex concentration was computed by taking the ratio of the immunocomplex to available binding sites, %Bound = C/Ab. For each interaction time, a control was performed to determine the amount of non-specific binding occurring at the filter interface. This value was subtracted before quantifying the immunocomplex concentrations for a given interaction time. We employ a Langmuirian one-to-one antibody-to-antigen binding model[47]. We choose this model as monoclonal antibody purification is known to result in protein unfolding, misfolding, and aggregation that may yield only one active binding site [74,75]. Experimental data was fit to the binding association and dissociation expressions[31].

Binding kinetic equations used: For k_{on}: $\%Bound = \%B_{max} \; x \; (1 - \exp(-k_{obs} \; x \; t_c))$ were the $\%B_{max}$ is the maximum amount of binding at equilibrium. The $k_{obs,}$ which is the observed association rate constant was computed using a nonlinear least squares curve fit to the association equation. For k_{off}: $\%Bound = (B_{max}-B_{min}) \; x \; \exp(-k_{off} \; x \; t_d)) - B_{min})$. Here B_{max} is the maximum amount of complex bound at $t_d = 0$ and B_{min} is the minimum immunocomplex signal at long dilution times. We present 2 significant figures in our measurements for k_{on} and k_{off}. This level of certainty depends on the spatial resolution of our imaging system, the certainty of our velocity, and antibody and antigen concentration measurements as well as the goodness of fit we used for the binding curves. We used a high speed; high megapixel resolution camera designed for quantitative fluorescence microscopy applications for developing calibration curves and imagining antigen interaction times with variations less than 10% from run-to-run. We then determined the goodness of our binding curve fit via R^2 values and used fit's with R^2>80%.

Transport modeling: We numerically modeled the antibody, antigen, and immunocomplex concentration for a series of time points for the KPAGE assay. Numerical models of the KPAGE system was performed using (MATLAB R2010b) The antigen concentration was selected at 30 times greater than the antibody concentration (similar to experimental concentrations) to ensure the antigen concentration remained constant during the antibody-antigen interaction with negligible depletion of antigen. Dissociation during association measurements was assumed negligible, given that a typical antibody-antigen pair[76] requires ~60 minutes to fully dissociate (k_{off}=1.88 x 10^{-3} s^{-1}).

Equations 1-3: Governing Equations: (diffusion, reaction, and convection)

A 1D diffusion, convection, and reaction model was developed to simulate the KPAGE assay. The change in antibody, antigen, and complex concentration were simulated as the antigen migrates to the antibody capture zone at varying electric fields. Modeling was performed via MATLAB using the "pdepe" solver. Dirichlet boundary conditions specified zero analyte concentrations at channel edges. Initial conditions were chosen to be Gaussians distributions.
The governing equations were:

$$\frac{\partial Ab}{\partial t} = -k_{on}Ag(Ab - c) + k_{off}c \qquad (1)$$

$$\frac{\partial Ag}{\partial t} = D\frac{\partial^2 Ag}{\partial x^2} - u_{Ag}\frac{\partial Ag}{\partial x} - k_{on}Ag(Ab - c) + k_{off}c \qquad (2)$$

$$\frac{\partial c}{\partial t} = +k_{on}Ag(Ab - c) - k_{off}c \ ) \qquad (3)$$

Parameters and values used in the system (units):

Ab = antibody concentration = 150 x 10^{-9} (M)
Ag = antigen concentration = 5 x 10^{-9} (M)
c = Ab-Ag immunocomplex concentration (M)
D = diffusional coefficient of a 30 kDa protein in a 3%T/3.3%C = 2.5 x 10^{-11} (m^2s^{-1})
k_{on}=association rate constant = 4.1 x 10^5 ($M^{-1}s$-1)
k_{off}=dissociation rate constant = 4.5 x 10^{-5} (s^{-1})
t=interaction time (s)
u_{Ag}=Velocity of antigen = (1000-1) x 10^{-6} (ms^{-1})

Figure 4.2: Simulations of antigen concentration reduction due to electromigation and diffusional effects

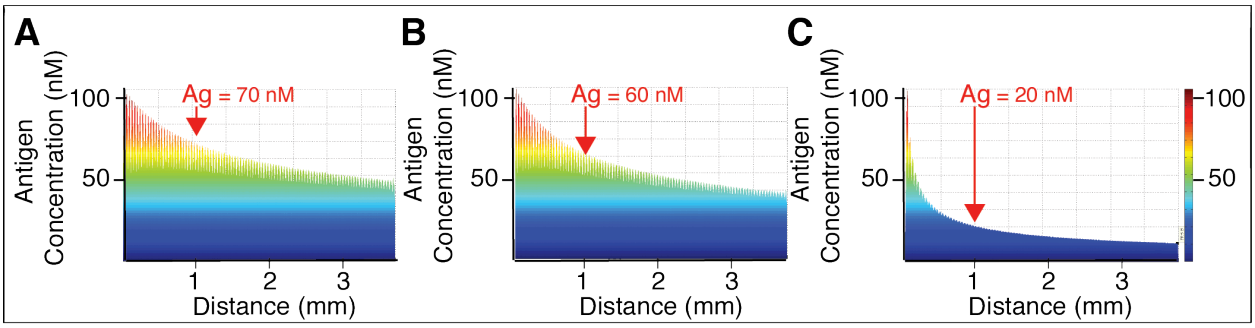

Figure 4.2: Simulations of the KPAGE assay were preformed. Here electromigration and diffusion of a Gaussian plug of PSA was modeled in Matlab as described above. Antigen electgromigrates through a 3%T/3.3%C gel channel at high, medium, and low electric-fields (e-fields) and the color bar represents local concentration of a Gaussian plug A: PSA concentrations decrease initially by 30% (from 100nM to 70nM) upon reaching antibody capture zone 1mm downstream at t=2.2 s after injection at a high e-field of 1738V/cm (u=450µm/s). B: PSA concentrations decreases further by 15% (from 70nM to 60nM) from its initial concentration at t=5.2 s at medium e-field of 1489V/cm (u=190µm/s). C PSA concentrations decreased by up to 71% (from 70nM to 20nM) from its initial concentration (A) at t=100 s at a low e-field of 150V/cm) (u=10µm/s).

Figure 4.3: Photo bleaching studies of PSA labeled in alexa fluor 488

Figure 4.3: Photo bleaching studies show minimal decrease (-4.4 ± 3%, n = 3) in fluorescence signal intensity for AF488 labeled PSA when imaged continuously for 600 s (100 ms exposure time, 30 nM PSA).

Figure 4.4: antibody shift into MWCO filter due to high electric fields

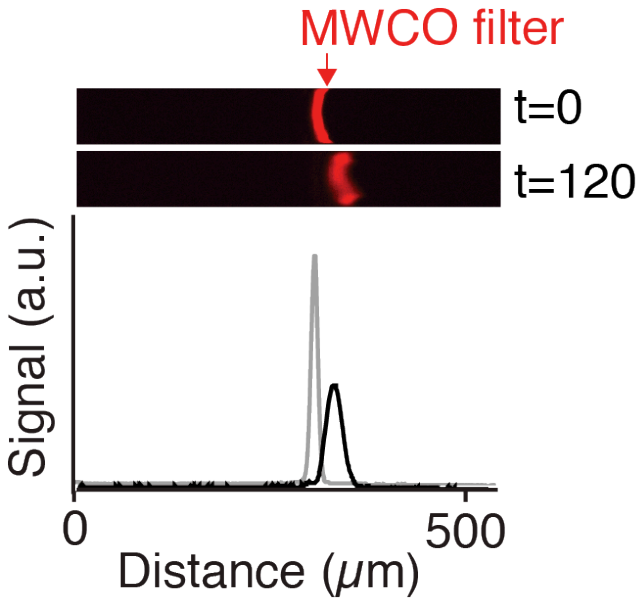

Figure 4.4: As antigen plug is electrophoresed through the immobilized antibody zone at varying electric field strengths, the antibody is observed to shift by as much as 24μm into the filter and spread by as much as 50% (n=3) at high E=1739 V/cm.

4. 4 Results and discussion

KPAGE assay design. To yield an efficient, scalable, and readily interpretable assay for determination of antibody-antigen kinetic rate constants, we explored a purely electrophoretic pseudo-homogeneous band-crossing format, as described in the *Materials & Methods* and briefly summarized here (Figure 4.4). During KPAGE k_{on} determination, a zone of fluorescently labeled antigen was electrophoresed through an immobilized zone of antibody for a known and controlled interaction time, t_c. Given sufficient t_c, electromigrating antigen binds to the immobilized antibody forming a stationary immunocomplex. Note that either antibody or antigen can be immobilized in the photoactive KPAGE system and only the larger of the binding pairs can be immobilized for the MWCO filter method, both with the un-immobilized analyte in excess. Several crossing experiments with distinct tc durations were performed, each using a zone of fresh immobilized antibody. Increasing or decreasing the t_c was controlled by varying the electrophoretic velocity of the antigen through adjustment of the applied electric field strength. At longer t_c, the amount of immunocomplex formed is higher (until equilibrium), with the amount of resultant immunocomplex directly related to k_{on} of the binding pair. To determine the dissociation rate, a zone of pre-equilibrated antigen-antibody immunocomplex was immobilized in the microchannel. Buffer was electrophoresed over the stationary immunocomplex for a set dilution time (t_d) and the decay in immunocomplex concentration was monitored. KPAGE offers a pseudo-homogeneous format that is reaction-limited, with mass transport of free antigen to immobilized antibody fast in comparison to the reaction, owing to small diffusional lengths (100 nm) defined by the porous gel matrix.

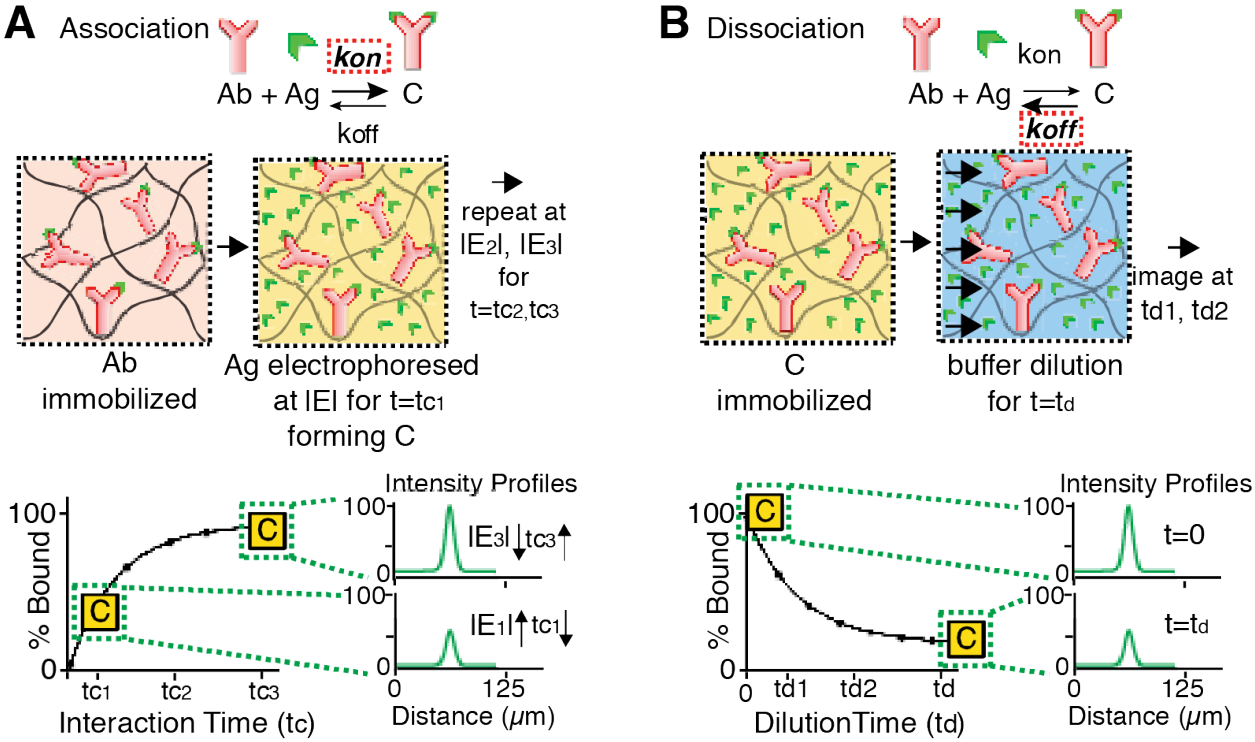

Figure 4.4. KPAGE schemes for determination of both association and dissociation rate constants: A) Association rate determination: A zone of antibody (Ab) is immobilized in a polyacrylamide gel. A plug of fluorescently labeled antigen (Ag) is electrophoresed through the stationary antibody for a set interaction time (t_c). Sufficient interaction time results in formation of stationary immune complex (C). By sweeping through a range of t_c experiments, the amount of complex formed for each condition allows estimation of k_{on}. Here, t_c is varied by controlling the electrophoretic velocity of the antigen through the applied electric field, E. **B)** Dissociation rate determination: A plug of immunocomplex is immobilized in the polyacrylamide gel and buffer is swept over the complex for a set dilution time, t_d. The time-dependent decay in the complex signal allows determination of k_{off}.

In designing the KPAGE assay, we first sought to determine the types of binding pairs well-suited for KPAGE analysis. We simulate the KPAGE assay and then consider assay requirements for three binding rate regimes: low, intermediate, and ultra-high (Figure 4.5A). The simulations estimate the range of association and dissociation rates using a 1D diffusion, convection, and reaction model. The parameter that dictates the KPAGE-accessible range for the association and dissociation rates depends on the electrophoretic velocity of the antigen, which controls the interaction time. The electrophoretic velocity of the antigen zone through the antibody capture zone is the same for both the MWCO filter and photoactive gel methods, and hence this model predicts the accessible regimes irrespective of the exact immobilization method employed. For k_{on}, KPAGE must allow ~4 measurements of immunocomplex formation before equilibrium is reached[31]. With the equilibrium time given by $\tau_{eq} = (k_{on}Ag + k_{off})^{-1}$, this criterion can be stated as: $t_c < (\tau_{eq}/4)$. An example of a low association rate constant system[77] is free prostate specific antigen (PSA) and a monoclonal antibody with a $k_{on} = 4.1 \times 10^4$ $M^{-1}s^{-1}$. For an intermediate system[77 78 79, 52,55] a $k_{on} = 4. \times 10^6$ $M^{-1}s^{-1}$ is appropriate. For an ultra-high[80] affinity binding pair such as biotin and streptavidin a $k_{on} = 4.52.2 \times 10^7$ $M^{-1}s^{-1}$ is appropriate. For low and intermediate association rates, the τ_{eq} was found to be within 10 s < τ_{eq} < 20 s. Given $t_c < \tau_{eq}$, we assume negligible dissociation. Using an electromigration-diffusion-reaction model, we estimate the fastest interaction time attainable as ~1 s. Thus, the KPAGE association assay must be capable of measuring ~4 distinct t_c values in the first 10 s. While this analysis suggests that assay operation is not well-suited to ultra-fast binding pairs (i.e., streptavidin-biotin), the analysis does suggest that KPAGE is well-suited to a wide range of antibody-antigen binding pairs (e.g., 1×10^4 $M^{-1}s^{-1}$ $\leq k_{on} \leq 1 \times 10^6$ $M^{-1}s^{-1}$), including those of interest in this work.

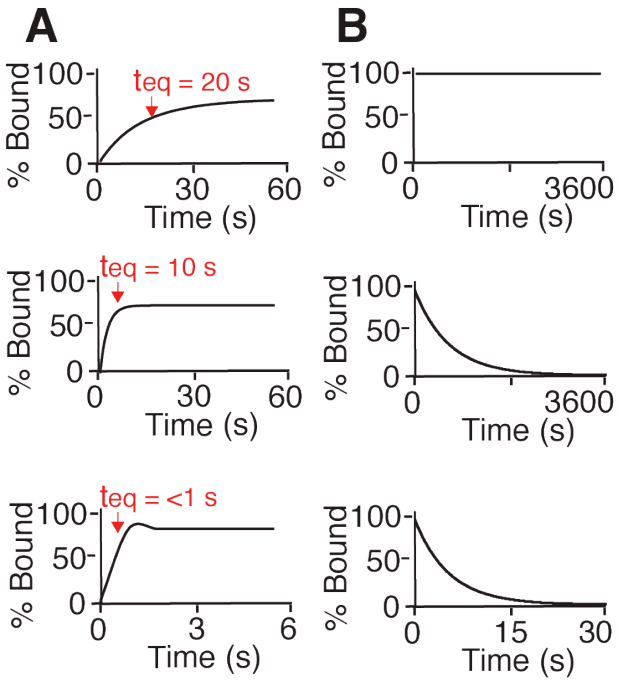

Figure 4.5 Binding kinetic regime simulations inform KPAGE applicability. A) Association kinetic rate constants in three association rate regimes: low, intermediate, and ultra-high. As association kinetic rate increases, the time to equilibrium decreases from 20 s to < 1 s. B) Dissociation kinetic rate constants in three dissociation rate regimes: low, intermediate, and high.

Low dissociation kinetic rates require unrealistic KPAGE measurement durations, whereas intermediate and high dissociation rates are measurable via KPAGE.

Similarly, for dissociation kinetic rate constant or k_{off} determination, we simulated a range of binding pairs (Figure 4.5B): one pair with a low dissociation rate (e.g., biotin[80] and streptavidin with $k_{off} = 7.5 \times 10^{-8}$ s^{-1}), one with an intermediate dissociation rate (e.g., PSA[76] with $k_{off} = 4.5 \times 10^{-5}$ s^{-1}) and one pair with a high dissociation rate (e.g., human serum albumin and ketoprofen[81] with $k_{off} = 0.227$ s^{-1}). In the limiting case of low k_{off} (Figure 4.5B), the simulation predicts a dilution time of 1 hour yielding minimal decrease in complex signal, by AUC determination. In fact, a dilution time of 7 weeks would reduce the AUC of the immunocomplex by just 5%, which is the minimum signal decrease needed to reliably compute k_{off} via KPAGE. Nevertheless, for typical antibody-antigen pairs, simulation results predict the majority of immunocomplex dissociating within 1 hour of dilution initiation, making dissociation readily measurable using KPAGE. Finally, simulation of high k_{off} systems predicts that the immunocomplex AUC should diminish notably within just the first 30 s of dilution.

Next, we sought to understand the applicability of KPAGE to measurement of k_{off}. For this analysis, we assume that newly dissociated and now electromigrating antigen (free antigen) does not re-associate with immobilized Ab during the assay duration. To scrutinize this assumption, we compare an "on-time" (t_{on}) and an "off-time" (t_{off}) representative of KPAGE. Assuming antigen is in surplus, we define t_{on} as the time required for antigen to bind with an antibody and form immunocomplex. Thus, t_{on} can be related to the antibody concentration, Ab, and the association rate, k_{on}, yielding $t_{on} = (k_{on}\ \mathrm{Ab})^{-1}$. $\tau = (k_{on}c + k_{off})^{-1}$We further define t_{off} as the antigen electromigration velocity, u_{Ag}, divided by the immobilized antibody zone length, L, yielding $t_{off} = L(u_{Ag})^{-1}$. Under KPAGE operating conditions and intermediate association rate kinetics, comparison suggests that the time needed for antigen to electromigrate past the immobilized antibody zone is substantially lower than the time needed for antigen to bind to antibody ($t_{off} << t_{on}$). For example for KPAGE with $t_{off} = 0.1$ and $t_{on} = 10$, at analyte velocities as fast as 500 μm s^{-1} , and antibody capture zones of 10-170 μm in axial length, dissociated antigen exits the immobilized antibody zone before rebinding with immobilized antibody. An upper limit on electric potential sourced by the high voltage power supply used for KPAGE limits the maximum electrophoretic velocity of the antigen zone.

KPAGE Determination of Association Kinetic Rate Constant, k_{on}

We applied KPAGE to determine k_{on} of a PSA and monoclonal antibody pair. First, we used a polyacrylamide MWCO filter to yield size-exclusion and, thus, immobilization of antibody at the filter interface (Figure 4.6A). We observed the (axial) length of the immobilized antibody zone ranging from 10-70 μm (n = 12 devices) with ~50% variation in the total mass of antibody immobilized, as determined by AUC measurements. As such, t_c was explicitly measured for each run from image sequences acquired during the band-crossing experiments. We observed immunocomplex signal increasing with longer t_c durations, as expected for $t_c < \tau_{eq}$. As shown in Figure 4.6B, binding curves plateau at 64% of the antigen bound in immunocomplex, with the asymptote value dependent on concentration of antigen and immobilized antibody. Interestingly, although the electromigrating PSA concentration was ~60 times greater than that of the

immobilized antibody, we did not observe saturation of the immobilized antibody under any t_c studied. We attribute this reduced binding occupancy (even at long interaction times) to possible steric hindrance of antibody binding sites owing to crowding at the MWCO filter interface[70] or due to high dissociation rates.

In light of the size-exclusion based immobilization mechanism used to determine k_{on}, we sought to further understand the role of non-specific adsorption of free protein, as the MWCO filter excludes species based on size. To characterize sources of non-specific binding at the MWCO filter we explored performance in four different cases: (Case 1) KPAGE with no antibody present, (Case 2) KPAGE with an immobilized off-target antibody (goat anti-mouse IgG (H+L)), (Case 3) KPAGE with PSA-specific antibody immobilized, and (Case 4) KPAGE with no polyacrylamide gel pore-size discontinuity and no immobilized antibody zone (i.e., uniform, bare gel). For each case, a high concentration zone of PSA antigen (10μM) was electrophoresed across the region of interest and any signal retained was quantified by calculating the AUC.

With no antibody present (Case 1), we measured a 23 ± 2% non-specific signal for the MWCO filter immobilization method. With off-target antibody immobilized at the MWCO filter (Case 2), we measured a 20 ± 4% non-specific signal. A uniform pore-size bare gel (Case 4) yielded no detectable signal. All of these cases were then compared to signal from immobilized on-target PSA antibody (Case 3), where we measured an AUC signal 5-fold greater than Cases 1 and 2. Taken together, we attribute non-specific signal to the presence of the pore-size discontinuity that forms the MWCO filter. As such, background signal correction was performed for each KPAGE measurement conducted using a MWCO filter, to account for any antigen non-selectively trapped at the pore-size discontinuity.

For PSA and monoclonal antibody pair, MWCO-filter based KPAGE reported a k_{on} value of 2 x 10^4 $M^{-1}s^{-1}$ ± 7% (n = 3, Figure 4.6B). In comparison, SPR determination of k_{on} for PSA monoclonal antibody pair[76] has been reported as 4.1 x 10^4 $M^{-1}s^{-1}$ ± 25%, thus showing appreciable agreement with KPAGE using the MWCO filter. When considering SPR, we note that this surface-based assay is known to be mass transport limited under a range of operating conditions. When operating in a mass transport limited mode, the binding reaction at the surface consumes free antigen faster than mass transport (diffusion, convection) can deliver fresh, unbound antigen to the surface. The development of a depletion boundary layer in free antigen concentration proximal to the surface causes SPR to report ~10-100x lower association kinetic rate constants when measured directly[59]. While a pseudo-homogeneous system such as KPAGE overcomes the k_{on} artifacts arising from concentration depletion boundary layers, our observations of the KPAGE system further suggest that local crowding of antibody at the filter interface may lead to a reduced ability for the immobilized antibody to bind to antigen owing to crowding artifacts (i.e., steric hindrance or epitope masking), as mentioned.

We next explored alternate means to locally immobilize antibody while overcoming the challenges of antibody crowding and non-specific interactions with the MWCO filter. As a second approach to immobilizing antibody, we utilized a polyacrylamide gel containing benzophenone methacrylamide monomer. This "photoactive" formulation allows UV-initiated covalent immobilization of a zone of antibody to the polyacrylamide gel through hydrogen abstraction (Figure 4.6C). In contrast to the MWCO filter immobilization approach, mask-based photopatterning of antibody allows use of a uniform pore-size polyacrylamide gel and relaxes the size-based assay design constraints. The antibody zone lengths ranged from 80-170 μm.

Importantly, we performed a study of non-specific interactions using the same set of control studies examined for the MWCO filter immobilization approach. Here, we measured a 3.8 ± 0.2 % non-specific signal for Case 1, a 3.5 ± 0.3 % non-specific signal for Case 2. In a uniform pore-size, bare gel (Case 4) no detectable signal was measured. All cases were then compared to signal from immobilized on-target PSA antibody (Case 3), where we measured a signal 33-fold greater than Cases 1 and 2. As an aside, we observed notably less variation in the run-to-run antibody mass loaded (8%) when using the photoactive gel as compared to the MWCO filter approach. We attribute tighter control of antibody immobilization to the uniform pore-size of the gel and, hence, similar electrical resistance of all fabricated microchannels (i.e., reduced chip-to-chip variation). Recall that protein and antibody are loaded into the gels electrophoretically.

After observing notably reduced non-specific interactions as compared to the MWCO filter approach, k_{on} for the PSA and monoclonal antibody pair was determined (Figure 4.6C). KPAGE with covalently immobilized antibody estimated a k_{on} of 2.7 x 10^5 $M^{-1}s^{-1}$ ± 12% (n = 3, Figure 4.6D) for the PSA and antibody pair. Like the MWCO filter method, the photoactive gel method sees a binding curve that plateaus at 64% of the antigen bound in immunocomplex. Saturation of the immobilized antibody did not occur, even at long interaction times. We attribute the observed plateauing behavior to high antibody concentrations and dissociation rates. In comparison, SPR can yield run-to-run calculation-based k_{on} variation near 25%[56,76,82], thus suggesting KPAGE is more robust than SPR.

Compared to the MWCO filter and SPR, the association kinetic rate constant measured for PSA and monoclonal antibody is an order of magnitude faster in the photoactive gel system. Further, the equilibration time is 3x faster than the equilibration time observed using the KPAGE MWCO filter approach (15 s). We hypothesize that the differences in observed kinetic characteristics stem from differences in the physical environment and mechanism underpinning antibody immobilization. Firstly, we note that the KPAGE system was operated under pH 8.4 buffer conditions to support electrophoresis, whereas the SPR studies cited were performed in a pH 7.4 buffer as is typical of SPR. The local pH influences the protein state and, therefore, electrostatic interactions and overall binding. Previous reports have observed that, as the pH increases, the association rates of antibody-antigen pairs can increase by as much as 85%[83] and dissociation rates can increase by as much as 16-fold[84,85]. In a study comparing an IgG antibody to an enzymatic protein similar to PSA, hen egg lysozyme (HEL), association rate increased by 33% by increasing the pH by just one unit (pH 7 to pH 8). Comparing PSA SPR results to our KPAGE results, we observed a 70% increase in association rates. These results follow the trend previously published[83] and are in range of what is to be expected when increasing the pH of the run buffer for this type of antibody-antigen pair. Secondly, for the MWCO filter, pore-sizes at

the filter interface are smaller than the antibody allowing antibody to be immobilized based on size exclusion. As antigen plug is electrophoresed through the immobilized antibody zone at varying electric field strengths, the antibody zone is observed to further electromigrate into the gel (up to ~25µm past the filter interface) and widen by 50% (n=3) (Figure 4.4). This localized concentration reduction and embedded nature of the immobilization potentially limits accessibility of epitope binding sites. In contrast, the photoactive gel immobilization approach yields stationary covalent attachment of the antibody to a uniform pore-size gel matrix.

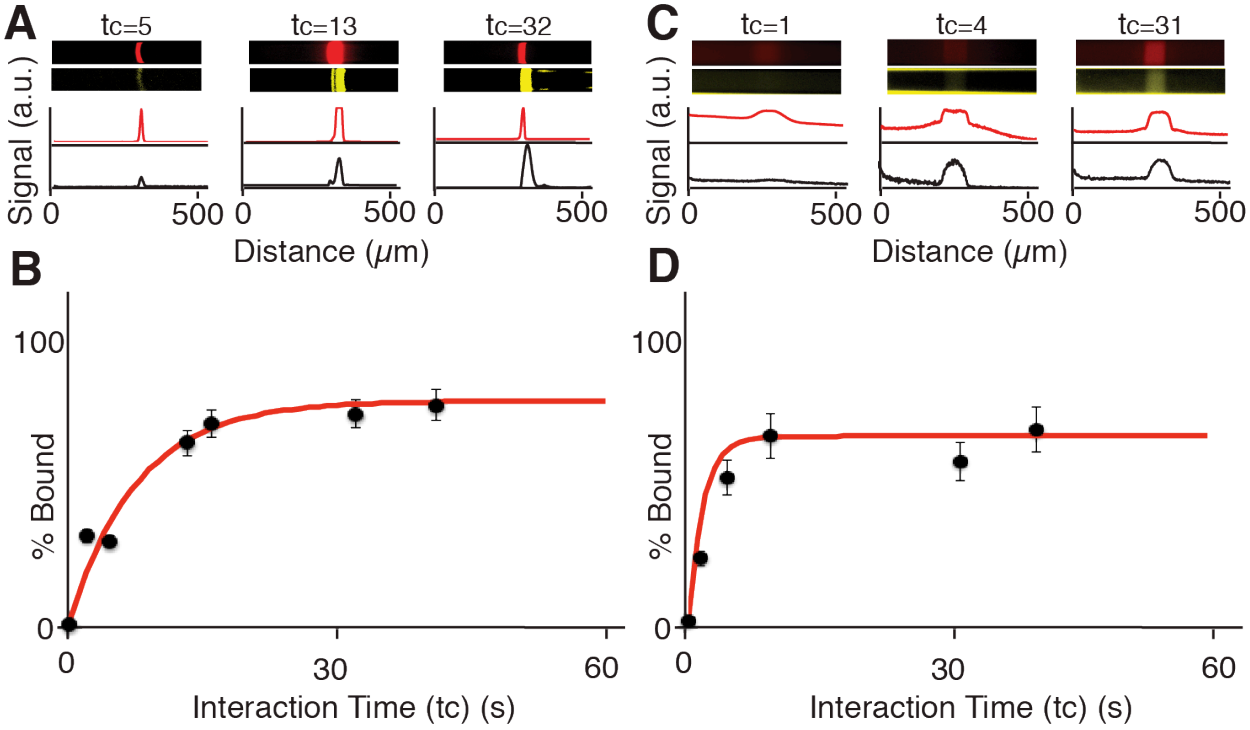

Figure 5.5 Direct determination of association rate constants with KPAGE. Two-color epi-fluorescence micrographs of immunocomplex (C, merged red and green fluorophore signals) formed after antigen (green fluorophore) has interacted with the immobilized antibody (Ab, red fluorophore) for a set interaction time, t_c. The MWCO filter antibody immobilization method (left panel) and the photoactive gel antibody immobilization method (right panel) are both shown. (A & C) Intensity profiles of immune complex peaks at different interaction times (t_c) points ranging from 0 - 60 s are quantified and shows that as t_c increases the AUC of the immune complex peaks increases. (B & D) Black circles represent on-chip measurements of PSA immune complex % Bound at different t_c . On-chip measurements of the association rate constant k_{on} was calculated from a 3-parameter binding curve fit model (red) and plotted against the measured PSA immune complex % Bound for each t_c. Error bars are calculated from three replicate trials. k_{on} for the affinity interaction of PSA was 2×10^4 $M^{-1}s^{-1}$ ± 7% for the MWCO filter method (left) and 2.7×10^5 $M^{-1}s^{-1}$ ± 12% for the photoactive gel method (right).

KPAGE Determination of Dissociation Kinetic Rate Constant, k_{off} and computed K_d

We next applied KPAGE to measure the dissociation rate constant of the PSA and monoclonal PSA antibody pair, here again comparing the MWCO filter (Figure 5.6A,B) and photoactive gel immobilization approaches (Figure 5.5 C, D). For both approaches, we observed time-dependent dissociation of immunocomplex, asymptoting to 20-30% at the longest dissociation times studied (i.e., 3600 s). KPAGE yielded two measurements for k_{off}, with the MWCO filter reporting 5.0 x 10^{-4} s^{-1} ± 7.5% and the photoactive gel reporting 4.7 x 10^{-4} s^{-1} ± 7.2%. Despite the differences in the physical environment and immobilization mechanism of both the MWCO filter method and the photoactive gel method, both methods yield similar k_{off} values. We hypothesize that despite steric hindrance or epitope masking that could be occurring in the molecular weight cut off MWCO filter method, once complex is formed, dissociation of the antigen upon buffer dilution occurs at the same rate at the photoactive gel. This type of behavior has been previously seen in a similar study[86] where they compared two types of antibody immobilization methods, (1) with a three-dimensional hydrogel-binding matrix (1µm in thickness) to (2) a dextran matrix (100 nm thickness). In this study, the association rate for the hydrogel-binding matrix was an order of magnitude lower than the dextran matrix[77], however, for the dissociation rates both methods were similar. The dissociation constant K_d computed from k_{off} and k_{on} for the MWCO filter and photoactive gel methods were 25 nM and 1.7 nM. Taken together, KPAGE by either immobilization method yields consistent k_{off} and K_d values. Literature reports based on SPR[76] establish k_{off} for PSA as 4.5 x 10^{-5} s^{-1} ± 15%, and computed dissociation rate constants of K_d=1.86 nM. k_{off} from SPR is roughly an order of magnitude lower than k_{off} determined by KPAGE and is the same order of magnitude for the computed K_d. Kinetic capillary electrophoresis determination of K_d values are comparable to SPR[61 87]. We hypothesize that differences in the measured values stem from differences in the pH of the binding system.

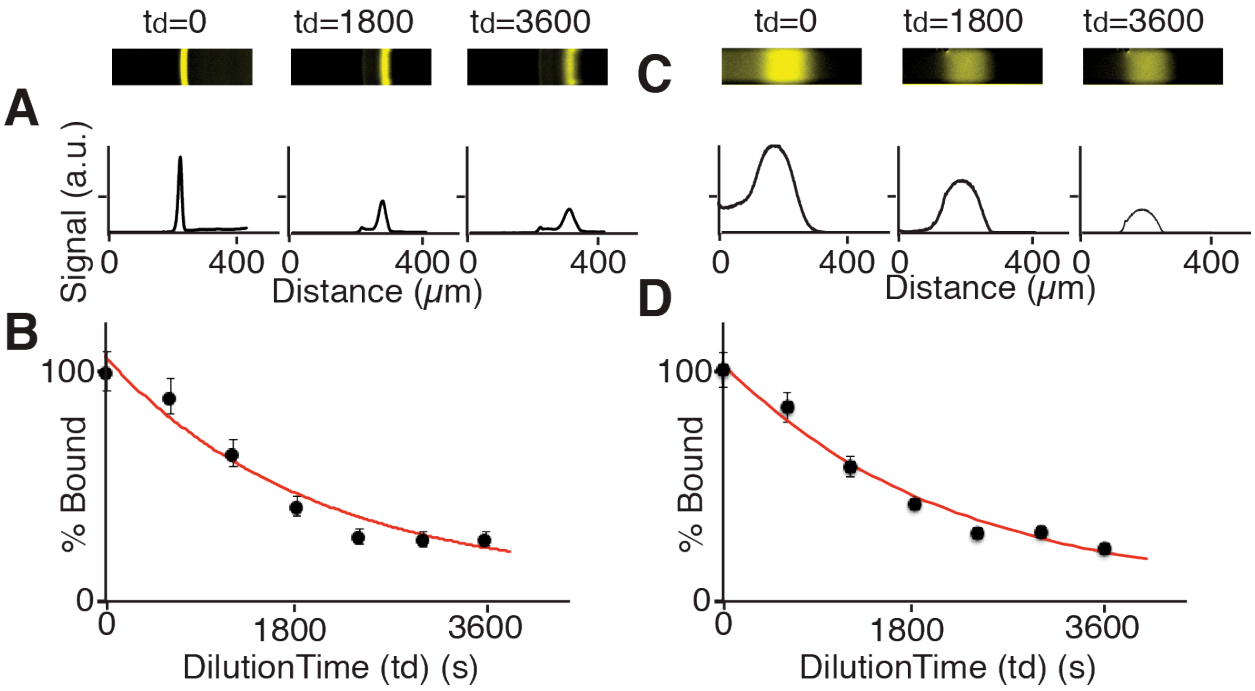

Figure 5.6 Direct determination of dissociation rate constants via KPAGE. Two-color epi-fluorescence micrograph time course of PSA immunocomplex dissociation (C, merged red and green fluorophore signals). The MWCO filter antibody immobilization method (left panel) and the photoactive gel antibody immobilization method (right panel) are shown (A & C). Intensity profiles of immune complex peaks at different dilution times (t_d) points ranging from 0- 3600 s are quantified. As t_d increases the AUC of the immune complex peaks decreases. (B & D) Black circles represent on-chip measurements of PSA immune complex % Bound at different t_d. On-chip measurements of the dissociation rate constant k_{off} was calculated from a 3-parameter binding curve fit model (red) and plotted against **the measured** PSA immune complex % Bound for each t_c. Error bars are calculated from replicate trials. k_{off} was determined to be 5.0×10^{-4} s^{-1} ± 7.5% for the MWCO filter method (left) and 4.7×10^{-4} s^{-1} ± 7.2% for the photoactive gel method (right).

KPAGE Comparison: molecular weight cut off (MWCO) filter method and the photoactive gel method

The MWCO filter method and photoactive gel method will each find use under specific assay constraints. The MWCO filter method should be employed (1) when binding partners in a pair differ considerably in molecular mass and (2) to immobilize the larger of two binding partners. Even with this rigid constraint, the MWCO filter is well-suited to measuring antibody-antigen interactions under native conditions (i.e., no covalent attachment) or for hydrophobic species. On this latter point, after exposure of the photoactive gel to UV, the gel becomes hydrophobic[7,73] and exhibits notable non-specific adsorption of hydrophobic species (lectins, carbohydrate-binding proteins)[88]. A phenomenon not observed with the MWCO filter. The photoactive gel is well-suited to study of binding between analytes of similar molecular mass. Both immobilization methods use electrophoresis to introduce analyte into the channels and, therefore, buffers used will need to support electrophoresis. The majority of proteins in their native state have isoelectric points below 7.5 and a typical buffer used for electrophoresis will have a pH 8-9. In addition, for the MWCO filter method, the gels can be reused up to 20 times by reversing the field and clearing out the complex in the filter with clear buffer. However, with the photoactive gels, the gels are limited to a single use. For both methods, after use the polyacrylamide gels can be removed from the microchannel network and chips re-used with new gels. Both the MWCO filter and photoactive gel methods were designed for adoption by well-equipped biology laboratories. In addition to microdevices, standard equipment and reagents (e.g, epi-fluorescence microscopes, polyacrylamide gel precursors) are required."

4.4 Conclusions

Here we report on the design, development, optimization, and characterization of KPAGE, a rapid, quantitative microfluidic-binding assay for direct quantification of kinetic rates for immunoreagent selection and quality assessment. We characterize each of two different methods of antibody immobilization: immobilization via a MWCO filter (where antibody is immobilized via size exclusion at a gel pore-size interface) and immobilization via a photoactive gel (where antibody is covalently attached to a polyacrylamide gel matrix via masking and UV exposure). A major KPAGE design consideration is fulfilled by allowing for pseudo-homogeneous reaction conditions, as compared to transport-limited heterogeneous systems such as SPR. Empirical and numerical analyses of the KPAGE assay were performed and suggest that this system is well-suited to measure a wide range of antibody – antigen binding pairs with association rates ranging from $1 \times 10^4\ M^{-1}s^{-1}$ to $1 \times 10^6\ M^{-1}s^{-1}$ and dissociation rates that range from $k_{off} = 4.5 \times 10^{-5}\ s^{-1}$ - $2.7 \times 10^{-1}\ s^{-1}$ to ultra-high dissociating pairs such as human serum albumin and ketoprofen. Characterization of k_{on} and k_{off} was performed for the well-characterized and widely reported PSA-monoclonal antibody pair. This low-infrastructure KPAGE assay provides a feasible means to realize rapid, quantitative, antibody screening, without the need for complex data interpretation or immobilization schemes. We see KPAGE as a potentially powerful binding screening assay to assess important but difficult to characterize interaction kinetics, such as protein-protein and protein-DNA.

Chapter 5. Kinetic rate determination enabled by electrophoresis in a microfluidic variable cross-section geometry polyacrylamide gel

Based on manuscript in preparation by Kapil, M. A., Pan, Y., Duncombe, T. A., & Herr, A. E. (2015).

5.0 Abstract

Antibodies are considered the workhorse molecular probe in the life sciences, clinical chemistry, and clinical medicine. There are over a million antibodies in production and massive libraries of protein-engineered antibodies being developed for a variety of therapeutics. Currently, there are no standard methods used for selecting and validating an antibody for an application of interest and problems with non-specific antibody binding, sensitivity, and reproducibility remain a major concern. High throughput, efficient, and easily adoptable analytical tools for the validation and selection of reliable antibody reagents would have a widespread impact. Therefore, we introduce the freestanding kinetic polyacrylamide gel electrophoresis (fsKPAGE) microfluidic assay that directly measures antibody−antigen association and dissociation rate constants, k_{on} and k_{off} in a single experiment. Here, antibody is immobilized in a single channel of varying cross-sectional widths allowing for precise control of the local electric field strengths. Fluorescently labeled antigen is then electrophoresed through the immobilized antibody. Upon crossing, the interaction yields a zone of immobilized immunocomplex and k_{on} is quantified by assessing the amount of immunocomplex that forms for a range of antigen− antibody interaction times determined by the local electric field strengths dictated by the geometry of the gel structure (channel width). To quantify k_{off}, immobilized zones of immunocomplex is subjected a buffer dilution. We determine k_{on} and k_{off} for prostate-specific antigen (PSA) and compare to gold-standard values. The fsKPAGE assay utilizes standard biology equipment and can be performed in a single experiment under 20 min, requiring only 45 ng of often limited antibody material. Thus, this technology offers a quantitative antibody-screening tool.

5.1 Introduction

Antibodies are critical reagents used from bench-to-bedside in approaches such as immunohistochemistry (IHC), ELISA's, western blots, immunoprecipitation (IP), to detect antigens of interest for a variety of research and diagnostic applications[89,90,91,92,93,94,95,96,97,98,99,100,101]. Currently there are over a million antibodies in production and many pharmaceutical and research institutions producing libraries of synthetic antibodies for a myriad of therapeutics [102,103,104,105.] Nevertheless, false positives (non-specific binding), false negatives (low specificity) and reproducibility (lot-to-lot, vendor variability) remain problematic and validation and selection of antibody reagent presents a critical challenge.

Currently, there are no consistent methods for the selection of the most widely used class of protein-binding reagent, antibodies[106,107]. Technologies that screen and characterize antibodies are laborious and time consuming. Methods such as enzyme linked immunosorbent assays (ELISA) and Surface Plasmon Resonance (SPR) provide initial screening but have limited kinetic information and are performed in a low throughput fashion. Antibodies are typically selected by conducting a series of time consuming and laborious equilibrium experiments, where the dissociation constant, K_d is determined. The K_d describes the dynamic equilibrium between the dissociation (unbinding) and association (binding) kinetic rates, $K_d = k_{off}/k_{on}$. Both ELISA and SPR are severely limited, as they do not provide, k_{off} & k_{on} independently due to mass transport limitations[108]. . Although K_d is widely used for antibody selection – and can be related to kinetic association and dissociation rate constants (k_{on} *and* k_{off}) – quantifying the association and dissociation rates directly and independently provides more specific information on binding

and unbinding. In other words, two antibodies with identical K_d values can have dramatically different binding kinetics, making performance for a specific application difficult to predict and making that metric of validation invalid. Hence, both k_{on} *and* k_{off} are needed for successful validation and selection criteria of immunoreagent [47,48,49,31,32,33]. Consequently, scalable, efficient, and easily adoptable analytical tools for informed selection of reliable antibody reagents would have wide impact. Previous work in this area produced by our group demonstrated kinetic measurements made in a polyacrylamide gel microfluidic chip format called kinetic polyacrylamide gel electrophoresis (KPAGE) [109]. In this study, an antigen zone is electrophoresed through a zone of immobilized antibody. Upon crossing, the interaction yields a zone of immobilized immunocomplex. $k_{on,}$ is quantified by assessing immunocomplex formation for a range of antigen-antibody interaction times. In KPAGE, interaction time is controlled by the velocity of the electromigrating antigen zone, which is determined by the strength of the applied electric field. Although parallelization is an option for this system, an important drawback from this work is that each data point that makes up the binding association curves are performed one at a time. A rapid, quantitative microfluidic-binding assay that can directly quantify kinetic rates in a single experiment could greatly improve immunoreagent validation, quality assessment, and selection. Therefore, we introduce a microfluidic free standing kinetic polyacrylamide gel electrophoresis (fsKPAGE) assay that asses important but difficult to characterize binding kinetic rates for protein-protein interactions using a easily adoptable format.

Here, antibody is immobilized in series in a single channel with varying cross-sectional channel widths. A form factor of a 96 well plate was used to utilize standard biology laboratory liquid handling technologies to allow for widespread adoptability. Antigen is then electrophoresed over the immobilized antibody for a given interaction time t_c dictated by the cross-sectional geometry. The interaction time is controlled by the local electric field, E which is inversely proportional to the channel width, where the electric field is dependent on the width of the channel, as defined by ohms law, where E=V/L=IR/L, which then leads to

$$E=I\rho/(wH) \quad (1)$$

which is directly proportional to the analyte electrophoretic velocity, $E \propto u$. The interaction time is then determined by the speed of the analyte, electrophoretic velocity. Association rates can then be determined in a single experiment by quantifying the amount of immunocomplex that forms for a given interaction time controlled by variable cross-sectional geometry. Subsequently, buffer is electrophoresed over immobilized immunocomplex and k_{off} rates are determined for further antibody validation.

5.2 Materials and methods

Apparatus and imaging

To quantify the amount of complex formed for association and dissociation rates, fluorescence images were collected using an inverted epi-fluorescence microscope equipped with CCD camera, filter cubes and an automated *x-y* stage as well. Large area imaging of the entire device was performed with a scan slide function controlled by Metamorph software (Molecular Devices, Sunnyvale, CA). A 2X objective (PlanApo, N.A. = 0.08, Olympus, Center Valley,PA) was used and the CCD exposure time was set to 100 ms. To quantify mobilities of antigen, images were collected using a ChemiDoc XRS Universal Hood II (Bio-Rad, Hercules, CA). Custom-made macros were developed and image analysis was conducted using ImageJ software (NIH, Bethesda, MD). Intensity plots were extracted by taking a region of interest (ROI) across the longitudinal axis of the gel. Post processing was performed using in-house algorithms implemented with MATLAB (R2014a) made by MathWorks (Natick, MA). A non-contact infrared thermometer with laser targeting (Westward 2ZB46) was used to determine gel temperature during electrophoresis.

Reagents: Solutions of 30% (w/v) (29 : 1) acrylamide/bisacrylamide were purchased from Sigma Aldrich (St. Louis, MO). Photoinitiator 2,2-azobis[2-methyl-N-(2-hydroxyethyl) propionamide] (VA-086) was purchased from Wako Chemical (Richmond, VA). GelBond PAG film and Gel Slick glass plate coating were purchased from Lonza (Base, Switzerland). Photo-masks were designed using AutoCAD 2013 (Autodesk, Inc., San Rafael, CA) and printed on mylar transparencies at CAD/Art Services (Brandon, OR). 10x Tris-glycine native electrophoresis buffer (25 mM Tris, 192 mM glycine, pH 8.3) was purchased from Bio-Rad. Benzophenone methacrylamide monomer (BPMA, (N-[3-[(4-benzoylphenyl)formamido]propyl] methacrylamide) was synthesized and characterized by PharamAgra Labs Inc. Stocks of BMPA at 100 mM in DMSO were stored at −20 °C until use. Proteins and antibodies were fluorescently labeled in-house using Alexa Fluor 488 and 568 protein labeling kits from Invitrogen and purified by Bio-Gel columns from Bio-Rad. Purified prostate specific antigen (PSA) and Anti-Prostate Specific Antigen antibody were purchased from Abcam. Alexa Fluor 568 Goat Anti-Mouse IgG (H+L) antibody was purchased from Life Technologies Corporation. For ELISA equilibrium experiments, white opaque 96 well microplates, were purchased (Thermo Fisher Scientific Inc., Waltham, MA). The microplate was incubated with 70µL of 0.01 nM of PSA monoclonal antibody labeled in Alexa Fluor 568 for 2 hours in room temperature on an Orbitron shaker. The microplate was then washed out 3 times using 1X tris-glycine and subsequently incubated with blocking buffer made of 1X tris-glycine and 1% bovine serum albumin (BSA) for 2 hours to prevent non specific binding. Free BSA was then washed out of each well 3 times with 1X tris-glycine. PSA labeled in Alexa Fluor 488 was then added to each well at 70µL raging in concentrations form 0.009 – 20 nM (n=3 for each concentration) and was incubated in room temperature until the reaction reached equilibrium for 1 hour. Each micro plate had three rows used for controls; one for blank wells, one for wells with just antibody, and one with wells with PSA incubated at max and min concentrations. The micro plates were imaged after PSA antibody immobilization on the plate and after PSA incubation using a fluorescence microplate reader (Tecan Infinite microplate reader, Mannedorf, Switzerland).

FsKPAGE Device Fabrication and Operation.

FsKPAGE devices were fabricated via UV photopatterning as described previosly[110]. The precursor solution contained 6% T acrylamide (w/v), 3.3% C bis-acrylamide cross-linker (w/w), and 0.5% VA-086 photoinitiator (w/v) and 2.5mM of BMPA. Prior to UV exposure, the precursor solution was degassed for 5 min under house vacuum with sonication. For FsKPAGE device fabrication a borosilicate glass substrate was used to place a mask that contained the device layout and features. Next a surface-functionalized polymer sheet (Gelbond) was placed on top of the mask. Two spacers, purchased from C.B.S scientific (MVS-0508R: Mini-Vertical Gel Wrap Spacer Set 0.5mm Thick x 8cm, Del Mar, CA) with a predefined thickness were aligned on two sides of Gelbond. Another glass plate was then laid on top of spacers. The precursor solution was pipetted into the gap between the Gelbond and the glass cover to attain a height of 500 μm. The precursor solution was then exposed to UV light through a 390 nm long pass filter to prevent BMPA activation (purchased from Edmund Optics, Barrington, NJ). The intensity of UV and UV exposure times were optimized for 6%T monomer concentration with 0.5% VOA86 at 30 mW/cm2 and 600 s exposure (measured by OAI 308 UV intensity meter, OAI, San Jose, CA). After UV exposure, the polymerized fsKPAGE devices were gently washed with water to remove unpolymerized monomers. After photopatterning, the fsKPAGE devices were soaked in run buffer for 15 min on an Orbitron shaker. When removed, a Rainin P2 pipet tip was connected to house vacuum and was applied to each well to remove residual unpolymerized monomers or run buffer via suction. fsKPAGE device was then placed into a custom made manifold for imaging and buffer wash steps (Figure 5.1). Two electrode wicks wetted with run buffer were aligned on top of both ends of the gel. Graphite electrodes were placed in contact with the electrode wicks. Sample solution was then manually pipetted into the sample wells at a volume of 0.05μL. The electrodes were then connected to an external high-voltage power supplier (Power-Pac HV; Bio-Rad Laboratories).

Figure 5.1: Custom made 3 dimensional printed manifold for imaging and buffer wash steps

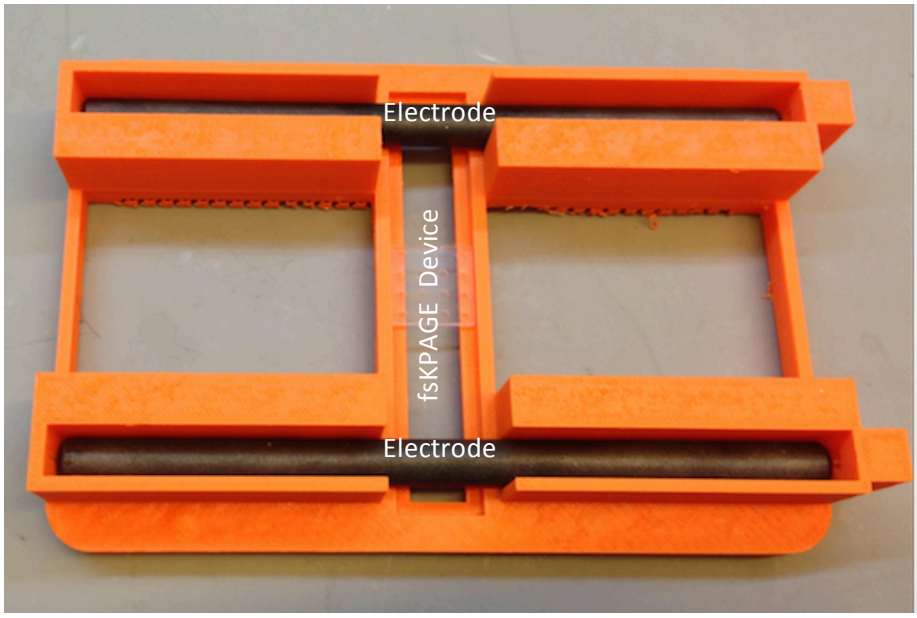

Figure 5.1: Custom made 3 dimensional printed manifold for imaging and buffer wash steps. The fsKPAGE device was cut such that extra gel bond surrounded the parameter of the gel and was placed in manifold. A Makerbot Replica 2 was used using an ABS true orange filament. Two electrode wicks were cut into 20 mm pieces (Electrode wicks long size, Filter cardboard, 240 x 6 x 1 mm, SERVA Electrophoresis GmbH, Heidelberg, Germany) and wetted with run buffer and aligned on top of both ends of the fsKPAGE device. Graphite electrodes were placed in contact with the electrode wicks. The electrodes were then connected to an external high-voltage power supplier (Power-Pac HV; Bio-Rad Laboratories).

FsKPAGE assay protocol:
To conduct fsKPAGE, first 0.05µL of antibody (Ab) (425 nM) was pippeted into the each well and electrophoretically injected into the channel longitudinally with an applied voltage of 855 V for 60 s (Step 1 of Figure 5.3B). Covalent attachment of Ab to the benzophenone containing polyacrylamide gel occurred through UV exposure via the Chemidoc Universal Hood II. Flood UV (350–365 nm) light was exposed to the gel with the gel facing the UV immersed in buffer for 6 min (see figure 5.2 for exposure time optimization). After UV exposure, unbound Ab was electrophoresed out of the gel in the transverse direction (Step 2 of Figure 5.3 B). Next, 0.05µL of antigen (Ag) (5.65 µM) was electrophoretically injected into each distinct cross-sectional area of the channel longitudinally with an applied voltage of 855 V for 30-60 s (Step 3 of Figure 5.3 B). The corresponding channel widths control the local electric fields and hence Ag mobilities and band-crossing interaction times (t_c) allowing interactions times in the range $10\ s < t_c < 60\ s$ (Step 4 of Figure 5.3 B). Fluorescence images of the entire device were collected continually during antibody-antigen interaction using the Chemidoc. This enabled monitoring of the immunocomplex formation and direct measurement of Ab-Ag interaction times for each distinct cross-sectional area. Ab-Ag are able to interact at 6 distinct t_c, forming immunocomplex. Unbound Ag is then electrophoretically washed off in the transverse direction (Step 5-6 of Figure 5.3 B). The gel was subsequently imaged using an epi-fluorescence microscope and the amount of complex formed was then quantified via area under the curve (AUC) analysis. The amount of immunocomplex that forms is directly proportional to the amount of time the Ab-Ag interacts. The dissociation rate determination was performed by electrophoresing buffer in the transverse direction, diluting the immunocomplex that was formed in steps 1-5 with a set dilution time (t_d). In this step, the time-dependent decay of the complex signal allows determination of k_{off}. Here, complex was subjected to buffer dilution for a dilution time (t_d) of 120 min while monitored *via* epi-fluorescence imaging. (See table 5.1 for voltage protocol used).

Figure 5.2: Protein capture optimization with polyacrylamide gel polymerization with benzophenone: Exposure time optimization via the Chemidoc Universal Hood II

The precursor solution contained 15% T acrylamide (w/v), 3.3% C bis-acrylamide cross-linker (w/w), and 1% VA-086 photoinitiator (w/v) and 1.6mM of BMPA. Prior to UV exposure, the precursor solution was degassed for 5 min under house vacuum with sonication. The free standing polyacrylamide gel was fabricated as stated in the methods section using a single channel mask with 1 mm square wells with a total gel thickness ~500 µm. The precursor was photo-polymerized with UV light until completion with and without a 390 nm long pass filter. The 390 nm long pass filter was used to prevent BMPA activation (purchased from Edmund Optics, Barrington, NJ) at 20 mW/cm2 for 60 s and 30 s without the filter. After polymerization, 1 µM of Ovalbumin (OVA, 45 kDa), Bovine Serum Albumin (BSA, 67 kDa) both labeled in Alexa Fluor 488 dye (purchased from Life Technologies Corporation) were injected into the gel via electrophoresis at 100 V/cm. After protein injection, the gel was exposed to UV light at (350–365 nm) for 1 and 6 min to photo-immobilize the proteins. The gels were then imaged after being soaked in buffer at times 0, 9, 18, 27 and 36 hours to determine protein loss due to diffusion and capture efficiency. With the long pass filter there is still signal at long diffusion times of 36 hours, with up to 6.73% non-specific binding of protein to the gel.

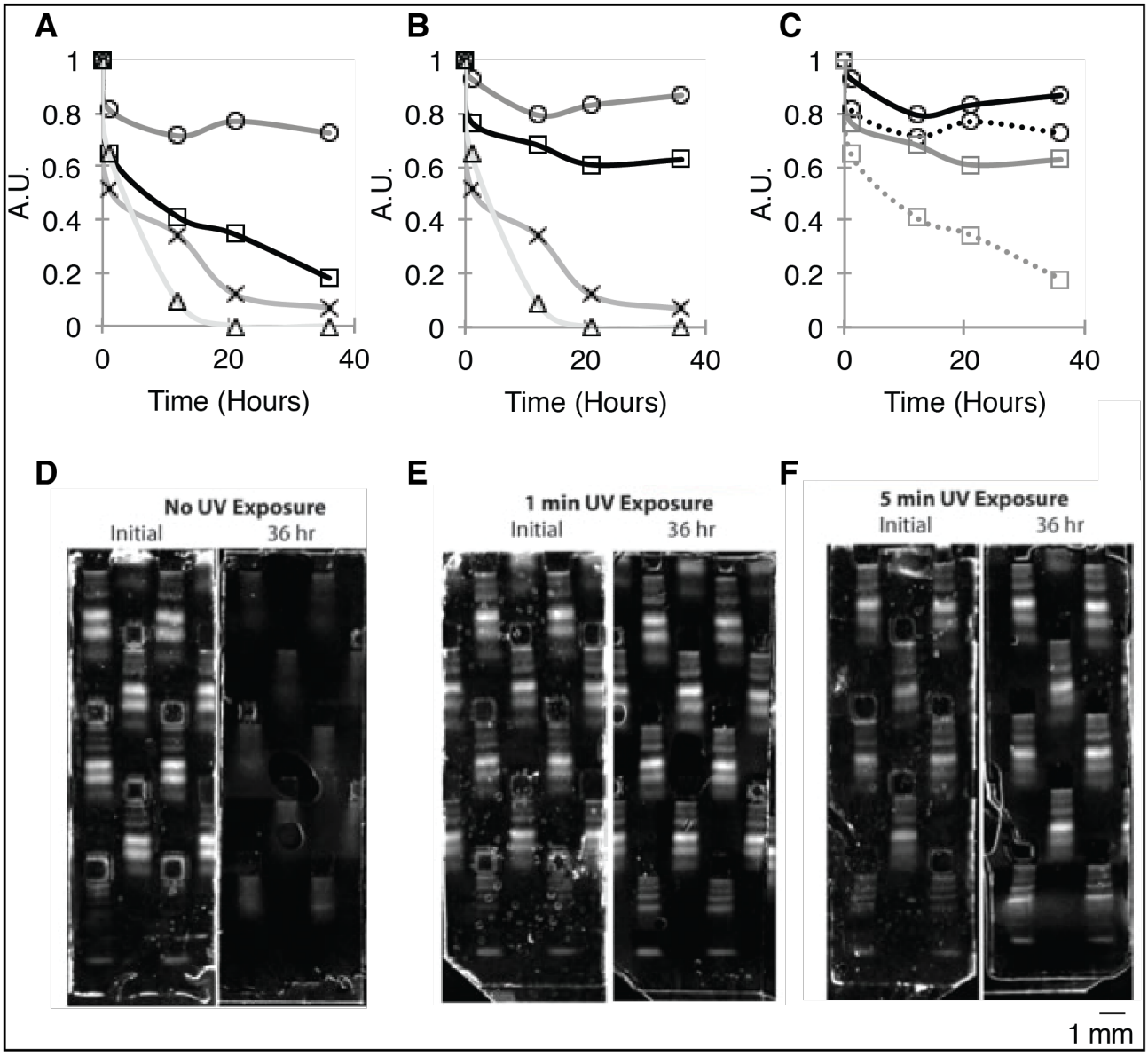

Figure 5.2: Protein capture optimization of polyacrylamide gel with benzophenone photo-polymerized with and without a 390nm long pass filter with UV exposure capture times of 1 min and 5 min with the Chemidoc Universal Hood II. Gels were then stored in buffer, allowing for protein to be diffused out at times 0, 9, 18, 27 and 36 hours. **A)** 1 min Chemidoc UV exposure protein capture using the long pass filter (circle), without the long pass filter (square), with no Chemidoc UV exposure with the long pass filter (x) and no Chemidoc UV exposure with out the long pass filter (triangle) at times 0, 9, 18, 27 and 36 hours in a bath of buffer. **B)** 5 min Chemidoc UV exposure protein capture using the long pass filter (circle), without the long pass filter (square), with no Chemidoc UV exposure with the long pass filter (x) and no Chemidoc UV exposure with out the long pass filter (triangle) at times 0, 9, 18, 27 and

36 hours in a bath of buffer. B) 5 min and 1 min Chemidoc UV exposure comparison: Captured protein using the long pass filter at 5 and 1 min exposure times (circle with the solid line at 5 min and circle with dotted line for 1 min), without the long pass filter (square with the solid line at 5 min and square with dotted line for 1 min). There is a 28% increase in capture efficiency using the long pass filter and 16 % increase in capture using the 5 min Chemidoc UV exposure with the long pass filter vs. 1 min Chemidoc UV exposure with the long pass filter. **C)** Images of BSA and OVA injected into lanes of photo-polymerized BPMA free standing polyacrylamide gels using the long pass filter with and without out protein captured into gels exposed to 1 min and 5 min exposure times with the Chemidoc. With the long pass filter there is still signal at long diffusion times of 36 hours, with up to 6.73% non-specific binding of protein to the gel.

fsKPAGE Steps	**Applied Voltage (V/cm)**	**Time (s)**
Antibody Loading	100	60
UV Exposure	-	300
Antibody Wash	100	300
Antigen Injection	100	30
Antigen Wash	100	300
Buffer wash	100	300-7200

Table 5.1. Voltage protocol for fsKPAGE assays, total assay time for association rates is less 20 min and association rates buffer dilution can vary from 5 min to 2 hours.

Estimation of interaction time, t_c: For k_{on} measurements, the t_c was defined as the time required for a plug of antigen to traverse through the immobilized Ab. Images of fluorescent antigen electromigrating through the immobilized Ab plug were taken, This capture region was designed such that we could obtain interaction times before the reaction reached equilibrium. The interaction time was then determined by computing the analyte electrophoretic velocity, u_{ag}, divided by the width of the antigen (w_{ag}) zone moving through the immobilized antibody zone, where $\mathrm{tc} = \frac{W_{Ag}}{u_{Ag}}$.

Estimation of kinetic rate constants k_{on} and k_{off}: Epi-fluorescence micrographs of the immunocomplex signals for each t_c and t_d were fitted to Gaussian distributions numerically (MATLAB R2014a). The area under the curve (AUC) of the immunocomplex signal was determined by integrating the Gaussian distribution. For k_{on} and k_{off} measurements, the AUC for each immunocomplex concentration was computed for each t_c and t_d. Controls for non-specific binding were performed with non-UV exposed gels, UV exposed gels, and gels with non-specific antibody present. We employ a Langmuirian one-to-one antibody-to-antigen binding model[47]. We choose this model as monoclonal antibody purification is known to result in protein unfolding, misfolding, and aggregation that may yield only one active binding site [74,75]. Experimental data was fit to the binding association and dissociation expressions to extract kinetic rates[31].

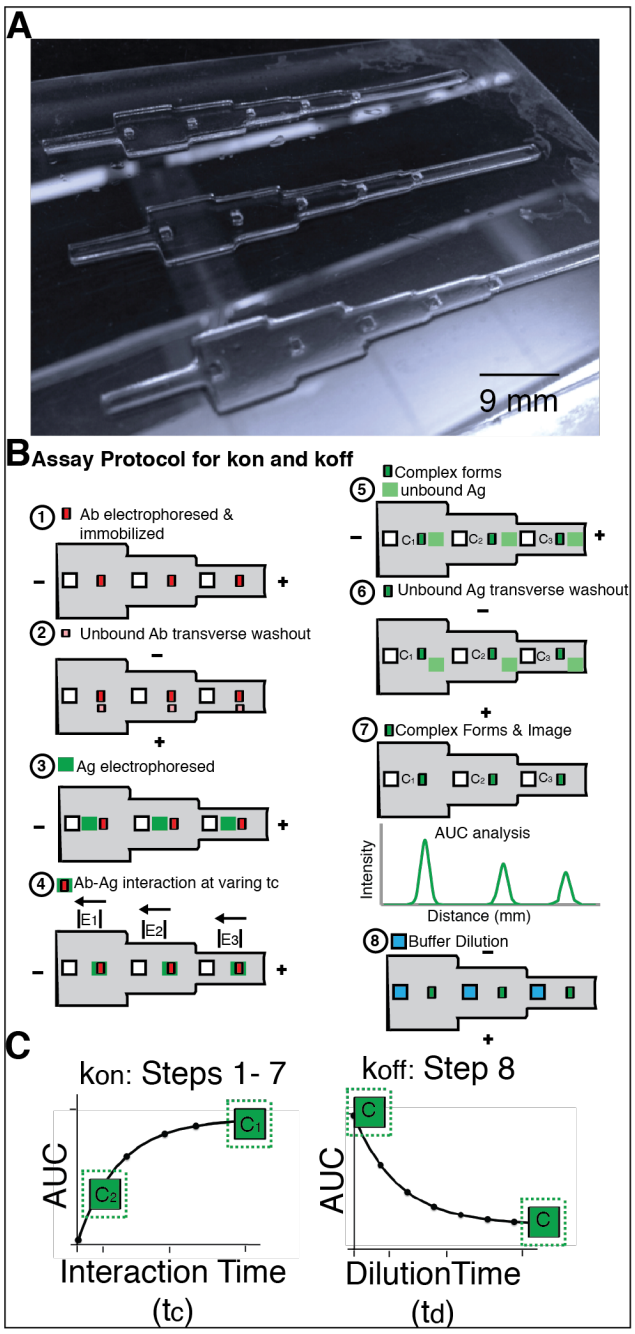

Figure 5.3 Free Standing Kinetic Polyacrylamide Gel Electrophoresis (fsKPAGE) enables rapid, quantitative measurements of antibody-antigen (Ab-Ag) binding kinetics. (A) fsKAPGE device fabricated using a photoactive polyacrylamide gel. The device geometry has 6 district cross-sectional channel widths allowing for precise control of the local electric fields, which dictates analyte velocity and interaction times. (B) k_{on} and k_{off} determination can be completed in 8 steps. Step 1. Immobilization of Antibody: Ab is pipetted directly into the wells and then electrophoresised into the channel and immobilized via UV exposure Step 2. Unbound Ab is washed out in the transverse direction Step 3. Ag is loaded into the wells and injected into the channel Step 4. Ab-Ag interacts at 6 distinct interaction times (t_c) dictated by the local electric fields (E_1-E_6) Step's 5 & 6. Complex forms and unbound Ag is electrophoretically washed off in

the transverse direction Step 7. After complex forms, the gel is imaged and quantification of immunocomplex is performed via AUC analysis: the amount of complex that forms is directly proportional to the amount of time the Ab-Ag Step 8. Dissociation rate determination. Buffer is electrophoresed over the complex and with a set dilution time (t_d), The time-dependent decay in the complex signal allows determination of k_{off}.

5.3 Results and discussion

FsKPAGE assay design.
In designing this assay, we sought to use the gel geometry to control the antibody-antigen interaction times to determine kinetic rates in a single experiment. Zones of antibody was chosen to be immobilized within a single channel and antigen to be electrophoresed through the immobilized antibody, interacting with the antibody for a given interaction time based on the cross-sectional geometry. The velocity of the antigen, u_{ag} depends on the electrophoretic mobility of the antigen, μ_{ag}, and the local electric field E, where

$$u_{ag} = E\mu_{Ag} \quad (1)$$

and time the antigen interacts with the immobilized antibody is defined as

$$t_c = \frac{w_{Ag}}{E\mu_{Ag}} \quad (2)$$

where t_c depends on $w_{Ag,}$ the width of the antigen plug and most importantly the local electric field strength. We chose to design our assay to have a form factor that is compatible with conventional laboratory liquid handling technologies (e.g., handheld multichannel pipettors, automated robotic fluid delivery systems). The lengths of each cross-sectional region were designed to match the 96 well-plate form factor, with well-to-well distances of each matching the well-to-well distances of the 96 well-plate. This allows for up to 8 distinct cross-sectional regions to be implemented in series for up to 8 immunocomplexes formed during a single experiment. The 96 well-plate form factor also allows for up to 12 experiments performed in parallel.

With the length of each distinct cross sectional-area constrained by the 96 well-plate form, we sought to understand how the cross-sectional area (width) affects local electric field for a given applied voltage. By applying a voltage across a channel with antibody immobilized in distinct regions in series, the local electric field can be controlled by increasing or decreasing the local resistance. The resistance is defined as $R=\rho L/A$ where ρ is the electrical resistivity of the buffer L *is* the channel length and A is the cross sectional area of the channel which is greatly dependent on the width (w) and height of the channel (H), $A = w\ x\ H$. Since L and H are constant through each cross sectional region, the electric field is dependent on the width of the channel, as defined by ohms law, where E=V/L=IR/L, which then leads to equation 1 as introduced in the introduction. $E=I\rho/(wH)$.

In order to make association rate measurements of typical Ab-Ag pairs with low and intermediate binding kinetics, interactions times must range above and below the time it takes for the reaction to reach equilibrium with τ_{eq} ranging from $10\ s < \tau_{eq} < 20\ s$ [109]. For a given antigen with a given electrophoretic mobility, the analytical solution for fsKPAGE assay implemented geometry with channel widths ranging from 3 to 8 mm. The channel widths were chosen such that for a given applied voltage, we could obtain interaction times above and below the equilibrium time. With an applied voltage of 100 V/cm, the field strength throughout each distinct cross-sectional area remains constant through each section in both the transverse and longitudinal direction allowing for tight control of Ab-Ag interaction times (see figure 5.4). The

interaction times were analytically calculated for free PSA[76] to a monoclonal antibody with an measured electrophoretic mobility of 6.8×10^5 $cm^2 V^{-1} s^{-1}$. Depending on the applied voltage, analytical interaction times range from 6 – 60 s with corresponding electric fields ranging from 50-200 V/cm (Figure 5.5 B subplot, where, x, circles and triangles represent, 200, 100 and 50 V/cm applied) allowing for interactions times above and below equilibrium, necessary for determining association rates. Experimentally, fsKPAGE was performed and the local e-fields and interaction times were calculated for PSA and then compared with analytical results. Two data sets were taken using a gel that had been pre-fabricated and stored in two different storage methods. One data set, (i) was taken from a gel that had been stored in 1x tris-glycine for 1 month in a aluminum foil covered petri dish in 4°C and another, data set (ii) had been incubated in fresh 1X tris-glycine for 15 min prior to use (Figure 5.5, data set (i) are the red and black diamonds and data set (ii) are the red and black squares). In data set (i), greater variation was observed with interaction times ranging from 10 – 60 ± 8 s. Data set (i) also had as much as 50 % slower interaction times than gels that had been pre-incubated in fresh 1X tris-glycine with interaction times ranging from 10 – 30 ± 1 s. In addition data set (i) differed from analytical results from calculations by 50 % in both interaction times and local e-fields in comparison to just 10 % in data set (ii). This large discrepancy in calculated results and variation in interaction times for data set (i) is due to increased concentration in ionic strength in gels that had been stored for longer times due to evaporation. Experiments were performed to test ionic strength using different storage conditions, and the conductivity of the buffer increases by as much as 50% during electrophoresis within 10 days of storage**.** This increase in ions in the buffer solution affects the electrophoretic mobility μ as it is directly proportional to the zeta potential and debye length, and as the ionic strength increases, the debye length decreases, and mobility decreases, which would slow the interaction time, as experimentally observed.

Figure 5.4: Field strength throughout each distinct cross-sectional area in the fsKPAGE device

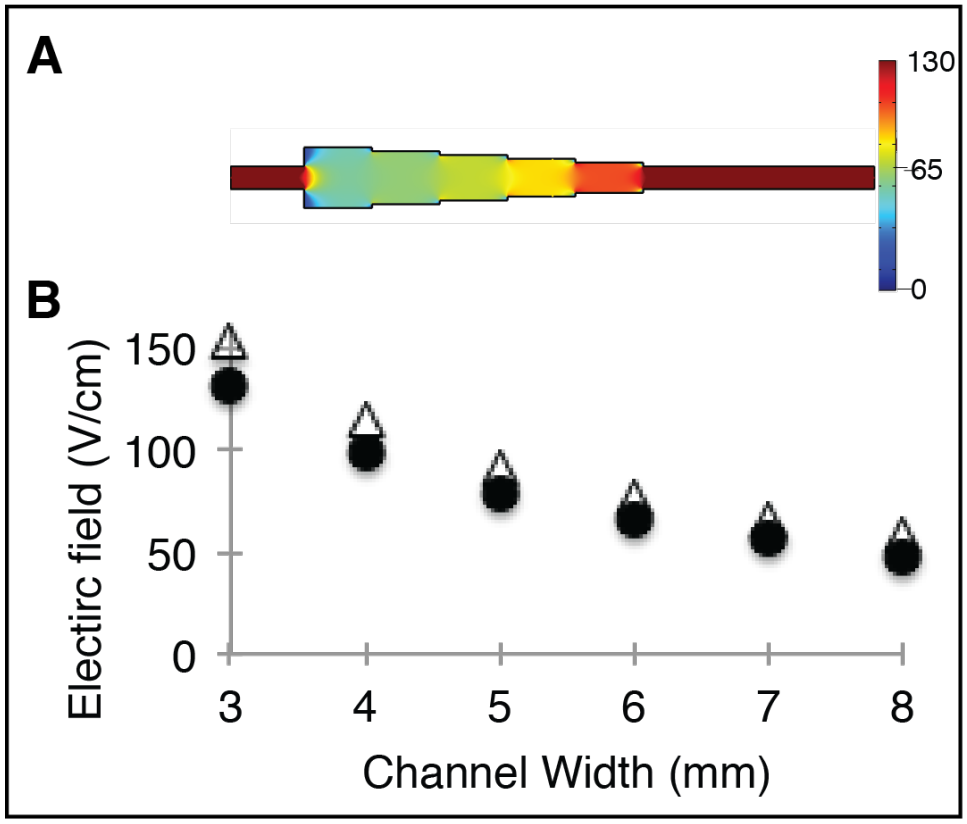

Figure 5.4: Simulations of the local electric field (e-field) were performed on COMSOL. (A) Simulations of the fsKPAGE assay with an applied voltage of 100 V/cm are shown. Local e-fields remained constant throughout each district channel width in both the transverse and longitudinal direction allowing for tight control of directionality and Ab-Ag interaction times. (B) Comparison of simulated results in red circles and analytical solutions are shown. A 20% difference from simulated results versus analytical results was found, and can be contributed to edge effects.

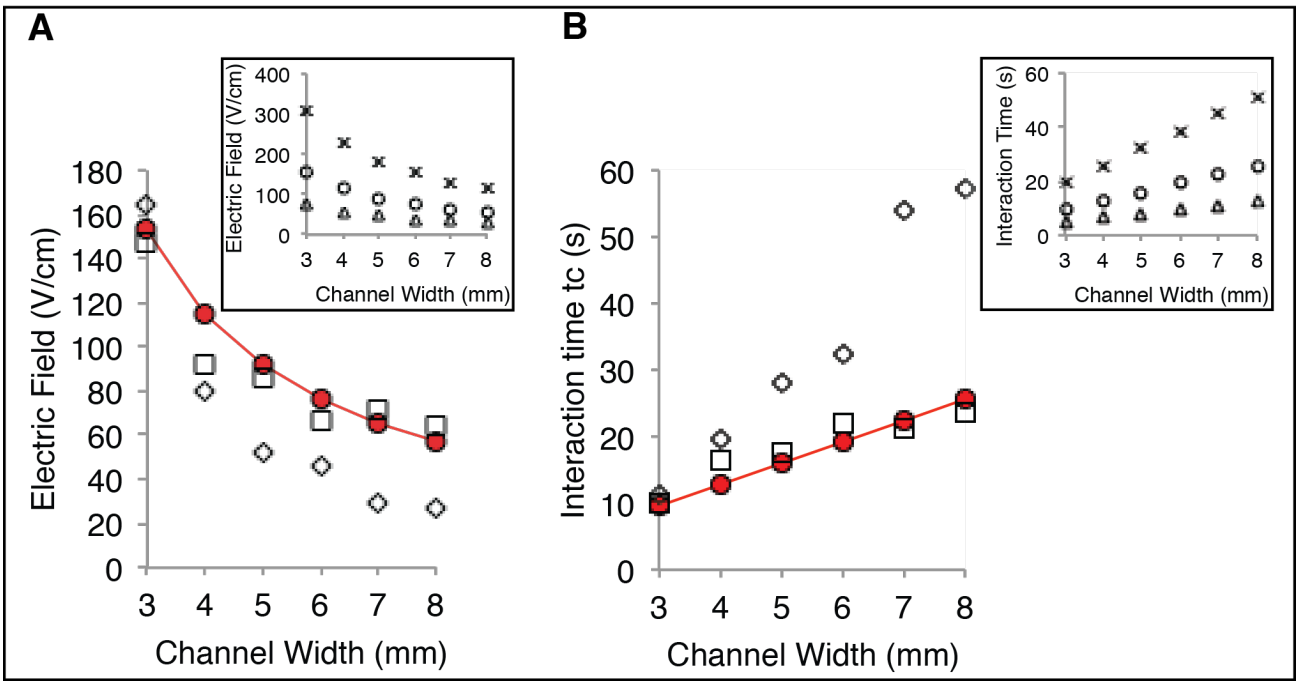

Figure 5.5 Geometry dictates local electric fields and interaction times. **A and B)** Analytical solutions of the local electric field (e-field) and interaction times were computed (red circles and line graphs) and plotted against experimental e-fields extracted from protein electrophoretic moblities (squares and diamonds at 2 different storage conditions) and observed interaction times (squares and diamonds) where the channel width is inversely proportional to the local e-field. **A and B subplot)** Analytical solutions of the fsKPAGE assay local electric fields and interaction times at increasing channel widths with an applied voltages of 50,100, and 200 V/cm, depending on the applied voltage, interaction times range from 6 – 65 s with corresponding local e-fields ranging from 24-263 V/cm where the x's, circles and triangles represent 200, 100, and 50 V/cm applied, allowing for interactions times above and below equilibrium, necessary for determining association rates.

KPAGE Determination of Association Kinetic Rate Constant, k_{on}

We applied fsKPAGE to determine k_{on} for a PSA and monoclonal antibody pair. We locally immobilized antibody by utilizing a polyacrylamide gel containing benzophenone methacrylamide monomer. This "photoactive" formulation allows UV-initiated covalent immobilization of a zone of antibody to the polyacrylamide gel through hydrogen abstraction. The antibody zone lengths ranged from 800 - 1000 μm. We performed a study of non-specific interactions in the gel using a set of control studies with three different cases. In each case, three replicates of n=3 were performed, using a new device for each replicate. In the first case (Case 1) we injected PSA in the gel that had not been exposed to UV, in (Case 2) PSA is injected into a UV exposed gel and in (Case 3) zones of off-target antibody was immobilized and PSA was subsequently injected. All of these cases were then compared to signal from immobilized on-target PSA antibody (Case 4). Here, we measured a 1.5 ± 0.2 % non-specific signal for Case 1, a 6.2 ± 1 % non-specific signal for Case 2 and in Case 3, 6.5 ± 2% was measured. All cases were then compared to signal from immobilized on-target PSA antibody (Case 4), where we measured a 90% increase in signal in comparison to Case 2 and 3. These same non-specific interactions were studied previously in a closed microfluidic chip system[109] and an increase of 50% in non-specific interactions was observed in this open gel format in case 1,2, and 3. We hypothesize that this increase in non-specific interactions is due the increase in BMPA concentration in the gel (from 1.1mM to 2.5mM), in which BPMA increases polyacrylamide hydrophobicity, and with an open gel format, evaporation during electrophoresis occurs which effectively can decreases gel pore size. Although this is a substantial increase from our previous work, the non-specific interactions occurring due to absorption in the gel does not interfere with the high signal of interest, which is 90% greater than the non-specific signal. k_{on} for the PSA and monoclonal antibody pair was then determined (Figure 5.6). FsKPAGE with covalently immobilized antibody estimated a k_{on} of 1.8 x 10^4 $M^{-1}s^{-1}$ ± 0.192 (n = 3, using a new device for each measurement) (Figure 5.6). This value was then compared to literature SPR[76] values and in house ELISA binding measurements, with computed association rates using the same buffer system used in the fsKPAGE for better comparison. SPR reported a value of 4.1 x 10^4 $M^{-1}s^{-1}$ ± 1.3 and ELISA, 2 x 10^4 $M^{-1}s^{-1}$ ± 1.03. For both ELISA and SPR, k_{on} for PSA to monoclonal antibody are within the same order of magnitude when compared to the fsKPAGE system. However both SPR and ELISA have larger run-to-run variation, 81% and 85% higher than fsKPAGE thus suggesting fsKPAGE is more reliable and robust.

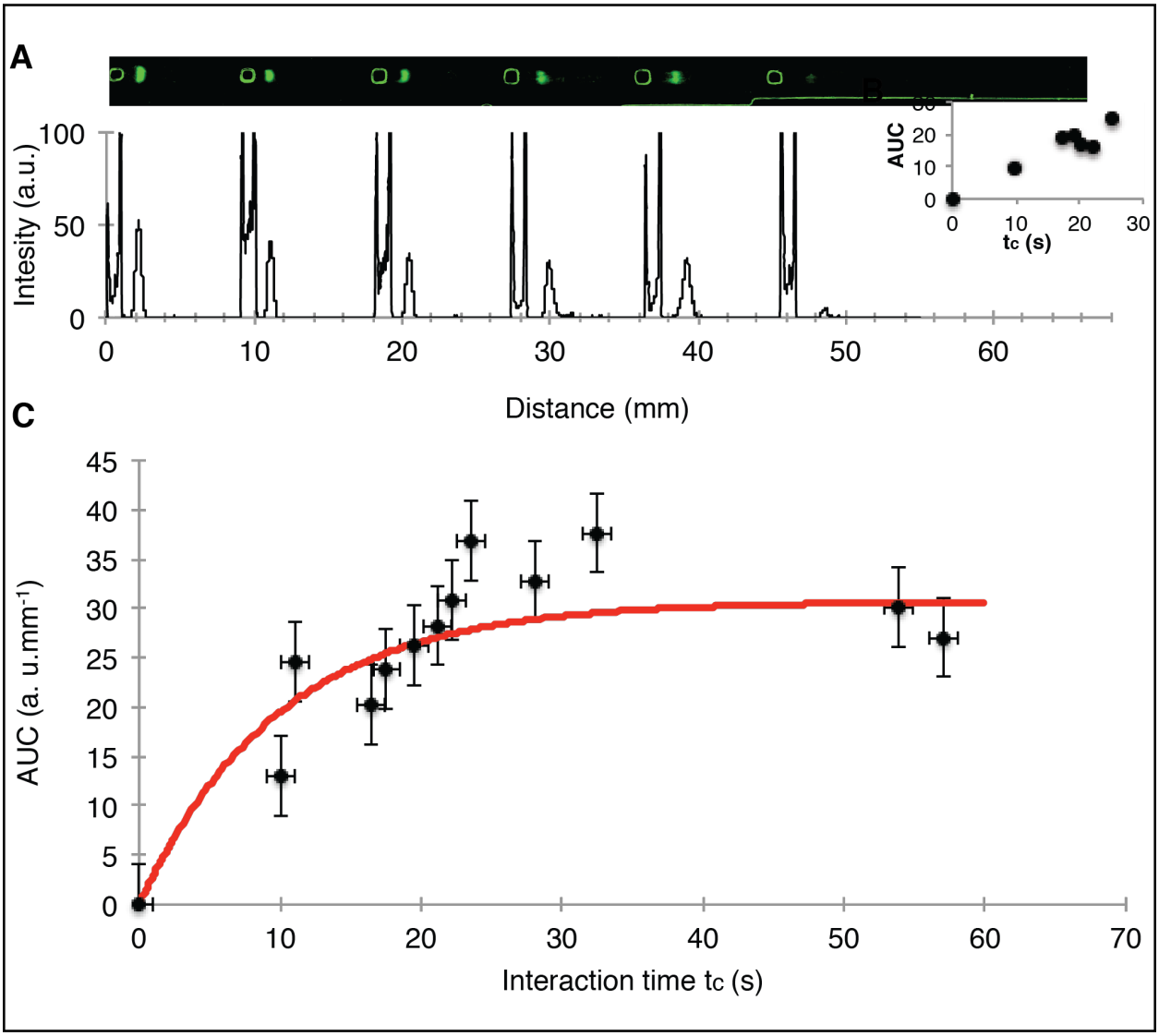

Figure 5.6 Direct determination of association rate constants with fsKPAGE. (A) Epi-fluorescence micrographs of immunocomplex signals formed after antigen (green fluorophore) has interacted with the immobilized antibody for a set interaction time, t_c. Intensity profiles of immune complex peaks at different interaction times (t_c) points ranging from 0 - 60 s are quantified and shows that as t_c increases the AUC of the immune complex peaks increases (B). (C) Black circles represent fsKPAGE measurements of PSA immune complex at different t_c . On-chip measurements of the association rate constant k_{on} was calculated from a 3-parameter binding curve fit model (red) and plotted against the measured PSA immune complex. Error bars are calculated from three replicate trials. k_{on} for the affinity interaction of PSA was 1.8×10^4 $M^{-1}s^{-1} \pm 0.19$.

KPAGE Determination of Dissociation Kinetic Rate Constant, k_{off} and computed K_d

We applied fsKPAGE to measure the dissociation rate constant of PSA and monoclonal PSA antibody pair (figure 5.7). We observed time-dependent dissociation of immunocomplex, decreasing from 100% and asymptoting to 47% at the longest dissociation times studied (i.e., 7200 s or 2 hr). FsKPAGE yielded k_{off} measurements, reporting 2.5 x 10^{-4} s^{-1} ± 2 s^{-1} . The dissociation constant K_d computed from k_{off} and k_{on} was 14 nM. Literature reports based on SPR[76] establish k_{off} for PSA as 4.5 x 10^{-5} s^{-1} ± 0.67 and in our ELISA measured dissociation rate, were determined to be as 3.0 x 10^{-5} s^{-1} ± 0.5 with computed dissociation rate constants of K_d=1.86 nM and 1.54 nM respectively. k_{off} from SPR and ELISA (pH 8.3, same as the fsKPAGE method) are both roughly an order of magnitude lower than k_{off} determined by fsKPAGE and the same order of magnitude for the computed K_d. We hypothesize that this differences in the measured values of dissociation rates stem from differences in how the fsKPAGE assay is run. The fsKPAGE assay is run at high electric fields for long dilutions times of up to 1-2 hours for a standard Ab-Ag pair. These long electrophoresis times increase assay temperature and can lead to joule heating and evaporation and hence affect dissociation.

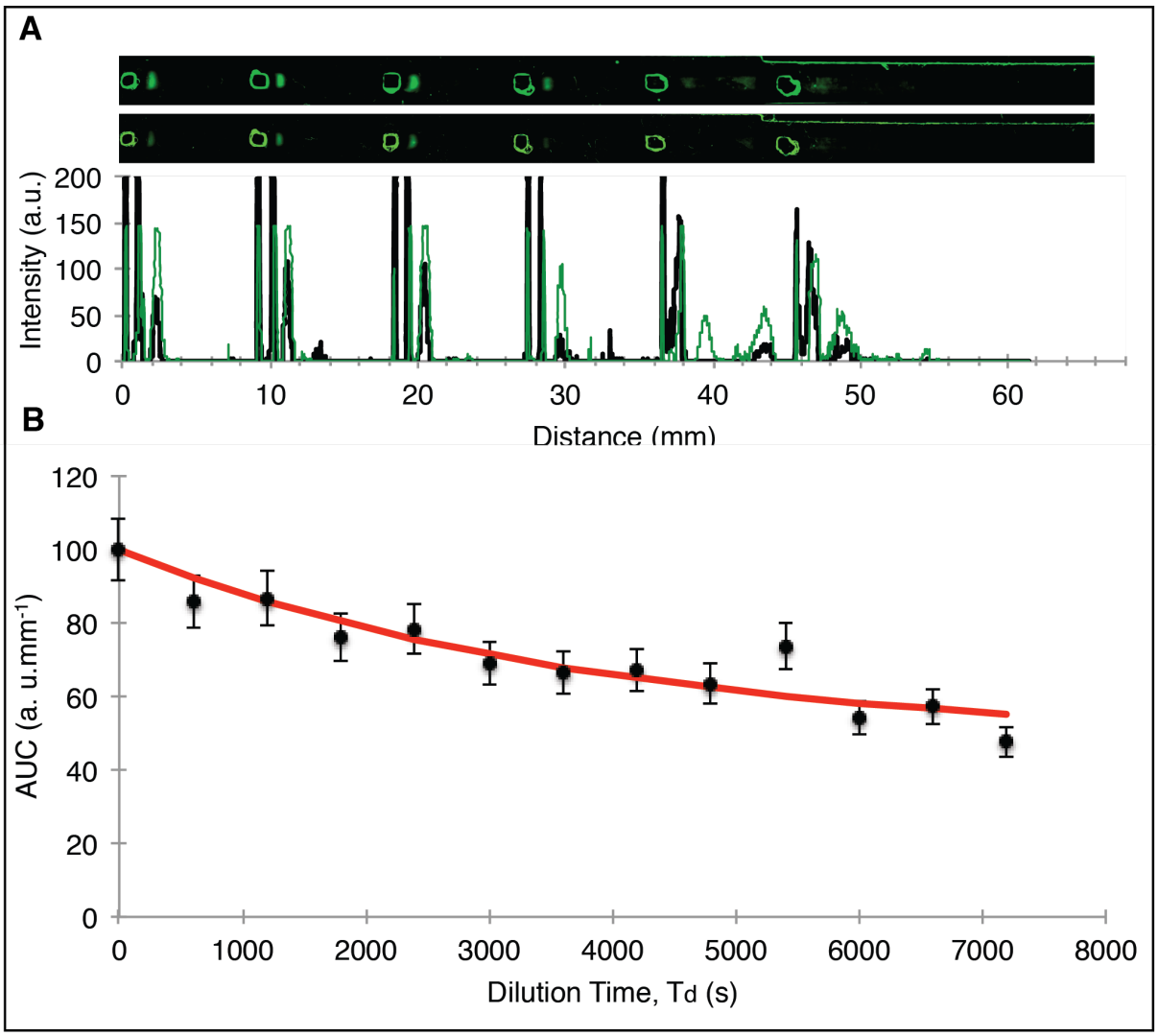

Figure 5.7 Direct determination of dissociation rate constants via fsKPAGE. (A) Epi-fluorescence micrograph time course of PSA immunocomplex dissociation (green fluorophore signal). Intensity profiles of immune complex peaks at different dilution times (t_d) points ranging from 0- 7200 s are quantified. As t_d increases the AUC of the immune complex peaks decreases. **(B)** Black circles represent fsKPAGE measurements of PSA immune complex at different t_d. Measurements of the dissociation rate constant k_{off} was calculated from a 3-parameter binding curve fit model (red) and plotted against **the measured** PSA immune complex for each t_d. Error bars are calculated from replicate trials. k_{off} was determined to be $2.5 \times 10^{-4}\ s^{-1} \pm 2$.

Thermal Effects of binding kinetics

Thermal Analysis of Open fsKPAGE **Structures**

The fsKPAGE format experiences thermal effects that affect binding kinetics in a different way than other gold standard or previously published methods such as SPR, and ELISA. fsKPAGE operates in open gel format, in which the generated joule heating is balanced by convection and evaporation. We can describe the heat balance by

$$E^2\sigma_g H = \dot{q}_C + \dot{q}_E \quad (4)$$

On the left-hand side of eq 4, we see heat generation due to electrophoretic induced joule heating given by the product of electric field (*E)*, fsKPAGE electrical conductivity (σ_g) and the height of the gel (*H*). The right-hand side represents heat loss from convection

$\dot{q}_C$ and evaporation $\dot{q}_E$, According to Langmuir's evaporation model and the Antoine

Equation describing[111] the temperature−vapor pressure relationship, both convective and evaporative heat loss increase with temperature, and equation 1 can be written as

$$E^2\sigma_g H = C_c(T_{gel} - T_{env}) + \Delta H_{Vap}(P_v - P_p)\sqrt{\frac{m}{2\pi R T_{gel}}} \quad (5)$$

where in eq 5 C_c is the heat transfer coefficient, T_{gel} and T_{env} is the temperature of the gel and environment respectively, ΔH_{Vap} is the vaporization of enthalpy, P_v and $P_p$are vapor pressure of liquid water and partial pressure of water vapor in air (at room temperature), *m* is the vapor molecule mass and *R* is the ideal gas constant. We compared the total amount of joule heating in the widest and thinnest parts of the fsKPAGE structure (8 and 3 mm wide gel) where the local electric fields are at the lowest and highest values. We experimentally measured the temperature and height of the gel after 60 and 120 s of electrophoresis at both the 8 and 3 mm width regions and analytically solved for the local temperature using eq 2 after 120 s. See below for a table 5.2 of values used and figure 5.8. The estimated gel temperature (t_{gel}) at the 8 mm wide region of the fsKPAGE structure matches experimental results with 0.54% error. The estimated gel temperature at the 3 mm wide region differs from experimental results by 45%. The higher error of the analytical estimation at the 3 mm wide region of the structure stems from the difficulty to accurately measure the partial pressure of water vapor in air. Joule Heating increases the gel temperature and accelerates the evaporation process (from 19°C to 42.4°C), which makes the moisture environment right above the gel indeterminable. Therefore, an estimated value was extracted from the empirical data of saturation pressure - temperature graphs and used for the calculation[112].

Physical and thermal changes due to thermal effects of open fsKPAGE Structures

Changes in the gel temperature and height affects binding kinetics depending on the binding pair in question. Changes in the gel temperature interfere with intermolecular binding forces that drive association or dissociation. Changes in gel height due to evaporation lead to changes in ionic strength of the buffer. For k_{on} measurements of PSA, the electrophoresis time ranges from 0-60 s. The gel height decreases due to evaporation and the local ionic strength increases by 3% and 11% in the 8mm and 3 mm width regions. Generally speaking, free ions can bind to charge groups of the antigen or antibody binding site on the epitopes or paratopes, obstructing their combination[113]. Previous studies on red cell antibodies conjugated with anti-D showed that reducing ionic strength from 0.17 to 0.03 M (6 fold decrease) increased the association rate constant 1000-fold [114]. In the fsKPAGE however, the ionic strength was increased from only

0.046 M to 0.047 and 0.051 M at the 8 and 3mm regions. Therefore, we believe that the small change in ionic strength has negligible effects on association rates and does not contribute to the differences in the observed kinetic rates.

However, we saw remarkable temperature changes during electrophoresis and we hypothesized this magnitude of temperature increase have considerable effects on association and dissociation of binding partners. Antibody-antigen interactions are known to be divided into cold and warm types in relation to their thermal optimal, which depends on the chemical nature of both the epitope and paratope and the type of bond that holds binding partners together[115]. All antigen-antibody bonds are weak physical bonds that involve primary and secondary bonds. The primary is the initial bond that first occurs when an antibody and antigen come in close contact from each other, usually a distance of several nanometers. This bond involves long-range forces such as ionic, hydrogen, and Van der Waals bonds (hydrophobic interactions). Secondary bonds hold the binding pairs together for an elapsed amount of time (ranging from milli seconds to days to even years for some pairs) and involve mostly Van der Waals forces. At that point, the overall strength of the binding depends on the goodness of fit between the two surfaces. Antibody-antigen pairs that rely on a primary hydrogen bonds and are known to be exothermic and are more stable at low temperatures, as in most carbohydrate antigen pairs[116]. Conversely, the strength of pairs that rely on a hydrophobic (combinations of hydrogen and Van der Waals) bonds increases with temperature[117]. Large temperature changes have little effects on the equilibrium constant K_d, where minimal changes were observed from temperature changes from 2 and 40 °C [118]. However in a separate study, the association and dissociation rates were shown to differ greatly as evident by an equilibrium experiment done on anti-D at 4 °C and 37 °C. In this study, the same pair with identical K_d's took 20 times longer to reach equilibrium at 4 °C that at 37 °C, proving that the association and dissociation rates independently are greatly affected by temperature separately but not quantifiable through the equilibrium constant[118,117, 119].

Comparison of gold standard methods

In this study, both the association and dissociation rates are higher in comparison to gold standard methods such as SPR and ELISA. The association rate remains within the same order of magnitude as SPR and ELISA, however increases by 25% and 65% for each respectively. Dissociation rates also increased by 80-89% in comparison to SPR and ELISA. These increases in rates are expected, as generally antibody–antigen complexes follow basic thermodynamic principles: increasing temperatures causes increases in both the association and dissociation rates and numerous previous studies have showed this overall trend [120 121 122]. Epitope mapping of PSA showed that the antigenic epitope contained a significant carbohydrate moiety and forms non-covalent hydrogen bonds [123,124]. PSA's epitope and non-covalent bond for PSA increases unbinding at higher temperatures due to the exothermic nature of hydrogen bonds.

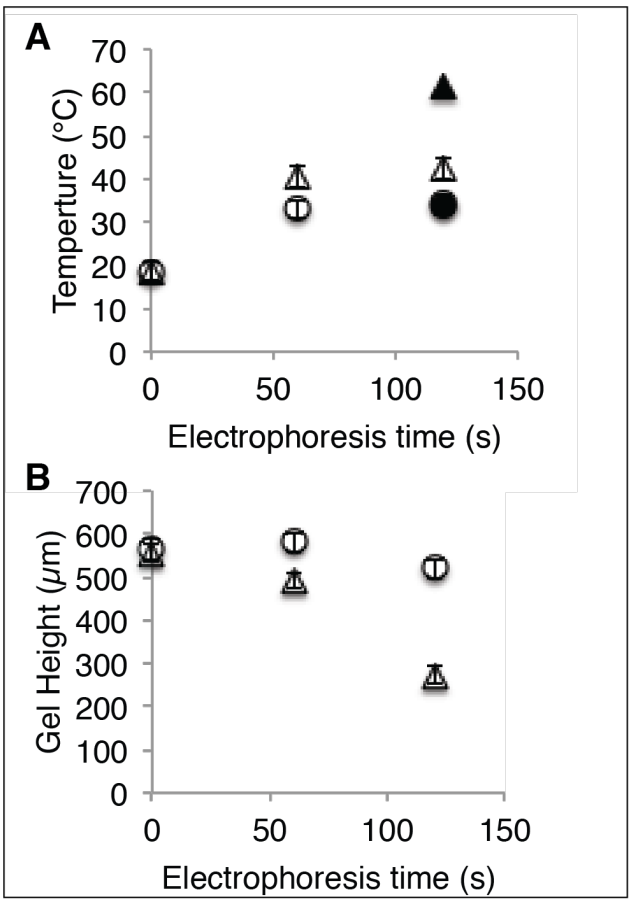

Figure 5.8 Thermal effects on Open fsKPAGE Structures during electrophoresis (A) The gel temperature increases for both the 8mm (circles) and 3 mm (triangles) width gels from 0-60 s stabilizing after 60 s. Analytical estimated values of the gel temperature were calculated for both the 8 and 3 mm width gels (black filled circle and triangle) and differ from experimental results by 0.5 and 45%. (B) Gel heights decreases minimally after electrophoresis times of 60 s, within the time frame of association rate measurements.

Table 5.2 Parameters used in analytical estimation of the temperature in gel and comparison to experimental results

Variable	Values used in analytical Solution
E (V/m) at 8mm wide gel	5736
E (V/m)	15297
σ_g (S/m)	.0389
H (m)	$5.55\ x\ 10^{-4}$
C_C (W/m^2K)	25
$T_{gel\ measured\ at\ 60\ s}$ (K) in 8mm wide gel	307
$T_{gel\ measured\ at\ 60\ s}$ (K) in 3mm wide gels	315
T_{env} (K)	291.75
ΔH_{vap} (KJ/Kg)	2257
P_v (Pa) in 8mm wide gel	4234
P_v (Pa) in 3mm wide gels	8624
P_p (Pa) in 8mm wide gel	4195
P_p (Pa) in 3mm wide gel	8279
R (J/mol K)	8.314
$T_{gel\ analytical\ estimation\ at\ 120\ s}$ (K) in 8mm wide gel	307
$T_{gel\ analytical\ estimation\ at\ 120\ s}$ (K) in 3mm wide gels	316

5.4 Conclusions

Here, we report on the design, development, optimization, and characterization of fsKPAGE, a high-throughput, quantitative microfluidic binding assay for direct quantification of kinetic rates in a single experiment. Varying the cross sectional area and designing the assay to fit a form factor easily adoptable using standard biology lab equipment fulfills a major fsKPAGE design consideration. The device geometry has 6 district channel widths allowing for precise control of the local electric field that dictates analyte velocity and interaction times. Numerical analyses of the fsKPAGE assay were performed by applying an electric field at 100 V/cm across the entire single channel with variable cross-sectional areas. Interaction times can then range from 10-60 s allowing for a vast variety of binding pairs measurable in this system. Characterization of k_{on} and k_{off} was performed for the well characterized and widely reported PSA−monoclonal antibody pair. This assay provides a feasible means to realize rapid, quantitative, antibody screening in a single experiment. We see fsKPAGE as a possible powerful binding screening assay to assess important but difficult to characterize interaction kinetics for protein-protein interaction as well as novel therapeutic development.

Chapter 6: Overall Conclusions

6.1 Conclusions

Microfluidic technologies for rapid, high-throughput screening and selection of antibodies for disease diagnostics and novel therapeutics: Selecting antibodies based on their antigen binding kinetic properties, such as their association and dissociation rate constants, k_{on} and k_{off}, can provide a quantitative metric that can further optimize and validate immunoreagent selection. These rate constants quantify the ability for an antibody to associate (bind) or dissociate (unbind) to a target analyte and determines inherent binding strength. Therefore a metric such as this has the power to eliminate problems seen by clinicians, researchers, and drug developers alike in regards to false positive, false negatives, and problems with reproducibility seen in antibody-based approaches and inform in assay design. Consequently, scalable and efficient analytical tools for informed selection of reliable antibody reagents would have wide impact. Here, we develop a rapid, quantitative quality assessment assay for screening and selection of improved immunoreagents to further the advancements of antibody-based approaches such as disease diagnostics and novel therapeutics. Here we introduce a Kinetic Polyacrylamide Gel Electrophoresis via three different approaches, K-PLE-IA, KPAGE and FsKPAGE. These microfluidic assays directly measure antibody-antigen association and dissociation rate constants, k_{on} and k_{off} and work to advances antibody-based proteomics by introducing a rapid immunoreagent quality assessment assay for the screening and selection of antibodies for disease diagnostics and novel therapeutics and provides a novel high-throughput screening tool for the development of new biomarker discovery, disease diagnostics, and novel therapies.

4.6 References

(1) Brennan, D. J., O'Connor, D. P., Rexhepaj, E., Ponten, F., & Gallagher, W. M. *Nature Reviews Cancer* **2010**, *10*, 12.
(2) Wu, A. R.; Kawahara, T. L. A.; Rapicavoli, N. A.; Riggelen, J. v.; Shroff, E. H.; Xu, L.; Felsher, D. W.; Chang, H. Y.; Quake, S. R. *Lab on a Chip* **2012**, *12*, 2190-2198.
(3) Hartmann, M.; Roeraade, J.; Stoll, D.; Templin, M.; Joos, T. *Anal Bioanal Chem* **2009**, *393*, 1407-1416.
(4) Leader, M.; Patel, J.; Makin, C.; Henry, K. *Histopathology* **1986**, *10*, 1315-1324.
(5) Ingvarsson, J.; Wingren, C.; Carlsson, A.; Ellmark, P.; Wahren, B.; Engström, G.; Harmenberg, U.; Krogh, M.; Peterson, C.; Borrebaeck, C. A. K. *Proteomics* **2008**, *8*, 2211-2219.
(6) Dedon, P. C.; Soults, J. A.; David Allis, C.; Gorovsky, M. A. *Analytical Biochemistry* **1991**, *197*, 83-90.
(7) Hughes, A. J.; Herr, A. E. *PNAS* **2012**, *109*, 21450-21455.
(8) Fitzgibbons, P. L.; Bradley, L. A.; Fatheree, L. A.; Alsabeh, R.; Fulton, R. S.; Goldsmith, J. D.; Haas, T. S.; Karabakhtsian, R. G.; Loykasek, P. A.; Marolt, M. J. *Archives of Pathology and Laboratory Medicine* **2014**.
(9) Bordeaux, J.; Welsh, A. W.; Agarwal, S.; Killiam, E.; Baquero, M. T.; Hanna, J. A.; Anagnostou, V. K.; Rimm, D. L. *Biotechniques* **2010**, *48*, 197.
(10) Towbin, H.; Staehelin, T.; Gordon, J. *Proceedings of the National Academy of Sciences of the United States of America* **1979**, *76*, 4350-4354; Burnette, W. N. *Anal Biochem* **1981**, *112*, 195-203.
(11) Wu, Y.; Li, Q.; Chen, X. Z. *Nature protocols* **2007**, *2*, 3278-84.
(12) Hou, C.; Herr, A. E. *Electrophoresis* **2008**, *29*, 3306-19.
(13) He, M.; Herr, A. E. *Journal of the American Chemical Society* **2010**, *132*, 2512-2513; He, M.; Herr, A. E. *Nature protocols* **2010**, *5*, 1844-56; Tia, S.; He, M.; Kim, D.; Herr, A. E. *Analytical Chemistry* **2011**, *83*, 3581-8.
(14) Johansen, K.; Svensson, L. In *The Protein Protocols Handbook, 2nd Edition*, Walker, J. M., Ed.; Humana Press, Inc: Totowa, NJ, 2002, p 1097.
(15) Phillips, T. M.; Wellner, E. F. *Biomed Chromatogr* **2006**, *20*, 662-7.
(16) Phillips, T. M.; Wellner, E. F. *Electrophoresis* **2007**, *28*, 3041-8.
(17) Phillips, T. M.; Wellner, E. F. *Electrophoresis* **2009**, *30*, 2307-12.
(18) Chen, H. X.; Busnel, J. M.; Peltre, G.; Zhang, X. X.; Girault, H. H. *Anal Chem* **2008**, *80*, 9583-8.
(19) Chun, H.; Chung, T. D.; Ramsey, J. M. *Anal Chem*, *82*, 6287-92.
(20) Apori, A. A.; Herr, A. E. *Analytical Chemistry* **2011**, *83*.
(21) Margolis, J.; Kenrick, K. C. *Nature* **1967**, *214*, 1334-6; Slater, G. G. *Anal Chem* **1969**, *41*, 1039-41; Margolis, J.; Kenrick, K. G. *Anal Biochem* **1968**, *25*, 347-62.
(22) Hughes, A. J.; Herr, A. E. *Anal Chem*, *82*, 3803-11.
(23) Lo, C. T.; Throckmorton, D. J.; Singh, A. K.; Herr, A. E. *Lab Chip* **2008**, *8*, 1273-9; Sommer, G. J.; Singh, A. K.; Hatch, A. V. *Lab Chip* **2009**, *9*, 2729-37.
(24) Shackman, J. G.; Munson, M. S.; Ross, D. *Anal Chem* **2007**, *79*, 565-71.
(25) Escobedo, C.; Brolo, A. G.; Gordon, R.; Sinton, D. *Anal Chem*, *82*, 10015-20.
(26) Bharadwaj, R.; Park, C. C.; Kazakova, I.; Xu, H.; Paschkewitz, J. S. *Anal Chem* **2008**, *80*, 129-34.
(27) Squires, T. M.; Messinger, R. J.; Manalis, S. R. *Nat Biotechnol* **2008**, *26*, 417-26.
(28) Urbanek, M.; Wu, X.; Vickery, K. R.; Kao, L. C.; Christenson, L. K.; Schneyer, A.; Legro, R. S.; Driscoll, D. A.; Strauss, J. F., 3rd; Dunaif, A.; Spielman, R. S. *J Clin Endocrinol Metab* **2000**, *85*, 4455-61.
(29) Tortoriello, D. V.; Sidis, Y.; Holtzman, D. A.; Holmes, W. E.; Schneyer, A. L. *Endocrinology* **2001**, *142*, 3426-34.
(30) Selby, C. *Ann Clin Biochem* **1999**, *36*.
(31) Goodrich, J. A.; Kugel, J. F. *Binding and kinetics for molecular biologists*; CSHLP: CSH, N.Y., 2007.
(32) Mironov, G. G.; Okhonin, V.; Gorelsky, S. I.; Berezovski, M. V. *Analytical Chemistry* **2011**, *83*, 2364-2370.
(33) Okhonin, V.; Petrov, A. P.; Berezovski, M.; Krylov, S. N. *Analytical Chemistry* **2006**, *78*, 4803-4810.
(34) Singhal, A.; Haynes, C. A.; Hansen, C. L. *Analytical Chemistry* **2010**, *82*, 8671-8679.
(35) He, M.; Herr, A. E. *Anal Chem* **2009**, *81*, 8177-84; Herr, A. E.; Hatch, A. V.; Throckmorton, D. J.; Tran, H. M.; Brennan, J. S.; Giannobile, W. V.; Singh, A. K. *Proc Natl Acad Sci U S A* **2007**, *104*, 5268-73; Meagher, R. J.; Hatch, A. V.; Renzi, R. F.; Singh, A. K. *Lab Chip* **2008**, *8*, 2046-53.
(36) Hou, C.; Herr, A. E. *Anal Chem*, *82*, 3343-51.
(37) Lee, S.-J.; McPherron, A. C. *Proceedings of the National Academy of Sciences* **2001**, *98*, 9306-9311.

(38) Sommer, G. J.; Singh, A. K.; Hatch, A. V. *Lab on a Chip* **2009**, *9*, 2729-2737.
(39) Squires, T. M.; Messinger, R. J.; Manalis, S. R. *Nat Biotech* **2008**, *26*, 417-426.
(40) Escobedo, C.; Brolo, A. G.; Gordon, R.; Sinton, D. *Analytical Chemistry* **2010**, *82*, 10015-10020.
(41) Brennan, D. J.; O'Connor, D. P.; Rexhepaj, E.; Ponten, F.; Gallagher, W. M. *Nat Rev Cancer* **2010**, *10*, 605-17.
(42) Lilja, H.; Ulmert, D.; Vickers, A. J. *Nat Rev Cancer* **2008**, *8*, 268-78.
(43) Carlsson, A.; Wingren, C.; Ingvarsson, J.; Ellmark, P.; Baldertorp, B.; Fernö, M.; Olsson, H.; Borrebaeck, C. A. K. *Eur. J. Cancer* **2008**, *44*, 472-480.
(44) Wu, A. R.; Kawahara, T. L. A.; Rapicavoli, N. A.; Riggelen, J. v.; Shroff, E. H.; Xu, L.; Felsher, D. W.; Chang, H. Y.; Quake, S. R. *Lab Chip* **2012**, *12*, 2190-2198.
(45) Friguet, B.; Chaffotte, A. F.; Djavadi-Ohaniance, L.; Goldberg, M. E. *Journal of Immunological Methods* **1985**, *77*, 305-319.
(46) Hawkins, R. E.; Russell, S. J.; Winter, G. *J Mol Biol* **1992**, *226*, 889-96.
(47) Karlsson, R.; Michaelsson, A.; Mattsson, L. *J Immunol Methods* **1991**, *145*, 229-40.
(48) Malmborg, A. C.; Michaelsson, A.; Ohlin, M.; Jansson, B.; Borrebaeck, C. A. *Scand J Immunol* **1992**, *35*, 643-50.
(49) Dandliker, W. B.; Levison, S. A. *IHC* **1968**, *5*, 171-83.
(50) Malmqvist, M. *Curr Opin Immunol* **1993**, *5*, 282-6.
(51) Nygren, H.; Stenberg, M. *Journal of Colloid and Interface Science* **1985**, *107*, 560-566.
(52) Hardy, F.; Djavadi-Ohaniance, L.; Goldberg, M. E. *J Immunol Methods* **1997**, *200*, 155-9.
(53) Karlsson, R.; Falt, A. *J Immunol Methods* **1997**, *200*, 121-33.
(54) Van Der Merwe, A. P. S. *Oxford, London,* **2001**.
(55) Nieba, L.; Krebber, A.; Pluckthun, A. *Anal Biochem* **1996**, *234*, 155-65.
(56) Myszka, D. G.; Morton, T. A.; Doyle, M. L.; Chaiken, I. M. *Biophys Chem* **1997**, *64*, 127-37.
(57) van der Merwe, P. A.; Bodian, D. L.; Daenke, S.; Linsley, P.; Davis, S. J. *JEM* **1997**, *185*, 393-404.
(58) Schuck, P. *Annu. Rev. Biophys. Biomol. Struct.* **1997**, *26*, 541-566.
(59) de Mol, N. J.; Plomp, E.; Fischer, M. J.; Ruijtenbeek, R. *Anal Biochem* **2000**, *279*, 61-70.
(60) Spisak, S.; Tulassay, Z.; Molnar, B.; Guttman, A. *Electrophoresis* **2007**, *28*, 4261-4273.
(61) Heegaard, N. H.; Olsen, D. T.; Larsen, K. L. *J Chromatogr A* **1996**, *744*, 285-94.
(62) Okhonin, V.; Petrov, A. P.; Berezovski, M.; Krylov, S. N. *Anal Chem* **2006**, *78*, 4803-10.
(63) Petrov, A.; Okhonin, V.; Berezovski, M.; Krylov, S. N. *J Am Chem Soc* **2005**, *127*, 17104-10.
(64) Jiang, C.; Armstrong, D. W. *Electrophoresis* **2010**, *31*, 17-27.
(65) Xiong, C.; Xia, Z.; Huang, R.; Chen, H.; Xu, P. *Sci. China Ser. B-Chem.* **2008**, *51*, 1087-1092.
(66) Bao, J.; Krylova, S. M.; Reinstein, O.; Johnson, P. E.; Krylov, S. N. *Anal Chem* **2011**, *83*, 8387-90.
(67) Drabovich, A.; Berezovski, M.; Krylov, S. N. *J Am Chem Soc* **2005**, *127*, 11224-5.
(68) Krylov, S. N. *Electrophoresis* **2007**, *28*, 69-88.
(69) Bousse, L.; Mouradian, S.; Minalla, A.; Yee, H.; Williams, K.; Dubrow, R. *Anal Chem* **2001**, *73*, 1207-12.
(70) Apori, A. A.; Herr, A. E. *Anal Chem* **2011**, *83*, 2691-8.
(71) He, M.; Herr, A. E. *Nat Protoc* **2010**, *5*, 1844-56.
(72) Tia, S. Q.; Brown, K.; Chen, D.; Herr, A. E. *Analytical Chemistry* **2013**, *85*, 2882-2890.
(73) Hughes, A. J.; Lin, R. K.; Peehl, D. M.; Herr, A. E. *PNAS* **2012**, *109*, 5972-5977.
(74) Bilgiçer, B. a.; Thomas, S. W.; Shaw, B. F.; Kaufman, G. K.; Krishnamurthy, V. M.; Estroff, L. A.; Yang, J.; Whitesides, G. M. *J. Am. Chem. Soc.* **2009**, *131*, 9361-9367.
(75) Shukla, A. A.; Hubbard, B.; Tressel, T.; Guhan, S.; Low, D. *J. Chromatogr. B* **2007**, *848*, 28-39.
(76) Katsamba, P. S.; Navratilova, I.; Calderon-Cacia, M.; Fan, L.; Thornton, K.; Zhu, M.; Bos, T. V.; Forte, C.; Friend, D.; Laird-Offringa, I.; Tavares, G.; Whatley, J.; Shi, E.; Widom, A.; Lindquist, K. C.; Klakamp, S.; Drake, A.; Bohmann, D.; Roell, M.; Rose, L.; Dorocke, J.; Roth, B.; Luginbuhl, B.; Myszka, D. G. *Anal Biochem* **2006**, *352*, 208-21.
(77) Yu, F.; Persson, B.; Lofas, S.; Knoll, W. *Anal Chem* **2004**, *76*, 6765-70.
(78) Singhal, A.; Haynes, C. A.; Hansen, C. L. *Anal Chem* **2010**, *82*, 8671-9.
(79) Borrebaeck, C. A. K.; Malmborg, A.-C.; Furebring, C.; Michaelsson, A.; Ward, S.; Danielsson, L.; Ohlin, M. *Nat Biotech* **1992**, *10*, 697-698.
(80) Srisa-Art, M.; Dyson, E. C.; deMello, A. J.; Edel, J. B. *Anal Chem* **2008**, *80*, 7063-7.
(81) Wang, H.; Wang, Z.; Lu, M.; Zou, H. *Anal Chem* **2008**, *80*, 2993-9.
(82) Myszka, D. G. In *Methods Enzymol*, Michael L. Johnson, G. K. A., Ed.; Academic Press, 2000, pp 325-340.
(83) Asish Xavier, K.; Willson, R. C. *Biophysical Journal* **1998**, *74*, 2036-2045.
(84) Schreiber, G.; Fersht, A. R. *J. Mol. Biol.* **1995**, *248*, 478-486.

(85) Dejaegere, A.; Choulier, L.; Lafont, V.; De Genst, E.; Altschuh, D. *Biochem* **2005**, *44*, 14409-14418.
(86) Wang, Y.; Brunsen, A.; Jonas, U.; Dostálek, J.; Knoll, W. *Anal Chem* **2009**, *81*, 9625-9632.
(87) Seifar, R. M.; Cool, R. H.; Quax, W. J.; Bischoff, R. *Electrophoresis* **2004**, *25*, 1561-8.
(88) van Oss, C. J. *J Mol Recognit* **2003**, *16*, 177-190.
(89) Sternberger, L. A.; HARDY, P. H.; CUCULIS, J. J.; MEYER, H. G. *Journal of Histochemistry & Cytochemistry* **1970**, *18*, 315-333.
(90) Dabbs, D. J. *Diagnostic immunohistochemistry*; Elsevier Health Sciences, 2013.
(91) Mino-Kenudson, M.; Chirieac, L. R.; Law, K.; Hornick, J. L.; Lindeman, N.; Mark, E. J.; Cohen, D. W.; Johnson, B. E.; Jänne, P. A.; Iafrate, A. J. *Clinical Cancer Research* **2010**, *16*, 1561-1571.
(92) Lerwill, M. F. *The American journal of surgical pathology* **2004**, *28*, 1076-1091.
(93) McCluggage, W. G.; Young, R. H. In *Seminars in diagnostic pathology*; Elsevier, 2005, pp 3-32.
(94) Hameed, O.; Humphrey, P. A. In *Seminars in diagnostic pathology*; Elsevier, 2005, pp 88-104.
(95) Milstein, C.; Cuello, A. **1983**; Schellekens, G. A.; Visser, H.; De Jong, B. A.; Van Den Hoogen, F. H.; Hazes, J. M.; Breedveld, F. C.; Van Venrooij, W. J. *Arthritis & Rheumatism* **2000**, *43*, 155-163.
(96) Lequin, R. M. *Clinical chemistry* **2005**, *51*, 2415-2418.
(97) Hughes, A. J.; Spelke, D. P.; Xu, Z.; Kang, C.-C.; Schaffer, D. V.; Herr, A. E. *Nature methods* **2014**, *11*, 749-755.
(98) Kawahara, A.; Yamamoto, C.; Nakashima, K.; Azuma, K.; Hattori, S.; Kashihara, M.; Aizawa, H.; Basaki, Y.; Kuwano, M.; Kage, M. *Clinical Cancer Research* **2010**, *16*, 3163-3170.
(99) Dressler, F.; Whalen, J. A.; Reinhardt, B. N.; Steere, A. C. *Journal of Infectious Diseases* **1993**, *167*, 392-400.
(100) Robertson, G.; Hirst, M.; Bainbridge, M.; Bilenky, M.; Zhao, Y.; Zeng, T.; Euskirchen, G.; Bernier, B.; Varhol, R.; Delaney, A. *Nature methods* **2007**, *4*, 651-657.
(101) Berglund, L.; Björling, E.; Oksvold, P.; Fagerberg, L.; Asplund, A.; Szigyarto, C. A.-K.; Persson, A.; Ottosson, J.; Wernérus, H.; Nilsson, P. *Molecular & cellular proteomics* **2008**, *7*, 2019-2027.
(102) Perchiacca, J. M.; Ladiwala, A. R. A.; Bhattacharya, M.; Tessier, P. M. *Proceedings of the National Academy of Sciences* **2012**, *109*, 84-89.
(103) Haupt, C.; Fändrich, M. *Trends in biotechnology* **2014**, *32*, 513-520.
(104) Jones, D. S.; Silverman, A. P.; Cochran, J. R. *Trends in biotechnology* **2008**, *26*, 498-505.
(105) Kariolis, M. S.; Kapur, S.; Cochran, J. R. *Current opinion in biotechnology* **2013**, *24*, 1072-1077.
(106) Collins, F. S.; Tabak, L. A. *Nature* **2014**, *505*, 612.
(107) Bradbury, A.; Plückthun, A. *Nature* **2015**, *518*, 27.
(108) Schuck, P.; Zhao, H. In *Surface Plasmon Resonance*; Springer, 2010, pp 15-54.
(109) Kapil, M. A.; Herr, A. E. *Analytical chemistry* **2014**, *86*, 2601-2609.
(110) Duncombe, T. A.; Herr, A. E. *Lab on a Chip* **2013**, *13*, 2115-2123.
(111) Pan, Y.; Duncombe, T. A.; Kellenberger, C. A.; Hammond, M. C.; Herr, A. E. *Analytical chemistry* **2014**, *86*, 10357-10364.
(112) Haynes, W. M. *CRC handbook of chemistry and physics*; CRC press, 2013.
(113) Reverberi, R.; Reverberi, L. *Blood Transfusion* **2007**, *5*, 227-240.
(114) Hughes-Jones, N.; Gardner, B.; Telford, R. *Immunology* **1964**, *7*, 72.
(115) Hughes-Jones, N. *Clinics in haematology* **1975**, *4*, 29.
(116) Moore, B. In *A Seminar on Antigen-antibody Reactions Revisited. Arlington VA: AABB*, 1982, pp 47-66.
(117) Hughes-Jones, N.; Gardner, B.; Telford, R. *Biochemical Journal* **1962**, *85*, 466.
(118) Hughes‐Jones, N.; Polley, M. J.; Telford, R.; Gardner, B.; Kleinschmidt, G. *Vox sanguinis* **1964**, *9*, 385-395.
(119) Hughes-Jones, N.; Gardner, B.; Telford, R. *Biochemical Journal* **1963**, *88*, 435.
(120) Xavier, K. A.; Willson, R. C. *Biophysical journal* **1998**, *74*, 2036-2045.
(121) Schwesinger, F.; Ros, R.; Strunz, T.; Anselmetti, D.; Güntherodt, H.-J.; Honegger, A.; Jermutus, L.; Tiefenauer, L.; Plückthun, A. *Proceedings of the National Academy of Sciences* **2000**, *97*, 9972-9977.
(122) Lipschultz, C. A.; Yee, A.; Mohan, S.; Li, Y.; Smith‐Gill, S. J. *Journal of Molecular Recognition* **2002**, *15*, 44-52.
(123) Pettersson, K.; Piironen, T.; Seppälä, M.; Liukkonen, L.; Christensson, A.; Matikainen, M.; Suonpää, M.; Lövgren, T.; Lilja, H. *Clinical chemistry* **1995**, *41*, 1480-1488.
(124) Troyer, J. K.; Feng, Q.; Beckett, M. L.; Wright, G. L. In *Urologic Oncology: Seminars and Original Investigations*; Elsevier, 1995, pp 29-37.